KATHOLIEKE UNIVERSITEIT
LEUVEN

FACULTEIT WETENSCHAPPEN
Departement Chemie
Afdeling Moleculaire en Nanomaterialen
Onderzoeksgroep Fotochemie en Spectroscopie

Structural insight into fluorescent protein properties by rational design and characterization of photoconvertible, photoswitchable and phototoxic fluorescent proteins.

door

Benjamien MOEYAERT

Promotor: Prof. J. Hofkens
Begeleider: Dr. V. Adam

Proefschrift ingediend tot het behalen van de graad van Master in de biochemie en de biotechnologie

Academiejaar 2009-2010

Acknowledgements

First of all, and foremost, I would like to thank Virgile for all the effort he put in introducing me in the world of fluorescent proteins. The discussions, measurements and coffee breaks we had taught me more than any book or lecture could. Thanks also to Peter and Hide, who were always ready to answer the questions that got me stuck. Charlotte, for amusing chats and help with the experiments. Also thanks to many the people from the lab, especially Jun-Ichi, Edward, Rob, Edouardo, Renée, Werner, Carine and Els, for their help. A special remark for prof. Yves Engelborghs, for allowing me to work at his facilities. Great thanks also to my fellow thesis students, for all the meaningful, but also senseless chats we had. And of course, this thesis would not have been made if there was no such group as the LPS group. I therefor would like to express my gratitude to prof. Johan Hofkens, for setting up this great research environment.

Mijn ouders en broers, bedankt voor de steun en de thuis die jullie boden. En natuurlijk Sarah-Ann, die me steeds zonder twijfelen door dik en dun steunt. Bedankt voor alle geduld, je luisterend oor en zoveel meer.

Benjamien

28 mei 2010

Contents

List of Figures

Nomenclature

*av*GFP	*Aequorea victoria* green fluorescent protein
p-HBI	4-(*p*-hydroxybenzylidene)-imidazolidin-5-one
APD	avalanche photodiode
BFP	blue fluorescent protein
CALI	chromophore-assited light inactivation
CCD	charge-coupled device
CFP	cyan fluorescent protein
cfu	colony forming units
CW	continuous wave
eGFP	enhanced green fluorescent protein
FIFO	first-in, first-out
FP	fluorescent protein
FPLC	fast protein liquid chromatography
FRET	Förster resonance energy transfer

FWHM	full width at half maximum
GFP	green fluorescent protein
IPTG	isopropyl β-D-1-thiogalactopyranoside
Ni-NTA	Ni^{2+}-nitrilotriacetic acid
PAFP	photoactivatable fluorescent protein
PALM	photoactivated localization microscopy
PBS	phosphate buffered saline
PCFP	photoconvertible fluorescent protein
PCR	polymerase chain reaction
PDT	photodynamic therapy
QC/MM	quantum chemical/molecular mechanical
RESOLFT	reversible saturable optically linear fluorescence transitions
ROS	reactive oxygen species
rpm	rotations per minute
RSFP	reversibly switchable fluorescent protein
SDS-PAGE	sodium dodecyl sulfate polyacrylamide gel electrophoresis
STED	stimulated emission depletion
STORM	stochastic optical reconstruction microscopy
TCSPT	time-correlated single photon counting
TN	Tris-NaCl
YFP	yellow fluorescent protein

Part A

Literature overview

CHAPTER 1

Fluorescent proteins

Since the 1990s, fluorescent proteins (FPs) have been invaluable as a tool for live cell imaging. Their influence on cell biology and many other related disciplines has been tremendous. It was therefore barely a surprise that the 2008 Nobel prize in chemistry was awarded to Osamu Shimomura, Martin Chalfie and Roger Tsien "for the discovery and development of the green fluorescent protein, GFP".

1.1 The discovery of *av*GFP

In the early '60s, Osamu Shimomura, then related to the Princeton University, described the molecules responsible for the green light emitted by the jellyfish *Aequorea victoria*. He found that a Ca^{2+}-dependent chromoprotein, aequorin, emits blue light that through Förster resonance energy transfer (FRET) is absorbed by another protein. This protein is fluorescent and emits light in the green part of the visible spectrum [1]. It was thus called green fluorescent protein (GFP).

It was some 30 years later that the gene coding for GFP, more precisely called *Aequorea victoria* green fluorescent protein or *av*GFP was cloned by Douglas Prasher [2]. Its potential as marker for gene expression, however, only became clear when Martin Chalfie cloned the *av*GFP gene into the nematode *Caenorhabditis elegans*, thus giving the roundworm a green color, as in

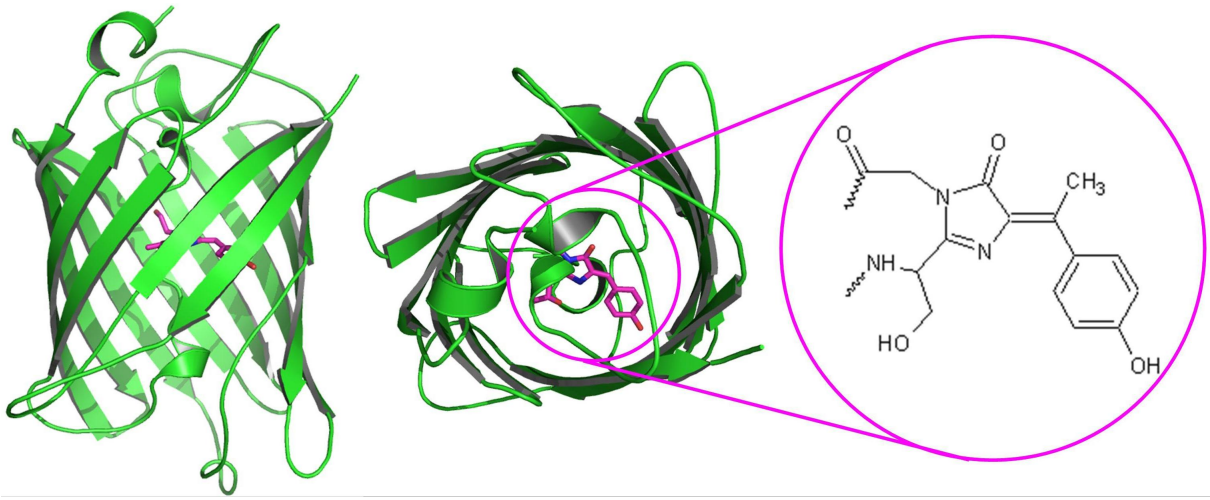

Figure 1.1: *First crystal structure of avGFP (PDB accession code: 1EMA) [4]. View from the side (left) and top view (middle) with the chromophore structure (right) in magenta.*

Figure 1.3 [3].

1.2 The protein and its chromophore

1.2.1 Protein structure

The *av*GFP consists of 238 amino acids (27 kDa). Its structure is made of 11 β-strands forming a cylindrical sheet with one α-helix running along the axis. The diameter of the can is approximately 24Å and the central axis has a length of about 42Å[4]. This particular structure motif is called a β-can and is specific for fluorescent and chromoproteins, the latter being colored, but non-fluorescent proteins (Lukyanov 2000). In the center of the β-can is the chromophore, shielded from the solvent (see Figure 1.1). It is essentially unaccessible by quenching molecules (for instance oxygen) due to the tight packing of the β-can and lack of clefts or tunnels towards the chromophore. Furthermore, the β-can forms a hydrogen network around the chromophore, thus keeping it a planar conformation. It is important to stress the strong relationship between the structure of the protein and its properties [5].

1.2.2 Chromophore structure

At the very heart of every fluorescent or chromoprotein is the chromophore. It is formed in a remarkable cyclization process, involving residues Ser65, Tyr66 and Gly67 (GFP numbering).

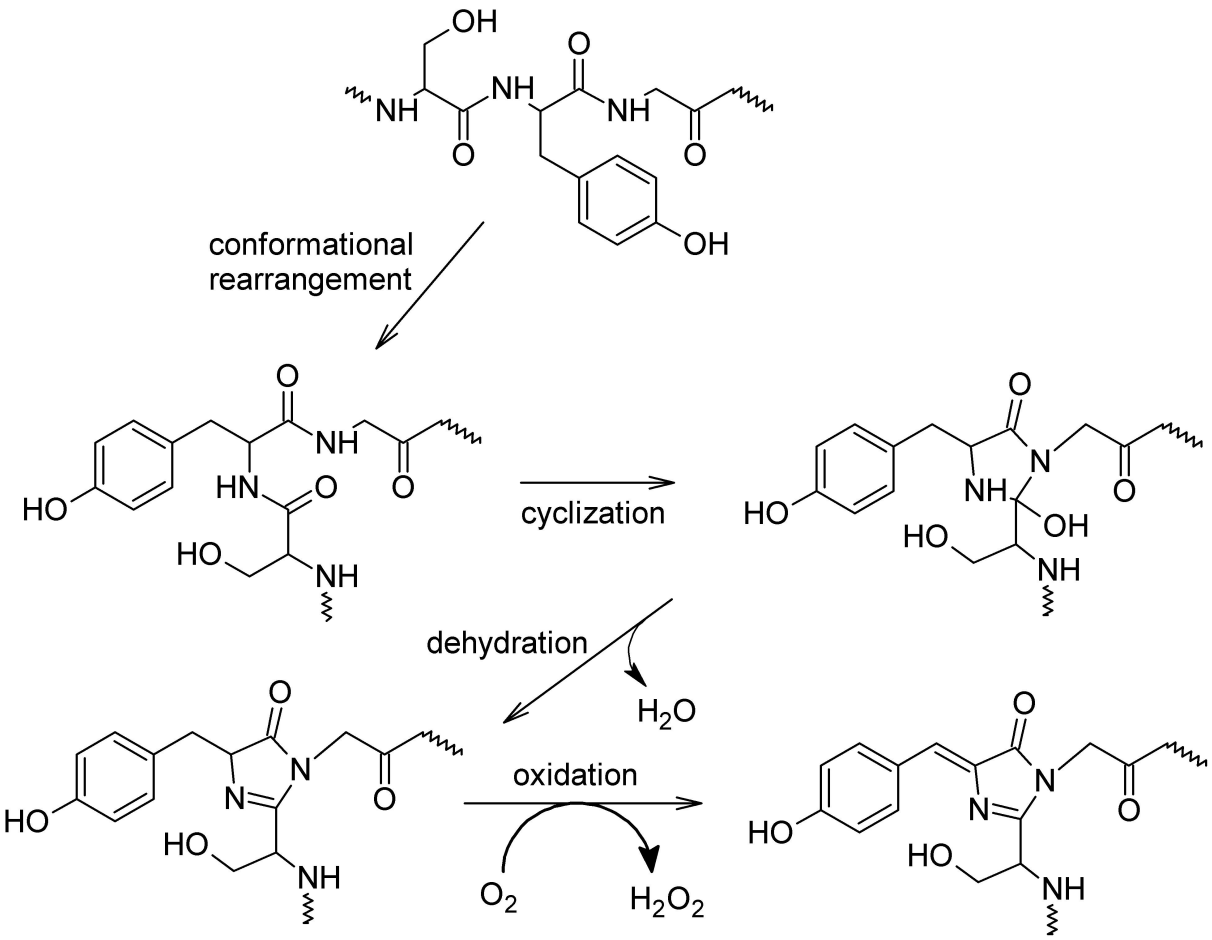

Figure 1.2: *Chromophore formation (adapted from [6]).*

The detailed mechanism consists of a conformational rearrangement that is directly followed by the formation of an imidazolinone ring system (the cyclization step), a dehydration step and an oxidation step (see Figure 1.2). This autocatalytical process occurs during a process called protein maturation and results in the formation of a 4-(*p*-hydroxybenzylidene)-imidazolidin-5-one (*p*-HBI) chromophore [6].

1.2.3 A success story

It is clear that a couple of very distinct properties have made GFP a versatile and reliable reporter gene. The most interesting aspect of GFP is that it works almost perfectly autocatalytically. That is, it requires no helper enzymes nor co-factors for maturation, except for O_2, which is ubiquitous anyway. This way, GFP can be introduced in principle in any organism [6]. The protein has for example been succesfully expressed in bacteria [3], yeast [7], plants [8] nematodes [3],

invertebrates [9] and vertebrates [10] (see Figure 1.3[1]).

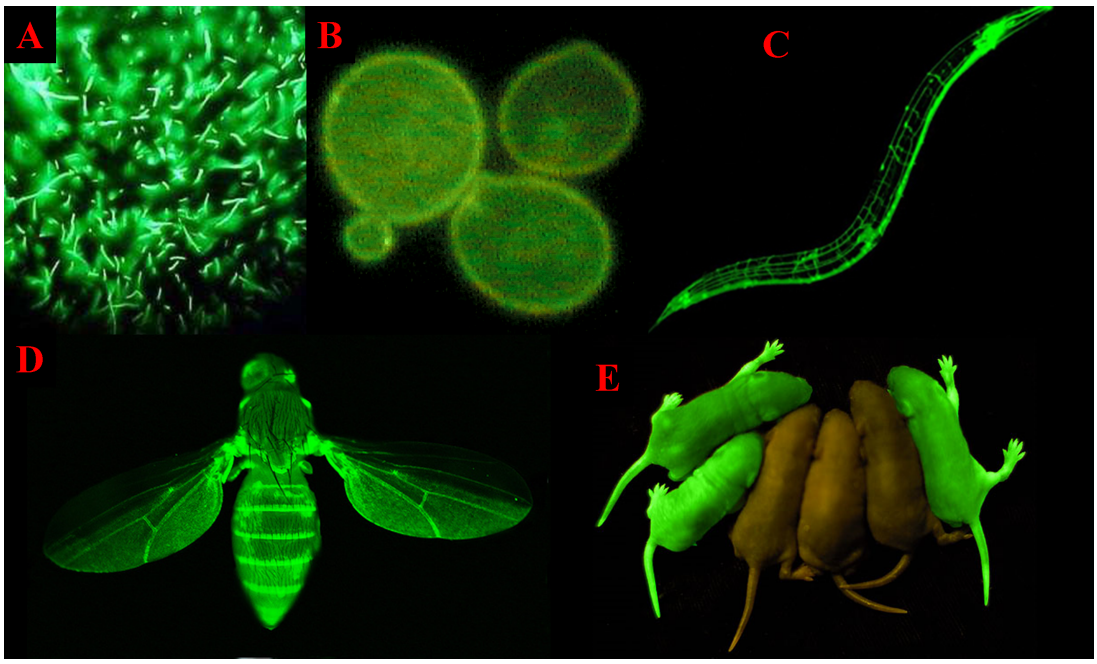

Figure 1.3: *Expression of GFP in (**A**) Escherichia coli, (**B**) Saccharomyces cerevisiae, (**C**) Caenorhabditis elegans, (**D**) Drosophila melanogaster and (**E**) Mus musculus.*

[1]Pictures were taken and adapted from

(**A**) http://www.microbelibrary.org/Laboratory%20Diagnostics/details.asp?id=707,

(**B**) http://stephen.johnston.faculty.noctrl.edu/Ras-GFP.gif,

(**C**) http://www.bcgsc.ca/people/msleumer/htdocs/fact_sheet/image004.jpg,

(**D**) http://www.hoxfulmonsters.com/wp-content/uploads/2008/10/glowing-fly.jpg and

(**E**) http://www.upenn.edu/pennnews/photos/704/mice.jpg.

CHAPTER 2

A color palette

From the moment people started to be aware of the great potential that GFP holds in terms of imaging, they have been looking for FPs with different spectroscopic properties. There are essentially two ways of doing this. One way is to look for organisms that express FPs and trying to clone the genes encoding them. The other way is based on mutational techniques allowed by molecular biology. The residues that form or surround the chromophore can be mutated, resulting in covalent modifications of the chromophore or its environment, thus influencing the fluorescence properties of the protein. Combinations of these two strategies are commonplace.

2.1 Fluorescent proteins from other organisms

Fluorescent proteins have untill recently been extracted and cloned from two classes of organisms: hydrozoa and anthozoa. The *av*GFP was derived from a hydrozoa species, while most of the other FPs come from anthozoa species. Figure 2.1 displays a relevant outtake of the cnidarian phylogenetic tree, together with wild type and engineered forms of FPs derived from the respective organisms. Only FPs that are relevant to what will follow in this thesis are mentioned in this figure. The number of FPs found in cnidarian species is in fact even higher and still increasing.

Recently, it was found that not only organisms found in the Cnidaria group express fluores-

cent proteins. In 2006, Masuda *et al.* reported on a yellowish-green fluorescent protein found in *Chiridius poppei*, a copepod that is member of the Bilateria group. It has a yellowish-green color and was thus called CpYGFP [11]. Another example is AmphiGFP, a GFP-like fluorescent protein that was found in three different amphioxus species, also members of the Bilateria. It was found that AmphiGFP consists of an 11-stranded β-barrel with fluorophore inside. Its primary structure is highly similar to the CpYGFP [12].

In 2009, the group of Roger Tsien brought out the first publication that introduces infrared fluorescent proteins (IFPs), derived from a bacterium called *Deinococcus radiudurans*. This bacterium produces a bacteriophytochrome (DrPbhP) that fluoresces. After deletion of the non-necessary domains and some point mutations that prevent oligomerization, this protein proved to fluoresce at ~720 nm. However, this is only the fact if the protein is supplemented with biliverdin IXα, normally produced by heme oxygenase I during heme degradation [13].

2.2 Fluorescent proteins made by mutagenesis

FPs can be mutated in parts of the chromophore and its microenvironment. The mutagenesis of the hydrozoan GFP towards its enhanced version called eGFP is a nice example of how the chromophore microenvironment influences the FP's behavior. A single mutation (S65T) has an influence on the protonation state of the chromophore, shifting the ratio between the neutral and anionic excitation peaks towards the anionic species. This resulted in increased fluorescence brightness and increased rate of fluorophore generation [14]. Introducing π-π interactions between the chromophoric Tyr hydroxyphenolate moiety and the inside of the β-barrel by mutating residue 203 to one of the four aromatic residues (His, Phe, Trp or Tyr) resulted in yellow fluorescent protein (YFP). Cyan fluorescent protein (CFP) and blue fluorescent protein (BFP) are in their turn the most known examples of chromophore-mutated FPs. They were made by mutating the chromophore Tyr towards a Trp and His, respectively.

Also, anthozoan FPs have been mutated in different ways. However, the wild types are mostly tetrameric, making them less suitable as reporters because their tetrameric nature has an influence on the probed molecule. additional mutagenesis efforts have been done to abolish the subunit interactions. All these efforts together resulted in a series of FPs called the mFruit series [15, 16, 17], because they are all called after a fruit having a similar color to the FP in

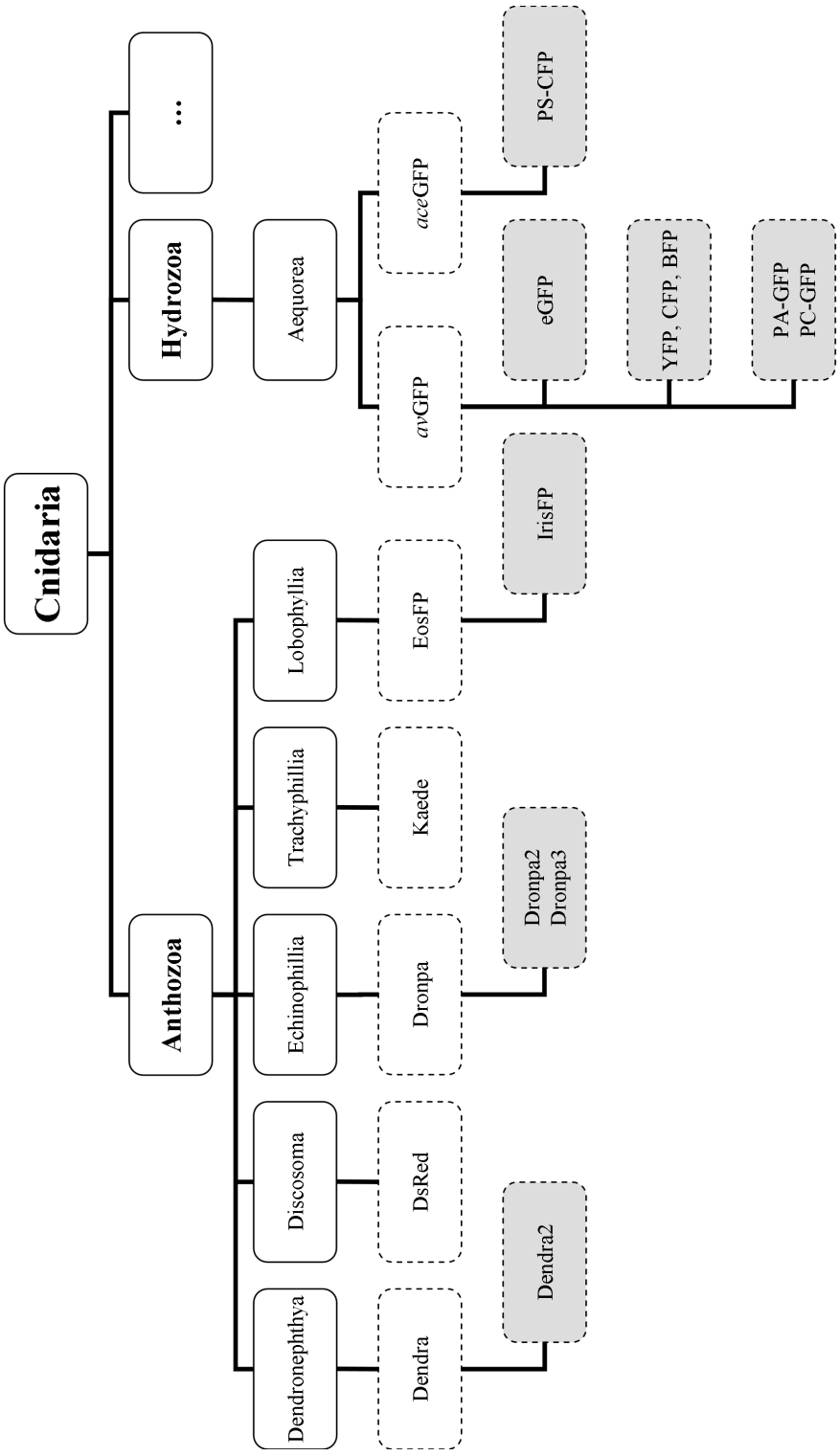

Figure 2.1: *Outtake of the cnidarian phylogenetic tree. Two classes (Hydrozoa and Anthozoa) and six geni (full line) are depicted. Wild-type FPs derived from these organisms are named (dashed lines), along with some mutants (dashed lines, grey).*

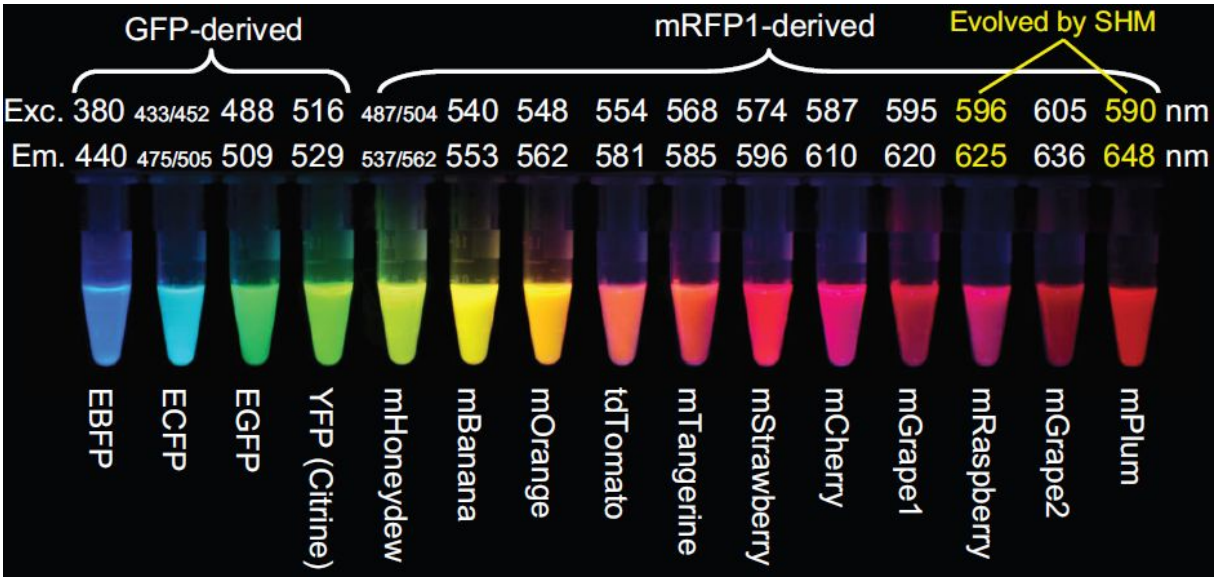

Figure 2.2: *The 2004 palette of nonoligomerizing fluorescent proteins (adapted from [18]).*

question. A nice series of engineered FPs, both hydrazoan as antozoan, was shown by Roger Tsien during his Nobel Lecture in 2009 (Figure 2.2).

CHAPTER 3

Intelligent FPs

Up to now, the fluorescent properties of FPs were only discussed in terms of excitation and emission wavelengths. However, next to this steady-state properties, some fluorescent proteins also exhibit time-dependent properties at the single molecule level that become visible at the bulk level. These properties, amongst others, broaden the possibilities for fluorescence microscopy and bring it to diffraction-unlimited levels.

3.1 Photoactivatable fluorescent proteins

Photoactivatable fluorescent proteins (PAFPs) are proteins that can change their spectra (would it be the absorption, emission, excitation or a combination of these) upon light irradiation. In referring to the reversible phototransformation between two forms of a chemical species, each having a different absorption spectrum, one also often speaks about photochromism. Roughly, two types of PAFPs can be named. The first ones are FPs that adopt a photoswitching behavior. These proteins can reversibly switch between a bright fluorescent and a dark non-fluorescent state and are therefore called reversibly switchable fluorescent proteins (RSFPs). The other group are the photoconvertible fluorescent proteins (PCFPs), which can irreversibly change their fluorescence emission from one color to another (see Figure 3.1). There is also one protein reported in literature, called IrisFP, that combines reversible photoswitching with irreversible

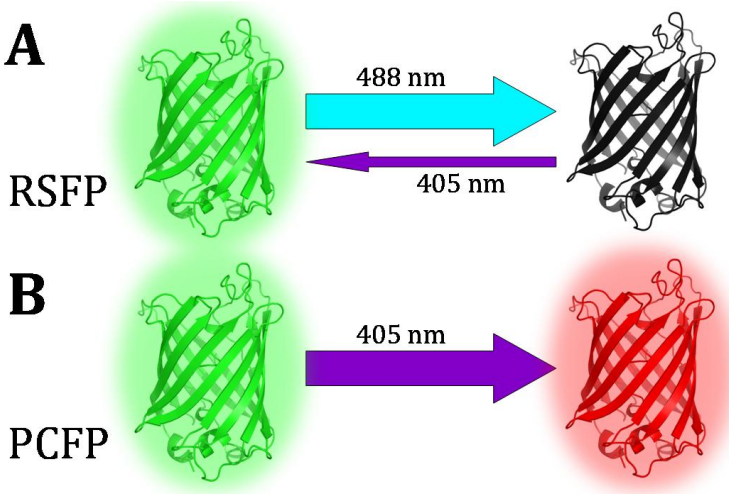

Figure 3.1: *(A) A green fluorescent RSFP can be switched to a dim state with prolonged and/or intense illumination with cyan light. Weak illumination with violet light brings the dim state quickly back to the bright state. (B) A green fluorescent PCFP can be irreversibly converted to a red fluorescent state with cyan light illumination.*

photoconversion [19].

3.1.1 Photoswitchable FPs

Photoswitching can be seen as a reversible bleaching event. That is, an RSFP can be converted from a bright fluorescent state to a dark non-fluorescent state by light irradiation. Short irradiation with another wavelength restores the fluorescence very quickly. With proper conditions for these proteins, this switching can be repeated more than 100 times.

For instance, the RSFP Dronpa shows two absorption bands, at 388 nm and at 503 nm [20]. The lower-wavelength absorption band can be attributed to the protonated form of the chromophore and the longer-wavelength to its anionic form. Exciting the protein at the 503 nm absorption band gives rise to bright fluorescence at 513 nm. However, the absorption band at 503 nm can be decreased by irradiating the protein at this wavelength, accompanied by an increase of the 388 nm absorption band. The result is a light-induced formation of a dark state. This dark state thermally recovers to the bright state at a rather slow rate, a process that is greatly enhanced by violet light irradiation (~400 nm). It has been proven at the single molecule level that this photoswitching process can happen up to 170 times before suffering from irreversible photobleaching [21]. Photoswitching kinetic parameters have been tuned by mutating the chromophore environment. This way, the photoswitching speed has been accelerated, resulting in rsFastLime (Dronpa_V157G) [22], but also slowed down, resulting in PDM1-4 (Dronpa_K145N) [23].

From what is described above, we can summarize that Dronpa is a negative photoswitcher, meaning that exciting the fluorophore leads to both excitation and off-switching. Interestingly, a single mutation of rsFastLime (rsFastLime_V157G) inverts the switching behavior from negative to positive switching. This means that irradiation with the excitation light results in both emission and on-switching, while the off-switching is done by irradiating the violet peak, corresponding to the protonated fraction. As this behavior is the opposite of Dronpa's behavior, this positive-switching fluorescent protein was called Padron [24].

3.1.2 Photoconvertible FPs

Two kinds of photoconvertible FPs exist. The first class includes PA-GFP [25] and PS-CFP [26] and involves a UV-violet light-induced decarboxylation step of the very conserved glutamate near the chromophore. Note here that this glutamate is not a chromophore-forming residue. However, the decarboxylation induces a rearrangement in the hydrogen bonding network surrounding the chromophore, thus altering the protonation state and inducing a hundred-fold fluorescence intensity increase and cyan-to-green emission shift, respectively.

The second class of PCFPs is the Kaede-like family of green-to-red PCFPs. UV-violet light induces a cleavage of the protein's mainchain between the amide nitrogen and C_α of the chromophore histidine, followed by the formation of a double formation between the C_α and C_β of the imidazolinone ring. This extends the π-conjugated system to this imidazolinone ring, causing a red shifted spectrum (see Figure 3.2). Examples of this class of proteins are Kaede [27], KikGR [28], EosFP [29] and Dendra [30].

For example, Dendra2 is an improved version of Dendra, said to be faster maturating and more brighly fluorescing. It is an efficiently photoconverting PCFP that shows an excitation maximum at 490 nm, with 507 nm emission [31]. Irradiation with 405 nm light irreversibly converts this green form to a red activated form that is excited at 553 nm with 573 nm emission [30].

3.2 Biotechnological applications of FPs

The overview of fluorescent proteins and their functionality has, up to this point, only focussed on FPs as convenient and versatile *labels*. However, FPs have been engineered to execute more

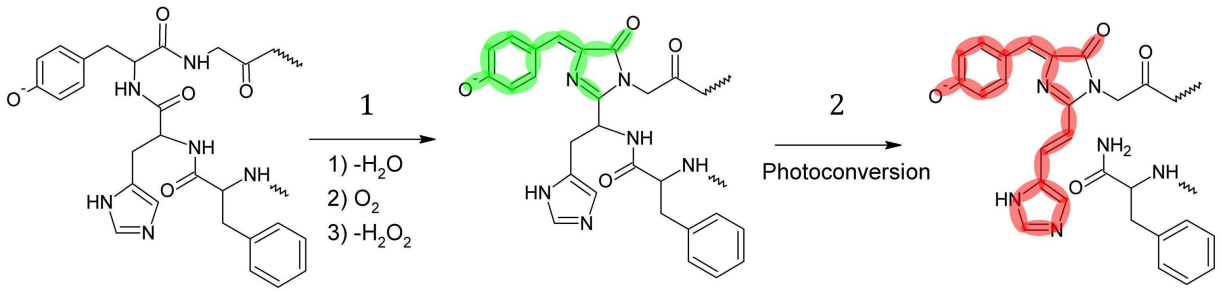

Figure 3.2: *(1) Autocatalytic chromophore maturation and (2) light-induced photoconversion to the red form. Adapted from [32] and [33].*

complicated tasks. They can, for instance, serve as a genetically encoded *sensors* for in situ measurements or be engineered to act as a *photosensitizer*.

3.2.1 FPs as sensors

The fluorescent properties of FPs are always strongly influenced by the pH of the medium, allowing the development of a genetically encoded biosensor based on a GFP mutant capable of sensing the local pH in a living cell [34]. More elaborate constructs have been made, for instance the cameleon type of calcium sensors. These constructs consist of two FPs, linked by a Ca^{2+}-binding domain. In the absense of Ca^{2+}, the two FPs are relatively far from each other, but in the presence of Ca^{2+}, a conformational change brings the two FPs in contact, close enough for FRET to occur [35]. These are only two examples. For a more complete overview and elaborate description, we refer to [36].

3.2.2 Photosensitizers

An interesting property of FPs is phototoxicity. Althought this might sound like a very much unwanted side-effect, it is the basis of chromophore-assisted light inactivation (CALI) [37, 38], a technique often used in cell biology. While conventional techniques of gene knock-out and RNA interference often suffer from transcriptional and translational compensation mechanisms, making measurements often unreliable, CALI can effectively and spatiotemporally delete a specific protein in the living cell. CALI makes use of a chromophore that reacts with oxygen to produce reactive oxygen species (ROS) upon excitation. These species are free oxygen radicals

like superoxide radicals or singlet oxygen and are thus very reactive. They react with any molecule in close proximity, destroying their structure and function. Thus, when a protein is targetted with such a photosensitizing molecule, and this latter gets excited, the protein is destroyed almost immediately, depending on the efficiency of ROS prooduction.

As an extension of this protein knockdown, photosensitizing small organic molecules (for instance porphyrin derivatives and phthalocyanines) have been used as a new way of treating several types of cancer, known as photodynamic therapy (PDT) [39]. In this technique, these small molecules are administered to the patient, after which the specific tissue is illuminated with red light (600-700 nm). Thereupon, ROS are produced, leading to cellular destruction. One of the major prerequisites for a good photosensitizer is at the same time a chief attraction, namely (dual) selectivity. The first selection is the localization of the photosensitizer. The second selective procedure is light delivery, that can be very precisely focused and confined.

KillerRed is a red fluorescent protein that has been engineered from the non-fluorescent GFP-like chromoprotein anm2CP, derived from a hydrozoan *Anthomedusae* species [40]. KillerRed shows a high phototoxic effect after green light (540 - 540 nm) irradiation. This way, it is indeed a genetically encoded photosensitizer. It destroys the function of a protein fused to it when excited, both in bacterial and mammalian cells [41]. In the light of what has been discussed in the previous paragraph, KillerRed could become a very exciting alternative to use in PDT.

Two crystal structures of KillerRed have been published [42, 43]. They have revealed that one of the key components contributing to the phototoxic behaviour is a channel filled with seven water molecules running from the the chromophore towards the bulk solvent along the axis of the β-barrel (see Figure 3.3. Another critical part seems to be a polar residue in the essentially apolar chromophore surrounding. The fluorescence itself also plays a critical part, as the long excited state lifetime is suggested to promote the interaction between chromophore and oxygen, thus giving rise to ROS production.

3.2.3 Diffraction-unlimited far-field fluorescence microscopy

One of the most interesting applications of photoactivatable fluorescent proteins is diffraction-unlimited far-field fluorescence microscopy [44]. Roughly two major techniques are in use. The first is the “reversible saturable optically linear fluorescence transitions” or RESOLFT

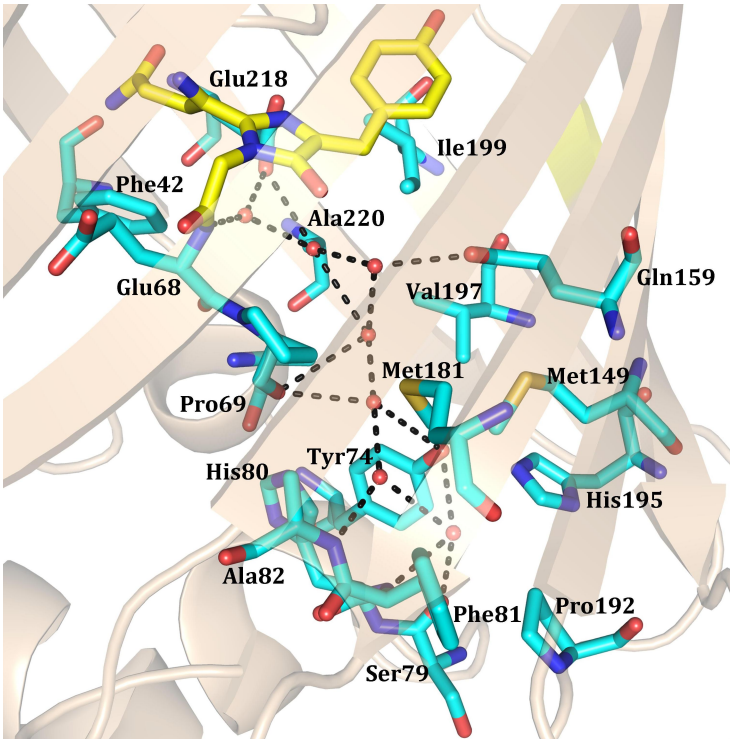

Figure 3.3: *Seven hydrogen-bonded (black dotted lines) water molecules (red spheres) form a water-filled channel running from the chromophore (yellow) to the bulk solvent (PDB accession code: 2WIQ). Oxygen atoms are represented in red, nitrogen atoms in blue and sulphur in orange.*

technique, of which stimulated emission depletion or STED is one of the most widespread implementations. STED microscopy is a scanning technique like confocal microscopy, meaning that the sample is scanned point by point. It makes use of a diffraction-limited focal spot of an excitation beam that excites the fluorophores from the S_0 to the S_1 state. Coaxially aligned with this excitation beam is a a doughnut-shaped depletion beam, red-shifted compared to the excitation wavelenght. This depletion beam promotes S_1-S_0 transitions in a doughnut shape around the exitation spot, essentially resulting in an excitation spot that is no longer diffraction-limited, allowing the excitation and thus the detection of a single fluorophore [45].

The second technique is called photoactivated localization microscopy or PALM when PAFPs are used and stochastic optical reconstruction microscopy or STORM when small organic fluorophores are used [46, 47]. In this technique, wide-field microscopes are used, that illuminate and excite the sample evenly and detect fluorescence using a charge-coupled device (CCD) camera. To achieve single molecule resolution, it is necessary to use photoactivatable fluorophores. In the case of photoswitchable fluorophores, all fluorophores are first brought into a photoinduced dark state. Due to thermal recovery or thanks to a short and weak illumination of light, some fluorophores are brought back into a fluorescing state. The duration and intensity of this activation light must be tuned so that every two fluorescing molecules can be distin-

guished from each other on the CCD camera. An image is then recorded untill all fluorophores are reversibly or irreversibly bleached. Then the cycle restarts, bringing some fluorophores back to a bright state, recording an image and then switching them off again, and so on and so forth. Every spot on every image is then fitted to a gaussian intensity profile. The peak of this profile can be considered as the position of the fluorophore. Important here is that the certainty about the position of the intensity peak, and thus the position of the fluorophore, is dependent on the number of photons that is detected. This means that a good probe for PALM or STORM microscopy switches from bright to dark slowly, so that a lot of photons can be detected, but switches back from dark to bright very fast, thus speeding up the acquisition time for a PALM or STORM measurement [23]. In an ideal case, the thermal recovery is so fast, that no light is needed to promote the backswitching to the bright state. This makes PALM/STORM setups much easier, as only one laser would be necessary.

CHAPTER 4

Structural insight into FP properties

The major question of this master's thesis will be:

> To what extent can structural knowledge about fluorescent proteins give us the tools to design their properties following a rational mutagenesis strategy and how will this provide us with further insight into the mechanistics of the designed molecular processes?

This indeed is a daring question, and certainly not a trivial one. As can be read above, the application of FPs for both fundamental as applied biological and biomedical sciences is immense, and it is expected that their importance will only become bigger. However, to keep practice up with new ideas, but maybe even more to improve and therefore fully understand existing FP and FP-based techniques, this fundamental knowledge is crucial.

This challenge will be taken up by three major projects. A directed mutagenesis procedure will be followed to make proteins that are both photoconvertible and reversibly photoswitchable. *First*, this will be done starting from the PCFPs Dendra2 and mEosFP. At the same time, the *second* approach starts form a photoswitchable protein (Dronpa). These proteins are studied in detail, crystal structures are available and much of the mechanistics is already known. Properties of IrisFP, the only protein known that already combines these properties, will serve as a guide for thinking out mutations that will serve the goal set. The resulting mutants will be fully and

thoroughly characterised to reveal insights into their working mechanisms.

A *third* part is the construction of a photosensitizing FP out of a non-photosensitizing one. eGFP will be mutated towards this goal. Structural insight into the mechanism of KillerRed phototoxicity will serve as a template here.

Part B

Projects

CHAPTER 5

Making mEosFP and Dendra2 photoswitchable

The discovery of photoactivatable fluorescent proteins and, amongst others, their diverse uses in cell biology [48], their possibilities in diffraction-unlimited far-field fluorescence microscopy [46, 49] and their applications in bionanotechnology, namely the field of genetically encoded biosensors [35], have led to a recent interest in the fundamental structural themes that are at the basis of photoactivation in FPs. The scientific community is not yet unambiguously sure about the exact mechanism of photoconversion (see Section 6.2). There has also been quite some doubt concerning the exact mechanism of photoswitching, but recent evidence confirms the mechanism by which light-induced protonation followed by cis-trans isomerization serves as the basis of photoinduced off-switching [50, 51].

Recent reporting on IrisFP [19] has led to a lot of interest in the FP research community. This particular protein shows both reversible photoswitching properties as well as the possibility to be photoconverted from green to red. Not only is IrisFP interesting from a mechanistic point of view, the possible applications are plenty. Two-color high resolution microscopy with one single FP is an obvious application. A more surprising use of IrisFP crystals is base-four data storage [52].

5.1 IrisFP unraveled

IrisFP is derived from the tetrameric photoconvertible EosFP by a point mutation that substituted the Phe173 for a serine residue. An additional mutation (F191L) slipped in, but has no further influence on the protein's behavior (V. Adam, personal communication). When the native green fluorescing form of the protein is illuminated with cyan light (488 nm), the anionic absorption band at 488 nm decreases, accompanied with a rise of the absorption band that is associated with the essentially non-fluorescent neutral species at 390 nm, thus switching off the fluorescence. Although the half-life of the dark form is over 5 hours, 405 nm light illumination restores the fluorescence within seconds. A continued excitation of the non-fluorescent neutral species with this 405 nm light converts the protein from the green- to the red-emitting state. This red state is also characterized by two absorption bands. The broad absorption band at about 450 nm stems from the neutral, non-fluorescent state of the red chromophore. The 551 nm absorption peak is caused by the fluorescent anionic species. In this red state, green light (eg. 532 nm laser light) induces exactly the same phenomenon as the 488nm light does in the green state. It brings the anionic excitation band down and the neutral absorption band up, thus resulting in off-switching of the fluorescence of the red species. The dark form of the red species has a half-life of over 3 hours, but, analogous to what violet light does to the green species' dim state, 440 nm light heavily accelerates backswitching from the red species' dark state to its bright state (See Figure 5.1).

As shown in Figure 5.2, the EosFP phenylalanine residue at position 173 occupies a voluminous space. Replacing it by serine (this is the EosFP-to-IrisFP-mutation) allows an extra water molecule (W2166) to fit in and binds both the Ser173 and the Thr59 side chains of IrisFP. The Met159 side chain, previously in van der Waals contact with the phenyl moiety of the chromophore, is flipped upwards allowing yet another water molecule (W2188) to fit in. This water molecule serves as an electron donor for the Ser142 side chain, lowering the bond energy between Ser142 and the hydroxyphenyl moiety of the chromophore, allowing light-induced protonation and subsequent cis-trans isomerization of the chromophore, leading to a dark state. Following this rationale, the engineered photoswitching properties can be fully understood from a mechanistic point of view. This in-depth insight will be validated in what follows by using it to rationally engineer photoswitching abilities into a photoconvertible FP [19].

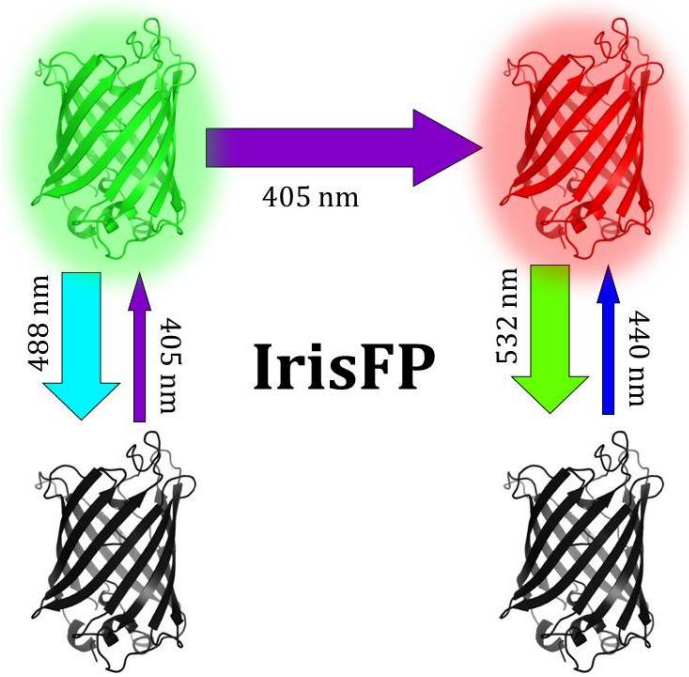

Figure 5.1: *IrisFP can be switched from a bright green state to a dim non-fluorescent state with prolonged and/or intense illumination with cyan light. Weak illumination with violet light brings the dim state quickly back to the bright state. Prolonged illumination with violet light converts the green form to the red form of IrisFP. This red form is fluorescent, but green light switches off the red form to a dim, non-fluorescent state. The fluorescence can be recovered by weak blue light illumination.*

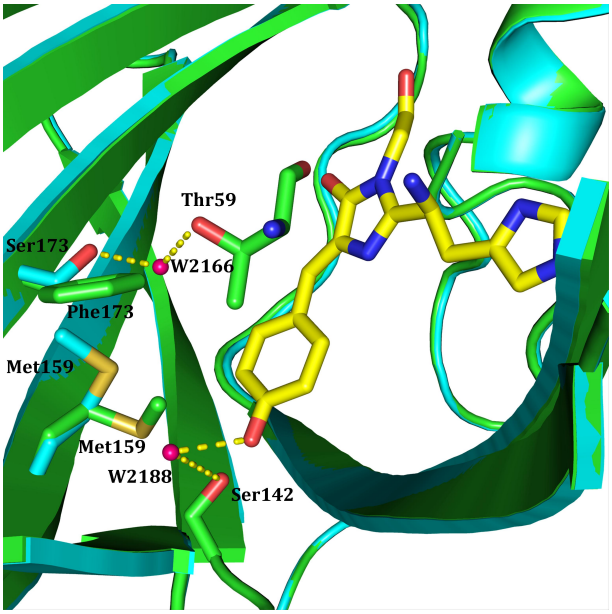

Figure 5.2: *Overlay of the EosFP (green, PDB accession code: 1ZUX) and the IrisFP (cyan, PDB accession code: 2VVH) crystal structure. Pink spheres are two IrisFP water molecules, the chromophore is shown in yellow. Mutating Phe173 towards a serine residue makes space for the W2166 water molecule to fit in, allowing the upwards flip of the Met159 residue, thus allowing an extra water molecule, W2188. Oxygen atoms are represented in red, nitrogen atoms in blue and sulphur in orange. Figure adapted from [19].*

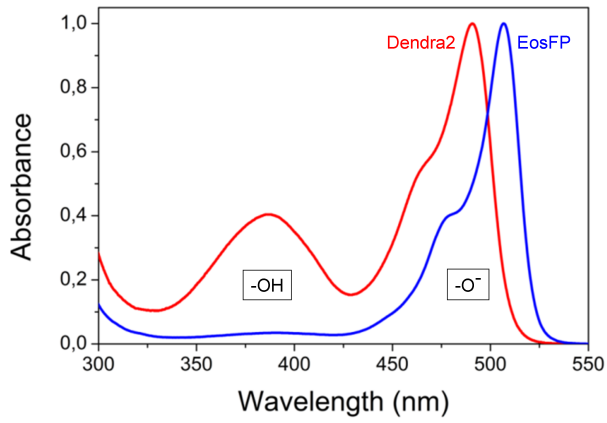

Figure 5.3: *Absorption spectrum of EosFP and Dendra2 (by courtesy of V. Adam).*

5.2 Making mEosFP photoswitchable

For most, if not all biological applications, monomeric FPs are better suited than their oligomeric variants. A double mutant of EosFP (V123T/T158H) proved to be monomeric and was therefore named mEosFP [53]. The structure of mEosFP is essentially identical to that of EosFP (Virgile Adam, personal communication). It should therefore be straightforward to make mEosFP photoswitchable: mutating Phe173 towards Ser, as was done to turn EosFP to IrisFP, should be sufficient to yield a monomeric variant of IrisFP, having both photoconversion and reversible photoswitching properties.

5.3 Dendra2 has a high photoconversion yield

Dendra is a monomerized form of DendGFP, a oligomeric PCFP derived from *Dendronephtya sp.* (see Figure 2.1) [30]. An additional mutation (V226A), increasing fluorescence brightness and maturation rate, transformed Dendra to the commercially available Dendra2 (Evrogen, Moscow, Russia). This protein is very similar to (m)EosFP, but has the advantage of maturating efficiently at 37 °C, as opposed to mEosFP, that does not fold and/or mature well above 30 °C. Moreover, the photoconversion quantum yield is much higher in Dendra2.

This last observation is most interesting when one wants to get insights into the structural basis of the photoconversion mechanism. In (m)EosFP, the Arg66 side chain N_η is in immediate contact (2,9Å) with the chromophore imidazolinone carbonyl group (see Figure 5.4). This interaction stabilizes increased electron densities located at the imidazolinone group, realized in the light- or pH-induced anionic form of the chromophore. The Arg66 residue in Dendra2,

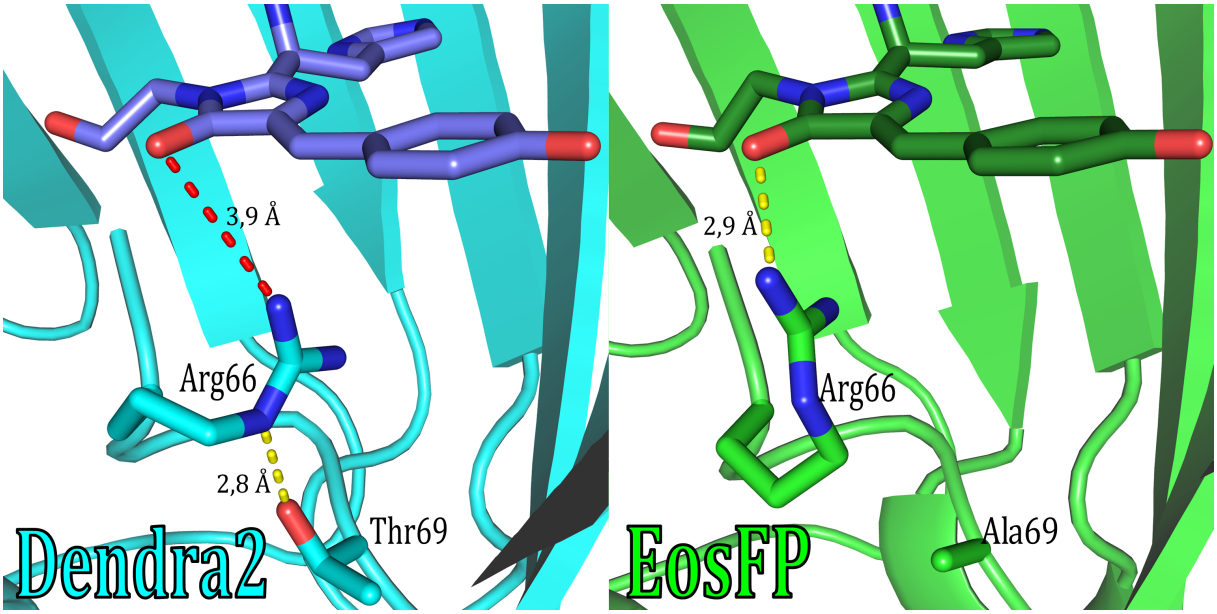

Figure 5.4: *Structural evidence for the observed difference in photoconversion efficiency in Dendra2 (cyan, PDB accession code: 1VZX) and EosFP (green, PDB accession code: 1ZUX). Oxygen atoms are represented in red and nitrogen atoms in blue.*

however, is pulled away from the chromophore by Thr69, that forms a hydrogen bond with its hydroxyl group to the N_ϵ of Arg66 (2,8Å). In (m)EosFP, this is not the case, as the latter has an alanine at position 69 that cannot interact with Arg66. As a result, the negative charge is more localized on the hydroxybenzylidene moiety, increasing its pKa and making it more prone to protonation. At a given pH, the protonated fraction of Dendra2 is thus bigger than in (m)EosFP, immediately giving an explanation for the much bigger 390 nm absorption peak of Dendra2 (see Figure 5.3) [31].

5.4 Making Dendra2 photoswitchable

Dendra2 is very similar to mEosFP in structure, but has some major advantages (see Section 5.3). It would thus be interesting to try to mutate Dendra2 to an Iris-like FP—that is, both photoconvertible and reversibly photoswitchable. To do this, the Phe173 residue in Dendra2 will, in analogy to the mutation that made IrisFP from EosFP, be mutated towards a serine.

5.5 Direct and indirect mutations towards photoswitching

As has been explained in Section 5.1, the mutation introducing the photoswitching ability in IrisFP makes use of a mechanism that is caused by a coordinated event involving at least two residues. The first one is of course Phe173, that is mutated to a serine residue. The second one is the Met159 residue which is, compared to EosFP, flipped upwards in IrisFP.

We will investigate whether it is possible to make photoconverting proteins photoswitchable by influencing the interaction between the fluorophore and its environment in another way compared to the EosFP-to-IrisFP-mutation. That is, instead of the F173S mutation that allows the upward flip of the Met159 residue, the methionine can be truncated by mutating it towards a small apolar residue, say alanine. This mutant is suspected to show similar behavior as IrisFP, as both would allow a water molecule to be introduced and serve as an alternative partner for Ser142. In other words, we expect that both the Dendra2_M159A and the mEosFP_M159A mutation will introduce photoswitching abilities in Dendra2 and mEosFP respectively.

As has been described in Subsection 3.2.3, to achieve the best results in PALM microscopy, one needs a fluorophore that switches on very fast, while the off-switching is rather slow [23]. In structural terms, this would mean a stabilization of the chromophore in its on-state, while having a rather unstable off-state. We thus have to create a FP that can switch, but in which this off-state is not favorable. The M159A mutants of both Dendra2 and mEosFP are expected to behave in such a way, as the trans conformation of the chromophore would be hindered by the Phe173. The rationale for this can be found in Figure 5.2. When Met159 is mutated towards an alanine residue, the W2188 is suspected to slip in, but not the W2166. In other words, the anionic hydroxyphenyl moiety of the chromophore will most probably find itself in a relatively hydrophobic region, thanks to the phenyl moiety of Phe173. Compared to the IrisFP case, where W2166 can stabilize the photoswitched conformation, this would no longer be true for the M159A photoswitched form.

But what about something intermediate then? Imagine a Dendra2 or mEosFP mutant that does not only bear the M159A mutation, but has also been mutated at the 173 position. Most obvious is of course the F173S mutation, but as this would create a rather big water-filled cavity, it seems unlikely that this double mutant will show intermediate switching behavior. A better option is mutating Phe173 toward a leucine. Leucine has a side chain that is not bulky, but not small either, thus enabling photoswitching. Moreover, it is hydrophobic, thus preventing

stabilization of the trans state. We will construct Dendra2_M159A_F173L to check whether this mutant is indeed a RSFP with switching properties intermediate between Dendra2_M159A and Dendra2_F173S.

CHAPTER 6

Making Dronpa photoconvertible

6.1 Dronpa is a photoswitcher

Dronpa is a monomeric RSFP, derived from the non-photoswitchable tetrameric protein 22G, that was isolated from an anthozoan Echinophillia species (see Figure 2.1). Two mechanisms have been proposed for this switching. Briefly, the first mechanism proposes that during photoswitching, cis-trans isomerization of the chromophore is the crucial event. Next to that, an equilibrium between a fluorescent anionic and a non-fluorescent neutral form exists in the cis state [54]. However, more and more evidence points towards a different mechanism. Doing both ensemble and single-molecule spectroscopy on Dronpa, S. Habuchi *et al.* proposed a detailed model for photoswitching. In this model, a light-induced protonation is the key to the off-switching mechanism [21]. This mechanism has been confirmed by femtosecond transient absorption spectroscopy [55].

Structural data supporting this mechanism was provided by H. Mizuno *et al.* using NMR spectroscopy [50]. They discovered that upon switching, the hydrogen bond that links Ser142 to the hydroxyphenyl moiety is disrupted, coupled to an increase in local flexibility of the β-barrel close to this residue. This immediately explains why 22G, the tetrameric mother protein, is not photoswitchable: the flexible region is held more rigid due to interactions between the

monomers in the tetramer. The flexibility of the chromophore in the trans state is also high. These observations confirm that in Dronpa, the rigidity of the chromophore is at least as important to fluorescence quantum yield than its cis-trans conformation. Yet another interesting piece of information that supports this mechanism comes from A. R. Faro *et al.* [51]. At a temperature of 100K, large structural rearrangements like cis-trans isomerization of the chromophore are not possible, but they proved that the spectroscopic signatures of reversible photoswitching are still possible. This all tends to show that photoinduced protonation is crucial for photoswitching and that the cis-trans isomerization process would be a secondary process.

6.2 What photoconverters have in common

There has been a lot of doubt about the mechanism of photoconversion. In 2003, Mizuno *et al.* proposed a mechanism of Kaede photoconversion involving a biprotonated His62 as a key residue for the β-elimination [32]. They were followed by Nienhaus *et al.* who, in 2005, proposed a mechanism on EosFP, also involving a biprotonated His62 [56]. In 2007, Hayashi *et al.* proposed yet another mechanism on Kaede photoconversion, again involving a biprotonated His62 as a key residue [57]. However, recent quantum chemical/molecular mechanical (QC/MM) calculations on EosFP by Lelimousin *et al.* [58] have shown that the probability of these mechanisms is very low, based on the energy profiles of the different intermediate states. Their calculations pointed towards a mechanism involving two intersystem crossings and a deprotonation of the His62 side chain, being reprotonated at the very end of the photoconversion.

Regardless of the mechanism, even regardless of which PCFP that is studied, the His62 residue, being part of the red species chromophore (see Figure 3.2), plays a crucial role in photoconversion. It is therefore not surprising that in all PCFPs known (Kaede, KikGR, EosFP, Dendra2...), the His62 residue is present. All PCFPs thus contain a His-Tyr-Gly chromophore.

6.3 Making Dronpa photoconvertible

As described above, His62 seems to play a crucial role in PCFPs. It is therefore straightforward, in order to engineer a photoconvertible variant of Dronpa, to think of mutating the Cys residue at position 62 towards a His residue. The resulting protein will be evaluated for photoconversion

properties. Of course, care has to be taken to also check whether the protein kept its initial photoswitching capabilities after the C62H mutation.

CHAPTER 7

Engineering photosensitizing properties in eGFP

The possible uses of genetically encoded photosensitizers as means of achieving spatio-temporal knockdown of proteins in the living cell or as photosensitizers in PDT have been discussed in Subsection 3.2.2. One of the major advantages of these applications is the spatio-temporal control of photosensitizer activity. Switching on or off light can be considered as immediate, and so would thus be the toxic effect of the photosensitizing molecule. Spatial control, on its part, can be achieved by careful focussing of the light beam. However, for all biological application, a small excitation volume is required, that is also controlled in size in the z-direction (the direction of the light path). This is extremely useful for targeting internal organs without damaging outer layers of tissue. Such focussing can be achieved by using two-photon excitation.

As discussed in Subsection 3.2.2, KillerRed seems at first sight a candidate to use in PDT. However, as the excitation of KillerRed peaks at 584 nm, two-photon excitation would require wavelengths in the 1200 nm range, which is out of the spectral window provided by the widespread Ti:sapphire lasers. It would be more convenient to have a genetically encoded photosensitizer that is two-photon excitable below 1000 nm. Therefore, we will try to engineer photosensitizing properties in eGFP.

As has been described in Subsection 3.2.2, two major structural elements have been proposed as being crucial for ROS-production in the photosensitizer KillerRed. The first is a water-filled channel spanning from the chromophore all the way to the bulk solvent. A sec-

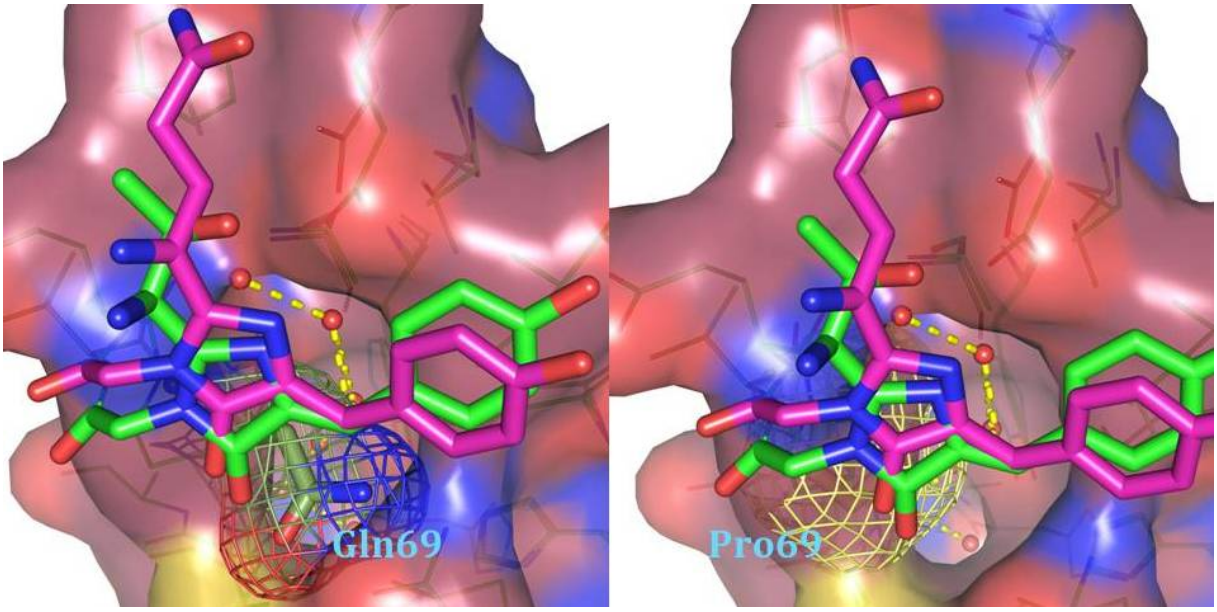

Figure 7.1: *Left: Water-filled channel (red spheres are water molecules, yellow dots are interactions between the water molecules) in KillerRed (red with pink chromophore). The tunnel is clearly visible, extending to the back of the picture. The opening linking the tunnel with the bulk solvent is not visible. From the superposed eGFP structure (dark green with light green chromophore), it is clear that the tunnel is only obstructed by a glutamine residue at position 69 (dark green with mesh). Right: Mutating glutamine 69 in eGFP to a proline residue (pale yellow) would allow the formation of a water-filled tunnel. PDB accession codes: KillerRed, 2WIQ; eGFP, 1EMA. Oxygen atoms are represented in red and nitrogen atoms in blue.*

ond feature is the existence of a negatively charged residue (Glu68 in KillerRed) in the mostly hydrophobic environment of the chromophore, a residue that is thus highly reactive [42].

The first mutation concerns the glutamine residue at position 69 in eGFP. As seen in Figure 7.1, this residue is located right where the water tunnel in KillerRed is located. At this particular position, KillerRed has a proline. This is an interesting residue, as its particular shape rigidly controls backbone conformation. In the visualization software, we can easily replace this Gln69 by a proline to have a very concise idea about the result of such Q69P mutation (Figure 7.1). Indeed, we now clearly see a channel appearing, analogous to the observations in KillerRed.

Secondly, eGFP does not have a charged residue in the hydrophobic pocket around the chromophore as KillerRed does. At the equivalent position of this glutamic acid in KillerRed, we find a hydrophobic valine in eGFP (see Figure 7.2). Making the analogy of what is true in KillerRed, the V68Q mutation is thus suspected to infer local energy instability and high

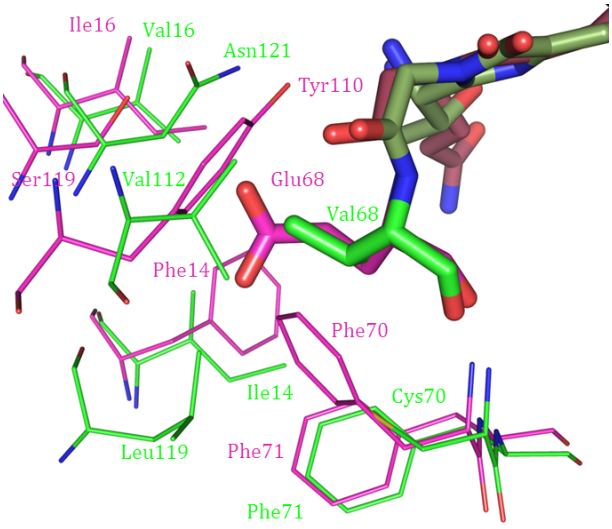

Figure 7.2: *Superposition of the KillerRed (pink with dark red chromophore) and eGFP (green with dark green chromophore) pocket surrounding Glu68 (KillerRed) and Val68 (eGFP). Oxygen atoms are represented in red and nitrogen atoms in blue.*

reactivity to the eGFP mutant.

To conclude, the eGFP_V68E_Q69P mutant will be made. It is suspected to have photosensitizing properties that will be tested. In these measurements, the non-mutated eGFP will serve as a negative control and KillerRed will be used as a positive control.

Part C

Materials and Methods

CHAPTER 8

General

8.1 Buffers

LB broth: 10,00 g tryptone, 5,00 g yeast extract, 10,00 g NaCl and distilled water for a total volume of 1 l. Medium was autoclaved at 121 °C before using.

LBA broth: LB broth with 100 mg/l of ampicillin added after autoclaving and cooling down to <50 °C.

SOC broth: 20,00 g tryptone, 5,00 g yeast extract, 0,583 g NaCl, 0,186 g KCl, 0,952 g $MgCl_2$, 1,204 g $MgSO_4$, 3,603 g glucose and distilled water for a total volume of 1 l. Medium was autoclaved at 121 °C before using. SOC broth = super optimal broth with catabolite repressor.

PBS buffer: 8,00 g NaCl, 0,20 g KCl, 1,44 g Na_2HPO_4, 0,24 g KH_2PO_4 and distilled water for a total volume of 1 l. The pH was adjusted to 7,4 with HCl or NaOH. The buffer was autoclaved at 121 °C before using.

TN buffer: 12,11 g Tris base, 17,53 g NaCl and distilled water for a total volume of 1 l. The pH was adjusted to 7,4 with HCl. The buffer was autoclaved at 121 °C before using.

8.2 Software

All figures of molecular models were made with the PyMOL software (The PyMOL Molecular Graphics System, Version 1.2r1, Schrdinger, LLC). Data analysis was done using OriginPro 7 (OriginLab, Northampton, MA) or Igor Pro version 6.1.0.0 (WaveMetrics, Portland, OR). Typesetting was done in LaTeX.

CHAPTER 9

Molecular biology

9.1 Transformation protocol

An aliquot of cells that were made competent using the Inoué protocol (as described in [59]) and stored at $-80\,^{\circ}$C were thawed on ice. Next, 0,5 µl of plasmid DNA ($\pm$200 µM) was mixed with 5 µl of these thawed competent cells and kept on ice for about 15 minutes. The cells were then put in a 42 °C water bath for 45 seconds, after which they were stored on ice for another 2 minutes. Subsequently, 100 µl of SOC broth was added and the bacterial suspension was put in a 37 °C incubator, shaking the tubes at 200 rpm (rotations per minute) for 20 minutes. The cells were then plated on LBA plates and incubated at 37 °C for one night.

9.2 Cloning protocol

All fluorescent protein cDNA sequences were cloned into a pRSet vector (Invitrogen, Merelbeke, Belgium). This was done using a polymerase chain reaction (PCR) with appropriate primers (Invitrogen). The forward primers contain a BamHI restriction site (**G**|**GATCC**), except for the Dronpa forward primer, that contains a KpnI restriction site (**GGTAC**|**C**). All reverse primers contain an EcoRI restriction site (**G**|**AATTC**) immediately upstream of a stop codon (*TAA*, except for KillerRed, that contains a *TGA* stop codon). All cloning primers are listed in

Primer name	Primer sequence
eGFP forward	5′ CGC**GGATCC**GATGGTGAGCAAGGGCGAGGAGC 3′
eGFP reverse	5′ CCG**GAATTC***TTA*CTTGTACAGCTCGTCCATGCCG 3′
mEosFP forward	5′ CGC**GGATCC**GATGAGTGCGATTAAGCCAGACATG 3′
mEosFP reverse	5′ CCG**GAATTC***TTA*TCGTCTGGCATTGTCAGGC 3′
IrisFP forward	same as mEosFP forward
IrisFP reverse	same as mEosFP reverse
Dendra2 forward	5′ CGC**GGATCC**GATGAACACCCCGGGAATTAACC 3′
Dendra2 reverse	5′ CCG**GAATTC***TTA*CCACACCTGGCTGGGCAG 3′
Dronpa forward	5′ GC**GGTACC**ATGAGTGTGATTAAACCAGAC 3′
Dronpa reverse	5′ CCG**GAATTC***TTA*CTTGGCCTGCCTCG 3′
KillerRed forward	5′ GGC**GGATCC**GATGGGTTCAGAGGGCGGC 3′
KillerRed reverse	5′ GGC**GAATTC***TCA*ATCCTCGTCGCTACCG 3′

Table 9.1: *Primers used for cloning FP sequences in pRSet. The forward primers contain a BamHI restriction site (*G|**GATCC***), except for the Dronpa forward primer, that contains a KpnI restriction site (***GGTAC**|**C***). All reverse primers contain an EcoRI restriction site (*G|**AATTC***) immediately upstream of a stop codon (*TAA*, except for KillerRed, that contains a* TGA *stop codon).*

Table 9.1, the PCR mixture and the temperature and time setup can be found in Table 9.2. The resulting PCR product was put on a 1,6 % agarose gel, the band containing the ±700 bp insert was cut out and purified using the QIAquick gel extraction kit (Qiagen).

Next, a double digest was done both on the empty vector and the insert, using Fermentas EcoRI and BamHI restriction enzymes in a 2× Tango buffer and incubating for 1 h at 37 °C. Enzymes were removed by 1,6 % agarose gel electrophoresis and the QIAquick gel extraction kit (Qiagen). Cut plasmid and cut insert were mixed with T4 DNA ligase (Fermentas) and incubated for 1 h at room temperature. The vector with insert was then transformed into JM109/DE3 cells (Promega) and plated out on a LBA agar plate. These plates were visually screened for fluorescent colonies using a transilluminator. These were then grown, miniprepped and sequenced.

Ingredient	amount (µl)	T (°C)	t (sec)	
forward primer (10 µM)	1	94	45	
reverse primer (10 µM)	1	94	45	
dNTPs (10 mM)	1	55	45	25×
Template (± 200 nM)	0,5	72	60	
10× Pfu buffer (+ Mg^{2+})	5	4	∞	
Pfu polymerase	1			
ultrapure water	40,5			

Table 9.2: *PCR mixture and settings for cloning of fluorescent protein cDNA.*

9.3 Site-directed mutagenesis

Site-directed mutagenesis was done using an optimized QuickChange protocol. Primers containing the desired mutation were designed and ordered (Invitrogen). A list of mutation primers can be found in Table 9.3. First, the mutation primer was phosphorylated by incubating the mixture described in Table 9.4 for 30 min at 37 °C. The mutated template strand was made by PCR (see Table 9.5). The original DNA strand was then degradated by adding a restriction enzyme that specifically cuts methylated DNA (DpnI) and incubating for 30 min at 37 °C. Next, the complementary strand was synthesized by PCR (see Table 9.6). The PCR product was transformed into JM109/DE3 cells, plated out and grown on LB agar plates supplied with ampicillin. Some colonies were inoculated at 37 °C overnight in 1,5 ml of LBA broth (composition see Section 8.1). Plasmid DNA was extracted using the GenElute HP Plasmid Miniprep kit (Sigma-Aldrich) and sequenced.

9.4 Protein purification

After transformation (protocol see Section 9.1), a single colony was inoculated in 1 ml LBA broth and kept at 37 °C for 4-6 h. This pre-culture was then poured into a flask containing 400 ml of LBA medium and kept at 37 °C overnight. In the morning, isopropyl β-D-1-thiogalactopyranoside (IPTG) was added to a concentration of 100 µM and kept for 24 h on 37 °C.

Mutation	Mutation primer
Dendra2_M159A	5′ GCAACATCAAC**GC**GGCCCTGC 3′
Dendra2_F173S	5′ CTGTGCGACT**C**CAAGACCACC 3′
Dendra2_F173L	5′ CTGTGCGACTT**G**AAGACCACC 3′
mEosFP_M159A	5′ GGTGATATTCAC**GC**GGCTTTGTTGC 3′
mEosFP_F173S	5′ CCGATGTGACT**CC**AGAACTACTTAC 3′
Dronpa_C62H	5′ GTGTTC**CA**TTACGGCAACAGG 3′
eGFP_V68E_Q69P	5′ CCTACGGCG**A**GC**C**GTGCTTCAGC 3′

Table 9.3: *Primers used for site-directed mutagenesis. Mismatches with the template are indicated in* ***bold****.*

Product	amount (µl)
Primer (100 M)	5
10x T4 PNK buffer	5
ATP (10 mM)	5
T4 PNK	1
ultrapure water	34

Table 9.4: *Mixture used for phosphorylating mutation primers.*

Ingredient	amount (µl)	T (°C)	t (sec)	
Template (± 200 nM)	1	65	300	
5' phosphorylated primer (10 µM)	1	96	30	
10× Pfu buffer	1	96	30	
10× Taq ligase buffer	1	55	60	25×
dNTPs (2,5 mM)	1,5	65	480	
Pfu polymerase	0,5	72	600	
Taq ligase	0,5	4	∞	
ultrapure water	13,5			

Table 9.5: *PCR mixture and settings for making a mutated template strand in the modified QuickChange protocol.*

Ingredient	amount (µl)	T (°C)	t (sec)	
Mixture from Table 9.5		65	300	
T7 primer (10 µM)	0,2	96	30	
dNTPs (2,5 mM)	1	96	30	
Pfu polymerase	0,2	55	60	2×
		68	900	
		72	600	
		4	∞	

Table 9.6: *PCR mixture and settings for complementary strand synthesis in the modified QuickChange protocol.*

After these 24 h, the culture looks brightly yellow-green and fluoresces. The bacterial suspension was then centrifuged for 15 minutes at 5000 rpm at 4 °C (Sorvall Evolution RC with SLA-1500 rotor). The pellet was resuspended in phosphate buffered saline (PBS buffer (composition see Section 8.1)) supplied with protease inhibitor (cOmplete Mini, Roche, 1 tablet / 10 ml) and lysozyme (1 mg/ml). The suspension was then frozen at −20 °C for one night, and thawed at room temperature the next morning, resulting in a slimy solution. This was then sonicated (Branson 102C sonifier tip connected to a Branson sonifier 450) using 12-second bursts, cooling the solution on ice between two bursts until the solution was no longer slimy. The sonicated solution was subsequently centrifuged at 8000 rpm for 10 minutes at 4 °C. The pellet appeared mostly non-fluorescent, while the supernatant was brightly colored.

The crude FP solution was then purified using metal affinity beads (Ni^{2+}-nitrilotriacetic acid (Ni-NTA) agarose resin) (Qiagen). Therefor, a small column (Pierce 29922 disposable 5 ml polypropylene column) was packed with 5 ml of Ni-NTA resin. The column was linked to a peristaltic pump (Pharmacia Peristaltic pump P-1). First, the column was equilibrated with 30 ml Tris-NaCl (TN) buffer (composition see Section 8.1) at a flowrate of 350 ml/h. Next, the crude FP solution was applied to the column at a slower flowrate of 25 ml/h. The column was then rinsed with 50 ml of TN buffer containing 5 mM imidazole to discard weakly bound proteins and impurities. Elution and fraction collection were done without peristaltic pump using TN buffer containing 200 mM imidazole.

The column was recharged using the peristaltic pump system at a flowrate of 350 ml/h by

first rinsing it with 50 ml of ultrapure water (Milli-Q, Millipore), followed by 50 ml of a 50 mM EDTA solution at pH 7,4. Then 50 ml of a 0,5 M NaOH solution was applied, followed by 50 ml of Milli-Q water. Next, a 5 mg/ml $NiCl_2 \cdot 6\,H_2O$ solution was pumped through (at a flowrate of 25 ml/h) and finally rinsed with 50 ml of ultrapure water. To prevent bacterial growth inside the column, the column was equilibrated with 20 % ethanol in ultrapure water for storage at 4 °C.

FP-containing fractions were subsequently purified using a fast protein liquid chromatography (FPLC) system equipped with fraction collector (ÄKTA Purifier with Frac-920, GE Healthcare, Diegem, Belgium). For FP purifications, a gel filtration column (HiLoad 16/60 Superdex 75pg, GE Healthcare, Diegem, Belgium) was used. After equilibrating the column with TN buffer, 1 ml of sample solution was injected. The column was ran at a set speed of 0,7 ml/min. UV absorption at 280 nm was followed. System parameters were set to collect fractions of 0,7 ml whenever this absorption exceeded 15 mAU. All fractions were visually inspected for fluorescence and fluorescent peaks were pooled for concentration and—if necessary—buffer exchange using a Vivaspin column (Vivaspin 15, 10 000 MWCO, Sartorius Stedim). The purity of the samples was checked by sodium dodecyl sulfate polyacrylamide gel electrophoresis (SDS-PAGE).

CHAPTER 10

Spectrometry and photochemistry

10.1 Spectroscopic characterization

10.1.1 Absorption spectra, fluorescence spectra and fluorescence landscapes

Absorption spectra were measured with a Shimadzu UV-1650PC spectrophotometer (Shimadzu GmbH, Duisburg, Germany). Excitation and emission spectra were taken with a PTI QuantaMaster fluorometer (Photon Technologies International, West Sussex, UK). Both for excitation and emission spectra, the excitation and emission monochromator slit was set to 1 mm.

For fluorescence landscapes, the fluorimeter was configured to measure emission spectra from X to 650 nm with excitation at X nm and in steps of 1 nm. This X was increased from 260 nm to 650 nm in steps of 5 nm. The data was then loaded into and processed with IgorPro.

10.1.2 Quantum yield calculations

Fluorescence quantum yields were measured by comparing the fluorophore to standards with known fluorescence quantum yields. For every sample, a dilution series was made, with an absorbance below 0,1 to avoid the inner filter effect. For every concentration, an emission

spectrum was taken and the integrated intensity was calculated. Having this data, it is possible to calculate the quantum yield using Formula (10.1) in which Q is the quantum yield, I is the integrated emission intensity, OD is the optical density and n is the refractive index. For all parameters, the subscript R refers to the value of the reference fluorophore. In fact, to maximize correctness and integrate the data measured for every dilution, the integrated emission intensity was plotted against the optical density of the sample at the excitation wavelength. These data points were fitted with a straight line going through the origin, and the slope of the curve was called m. This way, quantum yields can be calculated using Formula (10.2).

$$Q = Q_R \cdot \frac{I}{I_R} \cdot \frac{OD_R}{OD} \cdot \frac{n^2}{n_R^2} \tag{10.1}$$

$$Q = Q_R \cdot \frac{m}{m_R} \cdot \frac{n^2}{n_R^2} \tag{10.2}$$

10.1.3 Extinction coefficient measurement using pH-induced unfolding

In fully denatured conditions, the absorption of any FP that bears a chromophore consisting of a dehydrotyrosine residue linked to an imidazolone group is essentially the same, both in terms of maximum absorption wavelength (447 nm) as in exctinction coefficient (44000 $M^{-1} \cdot cm^{-1}$), as the molecular species that gives rise to this absorption is the same for any of these proteins. This observation immediately provides an accurate way of determining the exctinction coefficient of any FP that bears this particular chromophore. By increasing the pH using NaOH while measuring absorption spectra, it is possible to quantify the absorption at 447 nm of the fully denatured protein. Knowing that this absorption corresponds to an exctinction coefficient of 44000 $M^{-1} \cdot cm^{-1}$, it is possible to calculate back the extinction coefficient at any absorption peak at any pH.

10.2 Photoactivation

A setup fully dedicated to monitoring photoactivation behavior at the ensemble level was made. A schematic representation can be found in Figure 10.1. A cuvette (109.004-QS, Hellma, Kruibeke, Belgium) with FP solution was placed in a cuvette holder (CUV-UV, Ocean Optics, Duiven, Netherlands) that was connected by optical fibers (QP600-1-SR-BX, Ocean Op-

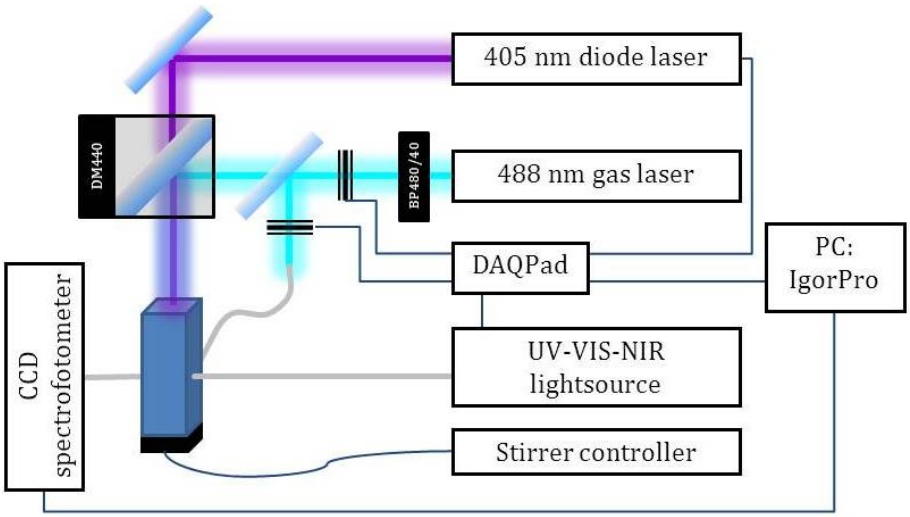

Figure 10.1: *Setup for analysis of photoactivation in fluorescent proteins.*

tics, Duiven, Netherlands) on the one side to a UV-VIS-NIR light source (DT-MINI-2-GS, Ocean Optics, Duiven, Netherlands) and on the other side to a miniature fiber optic spectrometer equipped with a 3648-element linear CCD-array (USB4000-UV-VIS, Ocean Optics, Duiven, Netherlands). Underneath the cuvette, a miniature stirrer (MINI 20, Sterico, Wangen, Switzerland) was placed. The cuvette could be illuminated from above with a 405 nm diode laser (CUBE, Coherent, Santa Clara, CA) and a 488 nm argon-ion laser (163 Series Argon-ion, Spectra Physics, Irvine, CA). The 488 nm laser light was filtered by a 480/40 bandpass filter and was then coaxially combined with the 405 nm light using a 440 nm dichroic mirror. Part of this 488 nm light was sent into an optical fibre that was connected to the cuvette holder, the 488 nm light beam being perpendicular to the UV-VIS-NIR light path. The 488 nm laser path striking the cuvette from above and from the side were both interrupted by an external shutter (SH05 Beam Shutter, Thorlabs, Dachau/Munich, Germany), the 405 nm diode laser and the UV-VIS-NIR light source are equipped with an internal shutter. All shutters were controlled by a data acquisition interface (DAQPad-6020E, National Instruments) that on its way was controlled by an Igor procedure developed in-house, also acquiring the CCD-array data.

10.3 Photoswitching

Photoswitching properties can be assessed by doing so-called “sharkfin” measurements, named after the particular shape of the plots. Such experiment consists of measuring fluorescence dur-

ing constant excitation of the fluorophore at the anionic peak maximum absorption wavelength. In our case, this was, depending on the excitation spectrum of the protein, 473 nm or 488 nm light. Superposed on this excitation light, a second light beam, with the wavelength that stimulates back-switching of the fluorophore to the on-state (here 405 nm), was repeatedly switched on and off. As a result, we can observe off-switching (473 nm / 488 nm alone) followed by back-switching (473 nm / 488 nm and 405 nm) that can both be fitted with an exponential function.

10.3.1 Photoswitching measurements

Photoswitching in absorption mode

Photoswitching properties were measured by two means. The first technique was done in solution using the setup described in Section 10.2. The sample was diluted until the maximum absorption was approximately 0,3. This dilution gave the best tradeoff in terms of avoiding too much inner filter effect on the one hand and noisy spectra on the other hand. In a first phase, the protein was switched off by illuminating 60 times 7,5 seconds with 488 nm light (2 W/cm^2). In a second phase, the 405 nm laser light (23 mW/cm^2) was also switched on for 20 times 7,5 seconds, thus switching on the proteins. The third phase consisted of exactly the same settings as the first, and the fourth was identical to the second. In the fifth and last phase, the 405 nm light was switched back off and so did the proteins, this time for 120 times 7,5 seconds. Using a self-written IgorPro procedure, these two sharkfins were fitted with a mono-exponential model.

Photoswitching in fluorescence mode

The second technique measures fluorescence on a microscope. Samples were prepared as follows. An aliquot of the FP solution was mixed with 50 µl of NiNTA beads and incubated for 15 minutes at room temperature. After short centrifugation at low speed ($<$ 3500 rpm), the supernatant was removed and an equal amount of ultrapure water was applied. After gentle mixing, the suspension was centrifugated once more and the supernatant removed. Again, an equal amount of ultrapure water was added and after gentle mixing, 20 µl of the slightly green-looking suspension was sandwiched between two 22 $\times$ 22 mm coverslip glasses (Knittel Gläser). The sides were sealed with silica grease to prevent solvent evaporation.

The samples were mounted on an inverted microscope (IX-70, Olympus, Tokyo, Japan) equipped with a scanning stage (Physik Instrumente, Karlsruhe/Palmbach, Germany). A continuous-wave (CW) Ar-Kr ion laser (Stabilite 2018-RM, Spectra Physics, Irvine, CA) produced 488 nm / 473 nm light that passed through a 480/40 bandpass filter and was then circularly polarized using a $\lambda/4$ phase plate combination for optimal excitation of all proteins in the illuminated area. A CW diode laser (Compass 405-25, Coherent, Santa Clara, CA) produced 405 nm light that analogously passed a 410/36 bandpass filter followed by a Berek's variable wave plate (Model 5540, New Focus, Santa Clara, CA), making it circularly polarized. Both beams were coaxially combined using a DM495 dichroic mirror. A dispersive lens ($f = 400$ mm) at the back aperture of the microscope ensured wide-field illumination by an oil immersion objective lens (100×, NA 1,3, Olympus). The excitation light plane was set to excite the bottom of a fluorescent-protein-coated bead. Fluorescence was collected by the same objective, passed through a 450 nm longpass filter, a 500 nm longpass filter, a 530/60 bandpass filter and finally detected by an avalanche photodiode (APD) (SPCM-AQR-14, Perkin-Elmer, Waltham, MA). Fluorescence was registered by a time-correlated single photon counting (TCSPT) card (SPC 630, Becker & Hickl, Berlin, Germany) using the first-in, first-out (FIFO) mode. All experiments were performed at room temperature. A schematic representation of this setup can be found in Figure 10.2.

To measure the extent and speed of photoswitching, and to make it comparable for all FPs, an identical illumination scheme was followed for all samples. The 488 nm / 473 nm laser light was attenuated to an intensity of 81,2 mW/cm^2, the 405 nm laser light objective intensity was 3,8 mW/cm^2. Extra neutral density filters were put in front of the APD, thus bringing the countrate between 5 000 and 20 000 counts per second. The data recording started with 10 seconds of measuring the APD dark count. Then the 488 nm / 473 nm laser was switched on alone until the emission intensity had dropped to only 20 % of the initial value. At this point, the 405 nm laser was switched on for 30,5 seconds, followed by an off-period of 40 seconds. This on-off cycle was repeated 20 times. After the last cycle, the sample was illuminated with only 488 nm / 470 nm illumination for some extra minutes.

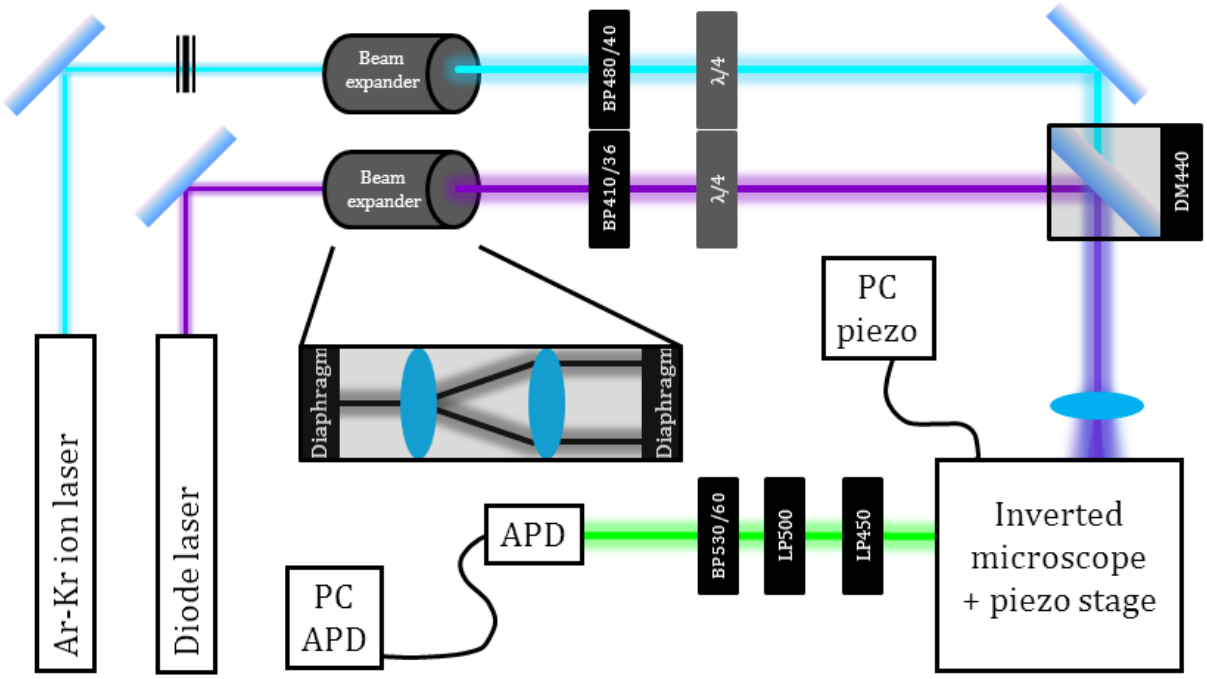

Figure 10.2: *Schematic representation of the setup used for sharkfin measurements. Cyan lines represent 488 nm laser light, purple lines indicate 405 nm laser light and the green line is the emitted light at about 500-515 nm.*

10.3.2 Analyzing the sharkfins

Sharkfin data analysis was done using IgorPro. A home-written FIFO analysis procedure was used to load in the data generated by the TC-SPT card. Analysis and fitting of the sharkfins with a mono- or bi-exponential model was done using a self-written IgorPro script.

10.3.3 Thermal recovery

Thermal recovery of the dark state was measured in absorption mode using the setup described in Section 10.2 and represented in Figure 10.1. First, the protein was switched off by 10 min illumination with 488 nm light (2 W/cm^2) and then left in the dark, recording a series of absorption spectra at regular timepoints. These regular timepoints are given in Table 10.1. After every time-lapse, a spectrum was recorded. From these spectrum series, the anionic absorption peak was plotted in time with $t = 0$ taken as the point where the off-switching 488 nm laser is stopped. The curve was then fitted by an exponential curve between $t = 0$ and $t = 3600$.

step number	number of spectra recorded	time-lapse between two recordings
1	12	10 sec
2	24	20 sec
3	20	30 sec
4	40	60 sec

Table 10.1: *Thermal recovery recording scheme.*

10.4 Photoconversion

In this work, photoconvertible fluorescent proteins have been photoconverted both in a preparative and analytical way.

10.4.1 Preparative photoconversion

Samples of photoconverted protein were prepared using a femtosecond laser setup as described in [60], producing 395 nm laser pulses of 200 fs (full width at half maximum (FWHM)). The power of the laser is over 800 μJ and was directed onto a 1 cm quartz cuvette. The protein solution was irradiated at room temperature for 24 hours while constantly stirring.

10.4.2 Analytical photoconversion

Photoconversion of Dendra2 and mEosFP mutants was followed using the dedicated setup described in Section 10.2. The sample was illuminated from the top with 405 nm light (0,6 W/cm^2) inside a small volume cuvette (105.251-QS, Hellma, Kruibeke, Belgium) without stirring. Absorption spectra were recorded every 2 minutes for 3 h.

10.5 Assessing photosensitizing properties

A bacterial aliquot was suspended in 2 ml PBS buffer and split in two samples. One sample was wrapped in aluminium foil to protect it from light. The other sample was irradiated for 30 min with white light from a xenon lamp that was passed through 20 cm of water to absorb infrared light, thus preventing direct damage to the cells and proteins. Directly afterwards, the

bacterial suspension was spread on a LBA plate and incubated at 37 °C overnight. The following morning, colonies were counted and expressed in colony forming units (cfu).

Part D

Results

CHAPTER 11

Results

11.1 Molecular biology

Several mutants were successfully made. The most interesting ones are: mEosFP_M159A, mEosFP_F173S[1], Dendra2_M159A, Dendra2_F173S, Dendra2_M159A_F173L, Dronpa_C62H and eGFP_V68E_Q69P. However, in all mEosFP mutants, an additional A69V mutation showed up. Tracing back this mutation, it turned out to be present in the original plasmid. Although it is located at a very interesting position (see Section 5.3), the mutation seems to have no profound effect on the properties of mEosFP and its mutants.

All proteins were purified in big quantities for spectroscopic characterization. They were also thoroughly purified to use for crystallization and structure determination.

[1] Also called monomeric IrisFP or mIrisFP because it is bears exactly the same mutation that made IrisFP out of the tetrameric EosFP

11.2 Spectroscopic characterization

11.2.1 Absorption

Dendra2 and mutants

Absorption spectra of Dendra2 and three mutants are shown in Figure 11.1. One interesting feature is the ±25 nm blue-shifted absorption peak of the mutants. Also remarkable is the strongly reduced absorption of the 380 nm peak in Dendra2_M159A and Dendra2_M159A_F173L while Dendra2_F173S is intermediate. We will come back to these results further on (Section 12.2). Note also the small absorption peak at ±315 nm, that we will assign in Subsection 11.2.2 to S_0–S_2 excitation.

Absorption spectra of mEosFP, two of its mutants and IrisFP (a mutant of the tetrameric EosFP) are shown in Figure 11.2. Here, we see that there is a again a ±25 nm blue-shift of the mutants compared to the wild-type mEosFP. Also, the FWHM of the deconvoluted highest-wavelength absorption peak is markedly broader for the mutants compared to the wild-type (mEosFP: ±18 nm, mEosFP_M159A: ±27 nm, mEosFP_F173S: ±32 nm and IrisFP: ±33 nm). This is probably due to more conformational freedom of the chromophore, as confirmed by the reduced quantum yield (see Table 11.2). This is less the case for Dendra2 and its mutants, probably because Dendra2 has a relatively big fraction of its chromophore in protonated and thus more flexible state (see Section 5.3).

There are no major differences in absorption spectrum between Dronpa and Dronpa_C62H, as can be seen from Figure 11.3. The exctinction coefficient of the mutant at ±505 nm seems to be higher, but this graph was only scaled to the 280 nm absorption peak. This finding should thus be confirmed.

11.2.2 Fluorescence

Green species excitation and emission spectra were taken and analyzed. Maximum excitation and emission wavelengths are mentioned in Table 11.1.

It is very hard to get a sample that contains the red species only. Therefore, fluorescence landscapes, rather than individual fluorescence spectra were acquired. Both the green and the partially photoconverted sample were recorded and scaled to their maximum emission signal of

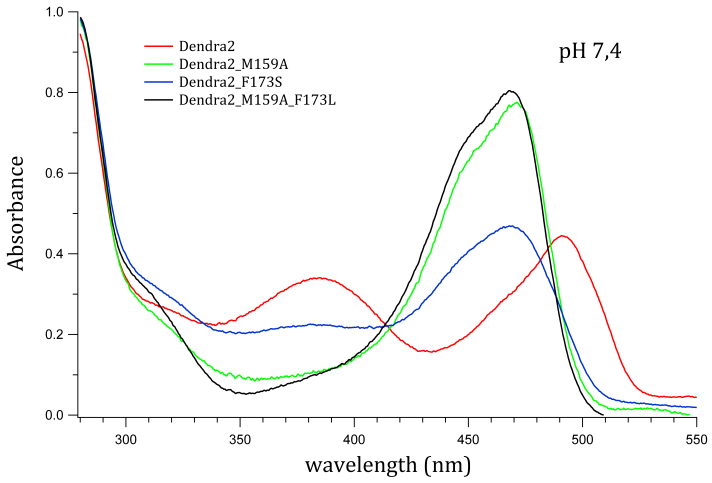

Figure 11.1: *Absorption spectra of Dendra2 (red) and three of its mutants: Dendra2_M159A (green), Dendra2_F173S (blue) and Dendra2_M159A_F173L (black). All spectra were taken at pH 7,4.*

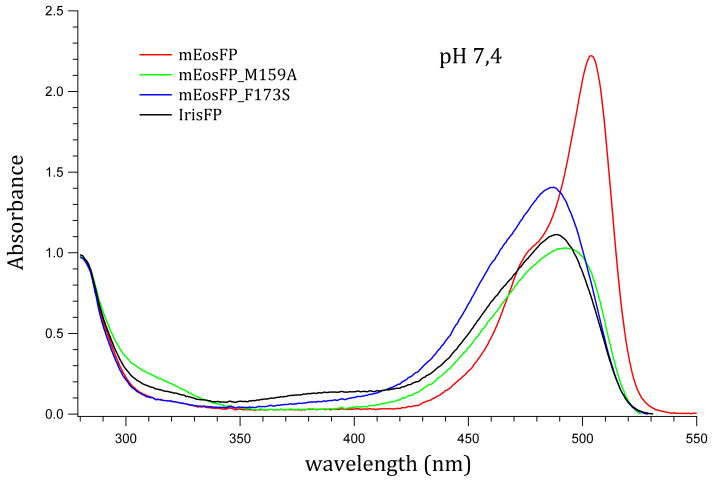

Figure 11.2: *Absorption spectra of mEosFP (red), two of its mutants: mEosFP_M159A (green) and mEosFP_F173S (blue) and IrisFP (black). All spectra were taken at pH 7,4.*

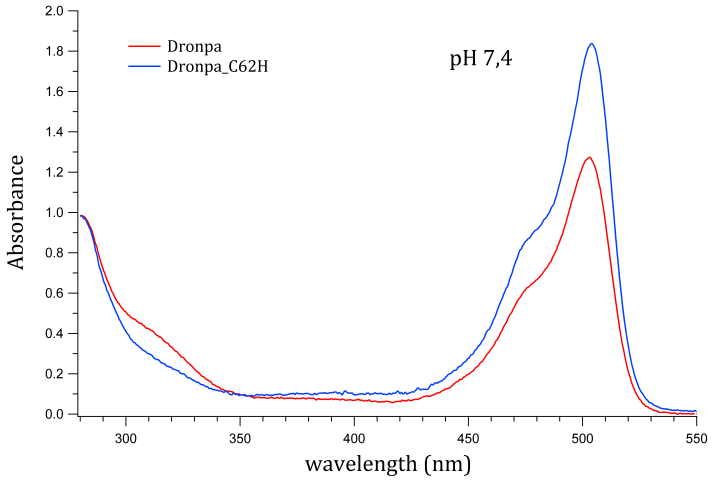

Figure 11.3: *Absorption spectra of Dronpa (red) and Dronpa_C62H (black). All spectra were taken at pH 7,4.*

	λem, max	λex, max
Dendra2	505nm	491nm
Dendra2_M159A	504nm	469nm
Dendra2_F173S	500nm	469nm
Dendra2_M159A_F173S	500nm	470nm
mEosFP	515nm	504nm
mEosFP_M159A	517nm	473nm
mEosFP_F173S	514nm	485nm
IrisFP	516nm	490nm
Dronpa	516nm	503nm
Dronpa_C62H	516nm	503nm

Table 11.1: *Maximum excitation and emission wavelengths for all mutants*

the green species. Subsequently, the green signal was subtracted from the partially photoconverted signal so that ultimately a dataset that only contains data on the red form of the protein was obtained. The colorscales of all landscapes is set to the darkest black for zero intensity and brightest white for the highest intensity peak.

Fluorescence landscapes were recorded for Dendra2, Dendra2_M159A, Dendra2_F173S and Dendra2_M159A_F173L, as shown in Figure 11.4. There are several things we can learn from these graphs. First of all, every intensity peak corresponds to a (local) excitation-emission maximum[2]. It should be noted that all peaks at $\langle 313, 387 \rangle$ correspond to the dim and broad fluorescent signal of imidazole, that was used during the purification to elute the proteins from the NiNTA resin. The diagonal line at $\langle \lambda, 2 \cdot \lambda \rangle$ is the second harmonic excitation light that is detected.

Dendra2 has the most complicated landscapes compared to the mutants, especially in its red form. In the green form of Dendra2, there is one major peak $\langle 505, 518 \rangle$, coming from the chromophore excitation and emission, together with a minor peak $\langle 280, 517 \rangle$ that comes from the excitation of aromatic residues in the protein that transfer their acquired energy to the chromophore. In the red state, the landscape gets much more complex. The major peak at $\langle 550,$

[2]We here introduce a notation for couples of local excitation and emission maxima. The expression $\langle P, Q \rangle$ should be read as a local excitation maximum of P nm with a corresponding local emission maximum of Q nm.

574⟩ bears a vibrational excitation shoulder at ⟨520, 574⟩. At lower excitation wavelengths, the neutral species of the red form becomes visible. Another prominent peak appears at ⟨320, 567⟩, which can be attributed to a S_0–S_2-transition after which a fast, non-radiative S_2–S_1 relaxation occurs and emission from the S_1 take place. For both the anionic and S_0–S_2 peaks, vibrational shoulders in the emission spectrum are visible[3].

As said, the mutants of Dendra2 have a much cleaner fluorescence landscape. In the green formDendra2_M159A, Dendra2_F173S and Dendra2_M159A_F173L all have a major ⟨470, 504⟩ fluorescence peak with a vibrational shoulder at ⟨460, 504⟩ in Dendra2_M159A and Dendra2_F173S being blue-shifted in excitation wavelength by 15-20 nm. The red form is much easier to interpret as compared to the red form of Dendra2. For all mutants, the prominent peak at ⟨530, 560⟩ with its vibrational shoulder at ⟨500, 560⟩ is apparent. Excitation due to S_0–S_2 transitions is, just like in Dendra2, present at ⟨320, 560⟩.

11.2.3 Quantum Yield

Quantum yield measurements were carried out as described in Subsection 10.1.2. Two different reference samples were used: fluorescein dissolved in 0,1 N NaOH and acridine yellow dissolved in methanol. The emission spectra were taken using excitation at 440 nm (for Dendra2_F173S, Dendra2_M159A and Dendra2_M159A_F173L plus acridin yellow as reference) and 470 nm (for Dendra2, mEosFP, mEosFP_M159A, mEosFP_F173S and IrisFP plus fluorescein as reference). Two plots of the integrated emission intensity (I) as a function of absorption maximum (OD) were made and the slope was calculated. This slope equals $\frac{\mathrm{I}}{\mathrm{OD}}$ and is known for the samples as well as for the references. As n (= 1,3330234), $\mathrm{n_R}$ (= 1,3299066) and $\mathrm{Q_R}$ is known ($\mathrm{Q_{fluorescein}} = 0,57$ and $\mathrm{Q_{acridin\ yellow}} = 0,90$), we can easily calculate the quantum yield. A cross-correlation between the two standards was made, in order to validate the procedure. The measured quantum yields were 0,59 and 0,86 respectively, being in a 5% error marge and thus validating the procedure.

However the method was validated by cross-referencing the two standards, there seems to be a rather big deviation of some of the values compared to the values in the literature. The

[3]It pops out that there are certain deviations from the wavelengths formulated here and apparent in Figure 11.4 compared to Table 11.1 and the literature. It is as of today not yet fully clear what causes these deviations, but an instrumental error of the fluorimeter is the most likely reason.

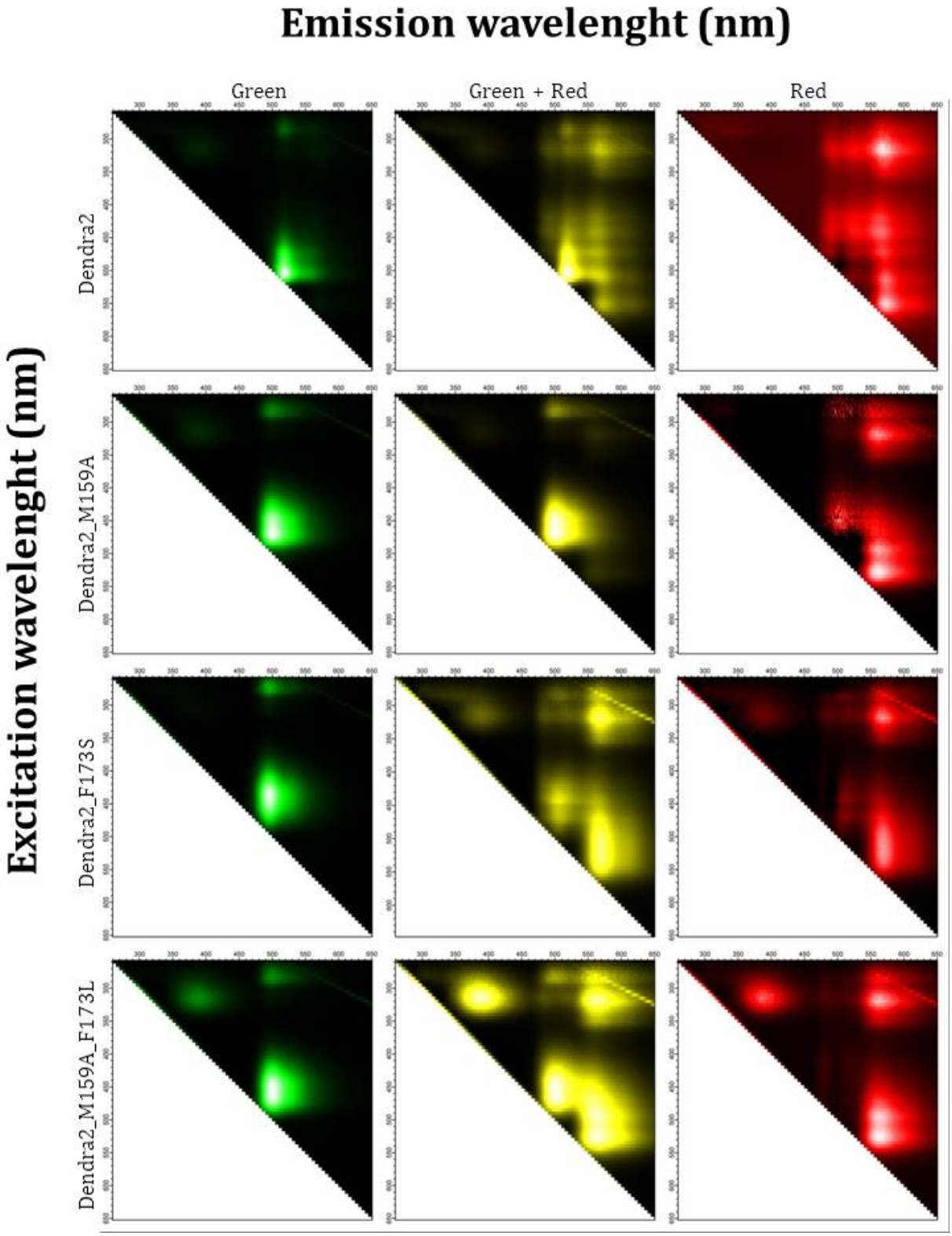

Figure 11.4: *Fluorescence landscapes of Dendra2, Dendra2_M159A, Dendra2_F173S and Dendra2_M159A_F173L in green (green) and partially photoconverted state (yellow). The calculated red species is shown in the right-hand column (red).*

Protein	Quantum Yield	ε ($M^{-1} \cdot cm^{-1}$)	Brightness‡
Dendra2	0,55 (**0,50**⋆)	**45 000**⋆	24,8
Dendra2_M159A	0,40	42 700	17,1
Dendra2_F173S	0,48	37 000	17,8
Dendra2_M159A_F173L	0,30	47 000	14,1
mEosFP	0,54 (**0,64** [53])	88 600	47,8
mEosFP_M159A	0,44	47 200	20,8
mEosFP_F173S	0,19	56 500	10,7
IrisFP	0,24 (**0,43** [19])	49 000 (**52 200** [19])	11,8 (**22,4**)

Table 11.2: *Quantum yields, extinction coefficients (ε) and brightness of Dendra2, mEosFP, IrisFP and mutants thereof. Values from the literature are shown in **bold** for comparison and validation. Extinction coefficients are calculated for the maximal absorption wavelength of the anionic species at pH 7,4.* ‡*Brightness was calculated as the product of the quantum yield and the extinction coefficient divided by 1000.* ⋆*Values taken from the website of Evrogen, the commercial supplier of Dendra2.*

samples will be measured again using an integrating sphere to get more precise values.

11.2.4 Extinction coefficient

From the extinction coefficient of the absorption peak at 447 nm of the denatured protein, it was possible to calculate the extinction coefficient of the anionic peak at pH 7,4. For this, a pH series ranging from pH 4,6 to complete pH-induced unfolding was measured. The first solution was measured at pH 7,4 (75 µl PBS buffer), after which 25 µl of sodium acetate buffer (1 M, pH 4,6) was added, followed by addition of aliquots of 5 µl of NaOH (0,1 M) until complete denaturation was reached. This way, the spectral series is useful for both extinction coefficient calculation as pKa determination. An example of one such experiment is shown in Figure 11.5. The extinction coefficients are represented in Table 11.2.

We also tried to measure the extinction coefficient of Dronpa_C62H. Strangely enough, this protein did not show any the spectral signature of unfolding. In fact, it kept it usual absorption spectrum up to pH 12,6. In other words, Dronpa_C62H seems remarkably stable at high pH. The extinction coefficient will be determined by the same means later on, but instead using urea or guanidinium chloride as denaturing agent.

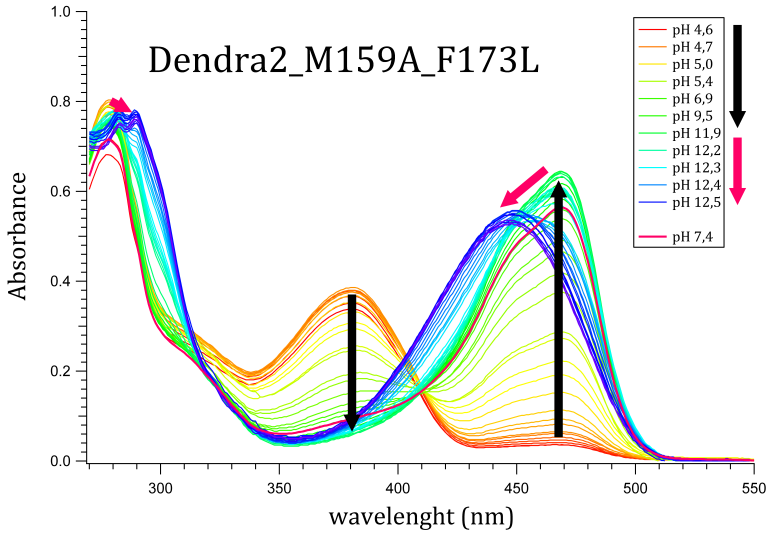

Figure 11.5: *Absorption spectrum series for pKa and extinction coefficient measurement. Black arrows represent spectral shifts due to deprotonation of the chromophore. Pink arrows show the spectral shifts due to denaturing of the protein.*

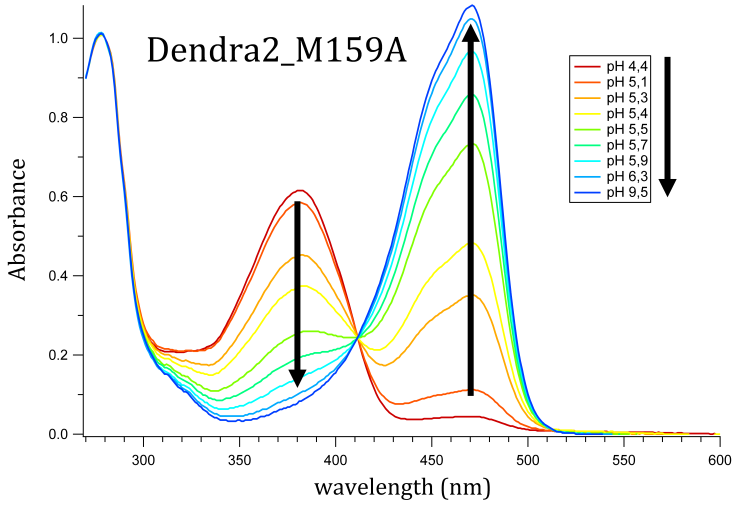

Figure 11.6: *Absorption spectra of Dendra2_M159A at different pHs.*

11.2.5 pH-dependency

Additional to the above experiment, pH series of some of the mutants was made, in order to study their behavior in acidic, neutral and basic conditions. A typical pH series (here from Dendra_M159A) is shown in Figure 11.6. Plotting the increase of the anionic species or the decrease of the neutral species absorption as a function of pH results in a sigmoid curve, that can be fitted using Formula 11.1. x_0 is the inflection point, giving the pKa value of the chromophore. Plot and fit for Dendra2_M159A are shown in Figure 11.7. The pKas can be found in Table 11.3.

$$y = \frac{A_1 - A_2}{1 + e^{\frac{x - x_0}{dx}}} + A_2 \tag{11.1}$$

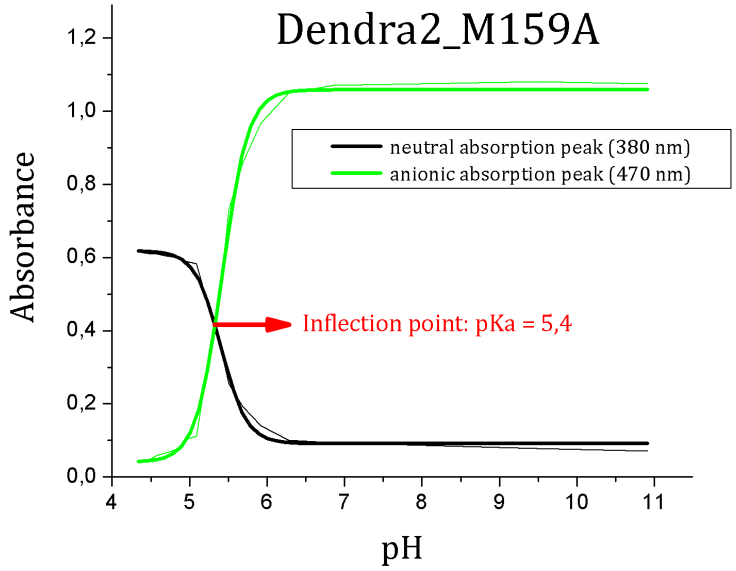

Figure 11.7: *The maximal absorption of the neutral (black) and anionic (green) species as a function of pH of Dendra2_M159A was plotted. The plots were fitted (thicker line) and the inflection point is calculated.*

protein	pKa
Dendra2	**7,1** [31]
Dendra2_M159A	5,4
Dendra2_F173S	5,5
Dendra2_M159A_F173L	5,2
mEosFP	5,2
mEosFP_M159A	5,0
mEosFP_F173S	5,4
EosFP	**5,8** [29]
IrisFP	5,4
Dronpa	**5,0** [20]
Dronpa_C62H	5,1

Table 11.3: *pKa values for Dendra2, mEosFP, EosFP and mutants thereof. Values that were taken from the literature are represented in* ***bold****.*

Protein	τ (min)
Dendra2	67,35 ± 3,16
Dendra2_M159A	186,69 ± 9,32
Dendra2_F173S	87,92 ± 0,64
Dendra2_M159A_F173L	154,65 ± 5,26
mEosFP	54,38 ± 2,04
mEosFP_F173S	52,26 ± 1,97
mEosFP_M159A	27,01 ± 3,65
Dronpa_C62H‡	5,77 ± 0,50

Table 11.4: *Photoconversion parameters. ‡Dronpa_C62H was measured using different light intensities and can therefor not be compared to the other proteins.*

11.2.6 Photoconversion

Dendra2 and mEosFP mutants

Photoconversion data on all PCFPs was recorded as described in Subsection 10.4.2. After a simple baseline correction, the absorption maximum of the green and red species were followed in time. These traces could then be fitted with exponential curves, be it mono-exponential (Formula 11.2) or bi-exponential (Formula 11.3). For all FPs, the appearance of the red species followed a first order exponential increase. This was not the fact for the disappearance of the green form, that showed mono- or bi-exponential decrease dependent on the particular FP. As was reasoned that photoconversion can be considered as the formation of red species, and not the disappearance of the green species, which is a sum of multiple processes (photoconversion and irreversible bleaching), only the rise in red absorption peak was used further on.

$$y = y_0 + A \cdot e^{(-\frac{x}{\tau})} \tag{11.2}$$

$$y = y_0 + A_1 \cdot e^{(-\frac{x}{\tau_1})} + A_2 \cdot e^{(-\frac{x}{\tau_2})} \tag{11.3}$$

The results of the fitting procedure are represented in Table 11.4.

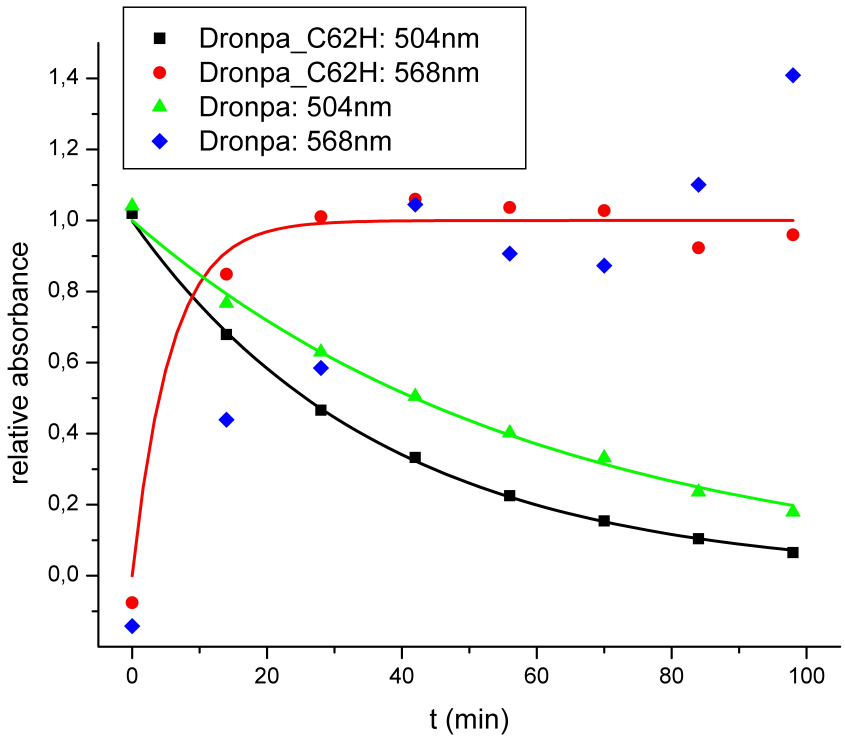

Figure 11.8: *Photoconversion of Dronpa and Dronpa_C62H.*

Dronpa and Dronpa_C62H

The photoconversion process of Dronpa_C62H with Dronpa as negative control was measured, although with a 405 nm laser intensity of 142 mW/cm^2. Absorption spectra were recorded every two minutes for 98 minutes. After baseline correction scaling to the 280 nm peak, the absorption at 504 nm (green species) and 568 nm (red species) were plotted in time and fitted with a mono-exponential (Formula 11.2). Results are shown in Figure 11.8.

The behavior of Dronpa cannot be explained by photoconversion. Although the green species seems to disappear, no clear evidence of the formation of a red species is visible. The signal that does show up at 568 nm can be fully attributed to noise or imprecise measurements and is in fact exaggerated due to the scaling procedure. The disappearance of the green peak can thus be considered as photobleaching. This means that the rate of photoconversion can only be assessed by the formation of a red absorbing species and not by the disappearance of the green species, because this last is again a combination of photoconversion and irreversible photobleaching. We can thus conclude that Dronpa_C62H is a photoconvertible fluorescent protein.

11.2.7 Photoswitching

Photoswitching was measured following absorption using the setup described in Section 10.2. Two characteristic results are shown in Figure 11.9. Graph **A** (IrisFP) shows very clearly the behavior of a reversibly switchable FP. Irradiation with 488 nm light (cyan bar) causes a decrease of absorption at the anionic peak and an increase at the neutral peak. When 405 nm light (purple bar) is switched on, exaclty the opposite happens: the anionic peak starts to grow again, at the expense of the neutral absorption peak. However, there is no 100% recovery to the fully deprotonated state.

In the same figure, graph **B** (mEosFP) shows a completely different behavior. A first observation is the much bigger noisiness of the signal. Secondly, the off-switching happens so slowly that the exponential nature is practically invisible. Thirdly, no plateau has been reached after 450 seconds of 488 nm light irradiation. However, the observed decrease of the anionic peak is not only due to irreversible bleaching of the fluorescent protein, as fluorescence can be recovered. The increase at the neutral peak proves that reversible transition from the neutral to anionic state and back again, is possible. The fact that there is however some irreversible photobleaching, is obvious from the fact that the on-switching is less intense for the second compared to the first maximal on-value. These results are remarkable, as mEosFP has up to now not been described as reversibly switchable.

Figure 11.10 shows the same kind of graphs of two of the mutants that were made. In part **A**, Dendra2_F173S is shown. Although Dendra2, the mother protein, shows similar behavior as mEosFP (data not shown), it is clear that Dendra2_F173, the daughter, is indeed reversibly switchable just like Dronpa and IrisFP are. Achieving this was one of the major assets of this thesis. Also Dendra2_M159A, Dendra2_M159A_F173L, mEosFP_M159A and mEosFP_F173S (mIrisFP), behave this way.

Remarkably, the behavior of Dronpa_C62H, shown in graph **B** of Figure 11.10 is very similar to that of Dendra2 and mEosFP. It is thus clear that Dronpa_C62H is not an IrisFP-like fluorescent protein.

This kind of measurements provides us with valuable data concerning photoswitching, but is not completely satisfactory for several reasons. First of all, we here measured absorption rather than fluorescence. There is a link between the two: comparison between the absorption and fluorescence spectra have showed us that excitation occurs at wavelengths corresponding

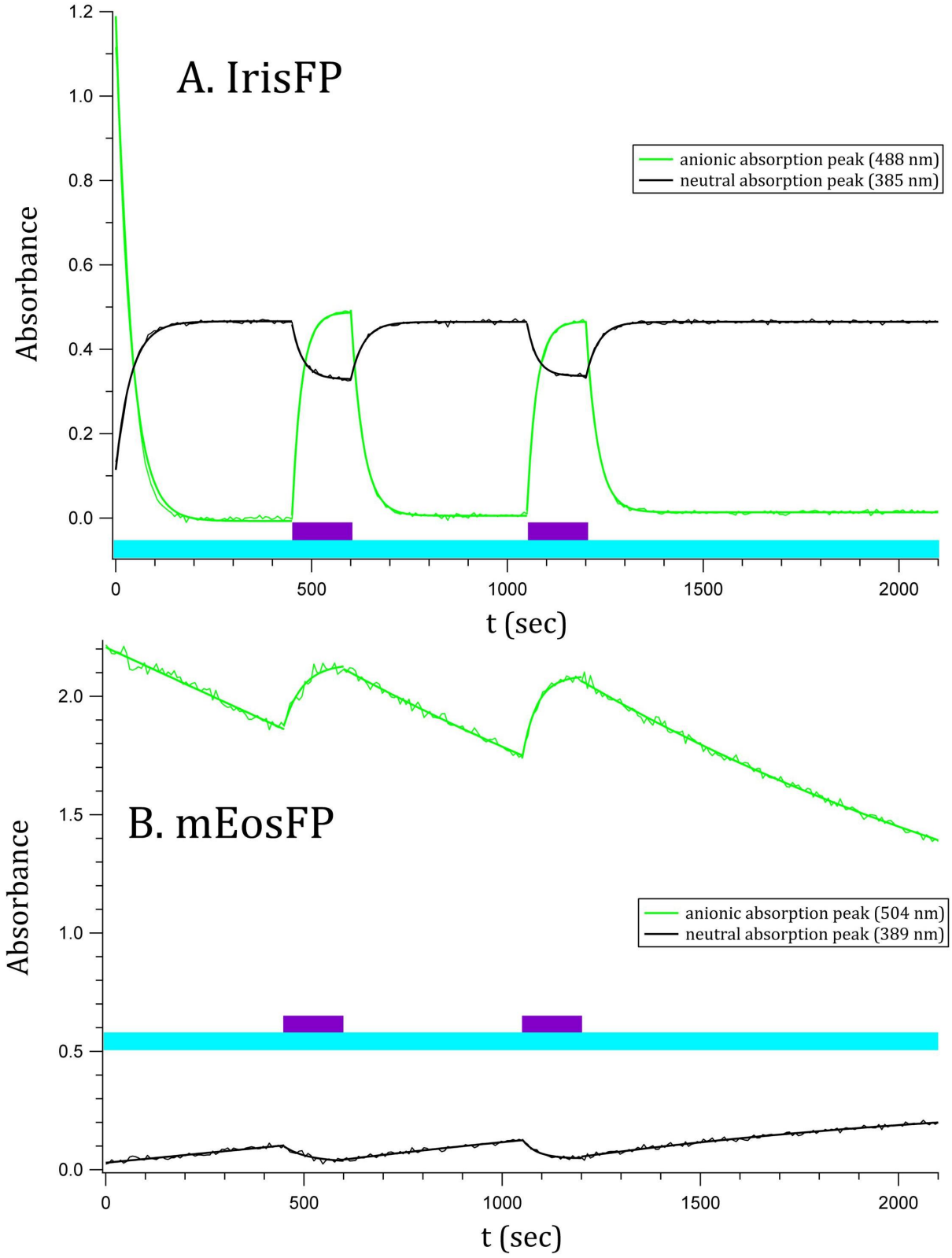

Figure 11.9: *Photoswitching of (**A**) IrisFP and (**B**) mEosFP was followed by irradiation of 488 nm light (cyan bar) and 405 nm light (purple bar).*

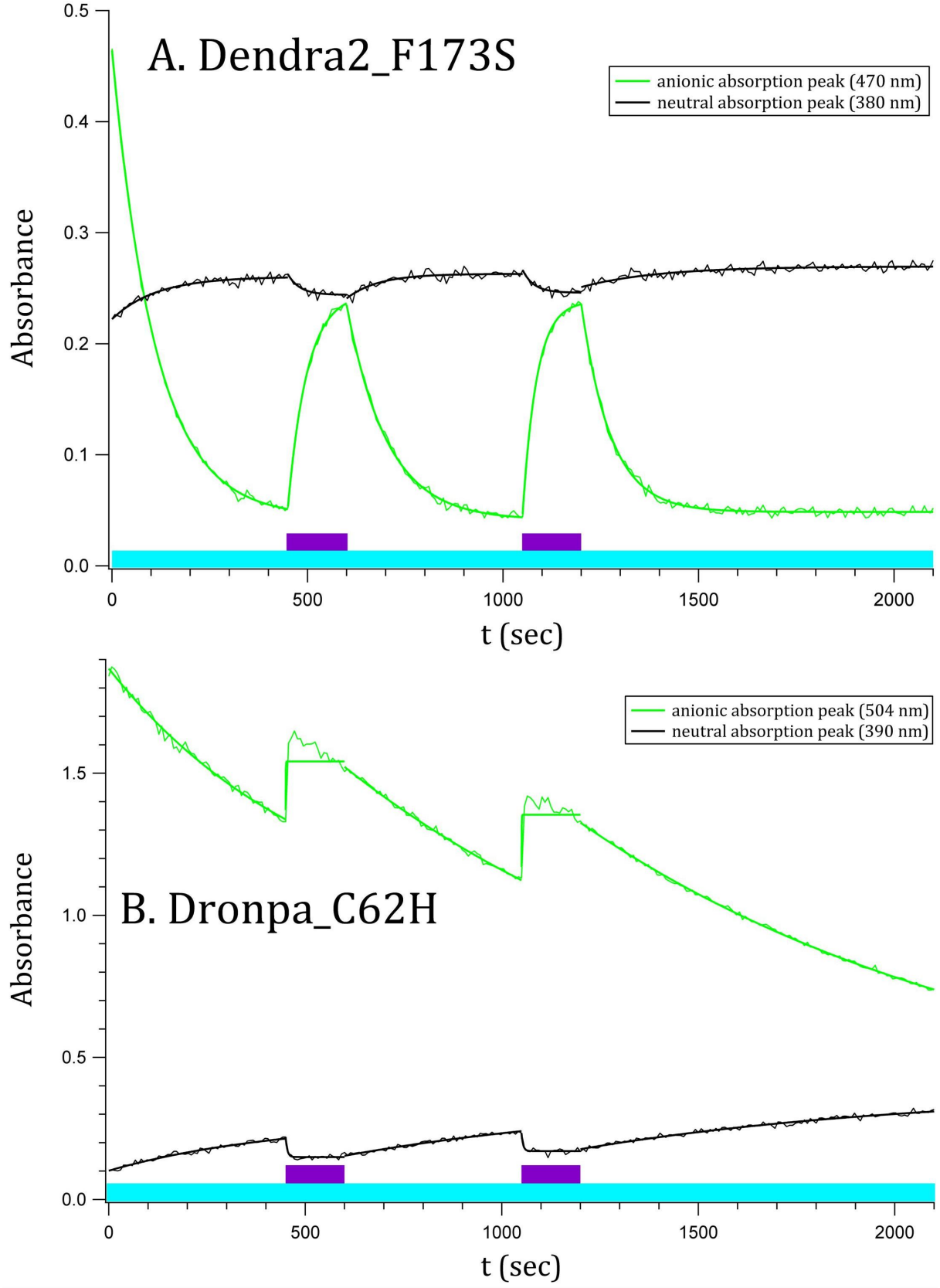

Figure 11.10: *Photoswitching of (**A**) Dendra2_F173S and (**B**) Dronpa_C62H was followed by irradiation of 488 nm light (cyan bar) and 405 nm light (purple bar).*

to the anionic absorption peak. However, this story is not black-and-white: recall from Figure 11.4 that the red neutral species of Dendra2 can indeed be excited. For all possible applications of these proteins, fluorescence rather than absorption is measured, so the above results do not exactly assess the parameters we are looking for. A second reason is that these absorption measurements are carried out in a cuvette, but again for all possible applications, these proteins will be used in a microscope system. Light intensities will thus be higher because of focussing, which could for instance also increase temperature, no mixing will take place... It is thus of major importance to also measure photoswitching properties on a microscope system. This is what has been done using the setup represented in Figure 10.2 and discussed there.

At first, the three Dendra2 mutants were probed and switched off using 473 nm laser light in this setup. After some very early attempts to do PALM experiments using 473 nm excitation light and comparing it to the results obtained by 488 nm excitation light, we observed much clearer blinking of the fluorescent proteins when exciting at the latter wavelength. This could be explained by the broad absorption peak ($\pm$31 nm) of the chromophore in its neutral state (see Figure 11.11). It extends to and even further than 488 nm. However, there is slightly less absorption at 488 nm. As irradiating the neutral species accelerates backswitching of the chromophore, we reasoned that 473 nm light is accelerating the backswitching more than the 488 nm light does, resulting in less clear blinking. In addition, mounting the 473 nm diode laser into the PALM system caused tedious alignment difficulties due to the rather divergent light beam. And finally, diode lasers producing 473 nm light are rather rare in basic PALM setups. These three reasons made us decide to characterize the photoswitching of Dendra2 mutants using 488 nm light for probing and off-switching. The results obtained in both experiments (using 473 nm or 488 nm light) were comparable (data not shown).

In a first attempt of fitting the sharkfins to mono-exponential curves, we observed that in some of the mutants there was a systematic error. This effect was sometimes hardly detectable, but present anyway. Therefor, we turned to a bi-exponential model that gave very neat fits. However, there is little reason to accept a bi-exponential model, as at the timeresolution of these kind of experiments, switching should be an apparent one-step event, and thus show mono-exponential behavior.

The reason for this bi-exponentiality could be found in the setup itself. At first, there was no lens right at the back aperture of the microscope (see Figure 10.2). This caused the probing light

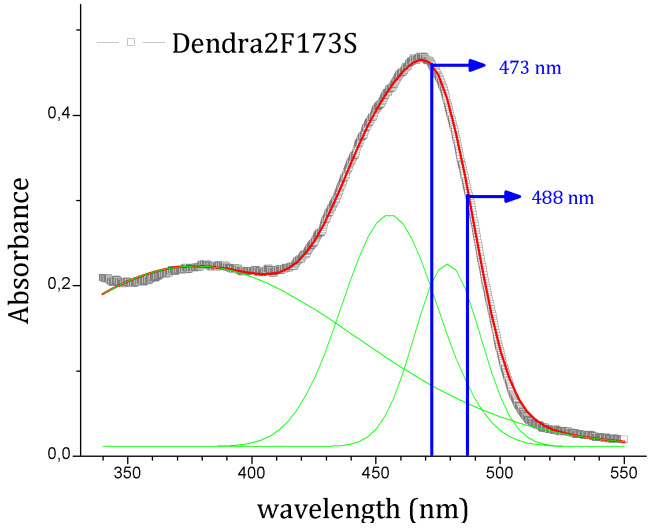

Figure 11.11: *Dendra2_F173S absorption spectrum (grey blocks) with gaussian peak deconvolution (green peaks). Reconstitution of the graph using the deconvoluted peaks is shown in red.*

and the detection spot to be of more or less the same size. However, the probing light has not a uniform, but a Gaussian intensity profile. This means that the molecules in the detection spot receive a different amount of photons depending on their position in the probing and detection area, leading to a deviation from the mono-exponential model. Therefor, the lens at the back aperture of the microscope was introduced. This lens assures a wide-field illumination, meaning that the probing light illuminates a large area, much bigger than the detection spot. In the detection area, the beam can thus be considered as uniform. The results following this technical optimization could indeed be fitted with a mono-exponential curve.

In Figure 11.12, the number of detected photons per half second is plotted in time for IrisFP (**A**) and mEosFP (**B**). Comparing these results with Figure 11.9, we can already see that both techniques of measuring photoswitching give at first sight similar results, except for the extent of irreversible bleaching. This last remark can be explained by the fact that on the microscope, we probe and detect the same molecules throughout the experiment, while in a cuvette, the solution is constantly stirred and the probed and detected molecules thus constantly refreshed. The same is true for Figure 11.13 and 11.10. It is clear from Figure 11.12 **B** and Figure 11.13 **B** that switchers and non-switchers show very distinct behavior.

As an ultimate negative control for photoswitching, the same measurements as mentioned above have been performed on eGFP. The results of this measurement is shown in Figure 11.14.

The sharkfins thus obtained were all automatically fitted to mono-exponential curves using the self-written IgorPro procedure. All resulting τ values are represented in Table 11.5 and

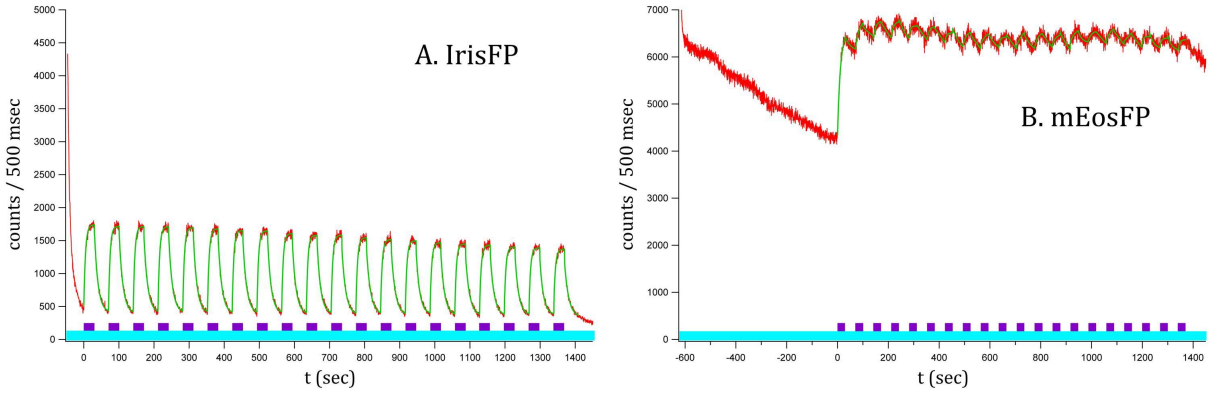

Figure 11.12: *Photoswitching of (**A**) IrisFP and (**B**) mEosFP was followed by irradiation of 488 nm light (cyan bar) and 405 nm light (purple bar).*

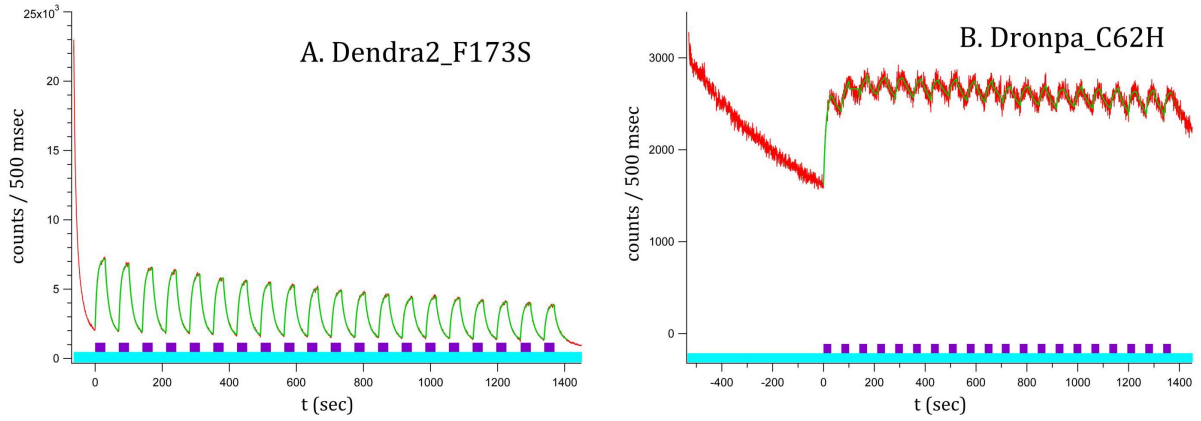

Figure 11.13: *Photoswitching of (**A**) Dendra2_F173S and (**B**) Dronpa_C62H was followed by irradiation of 488 nm light (cyan bar) and 405 nm light (purple bar).*

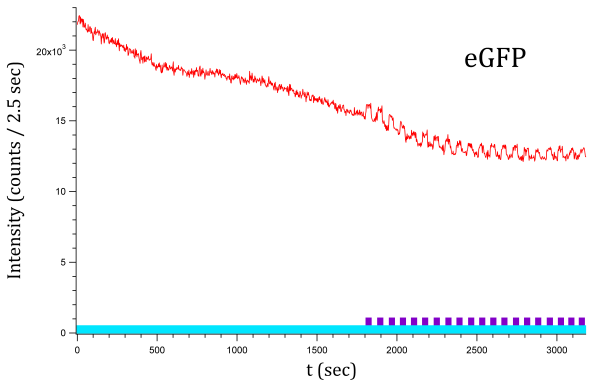

Figure 11.14: *Photoswitching of eGFP was followed by irradiation of 488 nm light (cyan bar) and 405 nm light (purple bar).*

expressed in seconds.

To cross-validate the results of both techniques used to assess photoswitching (i.e. using absorption in a cuvette or using fluorescence on a microscope), we checked whether there is correlation between $\langle\tau\rangle$ from the fluorescence measurements and $\langle\tau\rangle$ from the absorption measurements, both for on- as for off-switching. Indeed, a positive linear correlation is observed with a certainty of above 95% between the on- or off-switching parameters in fluorescent mode and the on- or off-switching parameters in absorption mode.

11.2.8 Thermal recovery

Thermal recovery was measured in absorption mode for all mutants that showed photoswitching behavior. First, the RSFP was switched off using 488 nm laser light (800 mW/cm^2) after which the protein was left in the dark, taking an absorption spectrum at regular timepoints, from $t = 0$ s to $t = 3600$ s. A typical result is shown in Figure 11.15 for Dendra2_M159A. The absorbtion maximum of the anionic species was plotted in time and fitted with an exponential curve. Using the parameters from this fitting procedure, listed in Table 11.6, the data was rescaled to fit Equation 11.4 and is shown in Figure 11.16. The values seem very low, meaning that the proteins seem to recover from the dim state very rapidly. All available literature point towards slower switching. One explanation might be that the probing light (200 - 900 nm light, $\pm$ 200 msec per spectrum) accelerates backswitching. Measuring this recovery in fluorescence mode or only using the halogen lamp and not the deuterium lamp in absorption mode might be necessary to have a better comparison to the published values.

$$y = e^{(-\frac{x}{\tau})} - 1 \tag{11.4}$$

11.2.9 Summary

Figure 11.17 summarizes the results described above. We represent τ_{on} on the x axis, τ_{off} on the y axis and the τ_{conv} is represented by the radius of the spheres. Note that the higher these values are, the slower the process occurs. IrisFP photoconversion was not measured here, its value was therefor arbitrarily set to the same value as mIrisFP (mEosFP_F173S), as they are structurally very similar. This is of course an approximation.

	Fluorescence		Absorption			
	on-switching	off-switching	on-switching		off-switching	
	τ_{on}	τ_{off}	τ_A	τ_N	τ_A	τ_N
Dendra2_M159A	9,62 ± 0,34	18,98 ± 0,67	38,91 ± 0,65	37,12 ± 5,98	155,20 ± 1,23	158,90 ± 10,06
Dendra2_F173S	6,49 ± 0,08	12,66 ± 0,15	39,92 ± 0,85	27,84 ± 5,06	89,67 ± 0,73	121,04 ± 10,12
Dendra2_M159A_F173L	5,30 ± 0,06	11,39 ± 0,12	32,32 ± 0,48	30,57 ± 2,55	79,21 ± 0,48	91,65 ± 3,37
mEosFP_M159A	4,30 ± 0,09	9,60 ± 0,16	33,74 ± 0,47	26,40 ± 1,06	43,98 ± 0,41	128,67 ± 5,84
mEosFP_F173S	4,46 ± 0,09	10,35 ± 0,17	21,25 ± 0,21	21,33 ± 0,91	31,69 ± 0,21	32,17 ± 0,60
IrisFP	4,38 ± 0,09	10,68 ± 0,18	22,62 ± 0,29	24,70 ± 0,94	30,70 ± 0,27	32,26 ± 0,48
Dronpa	10,71 ± 0,79	76,19 ± 41,20	32,27 ± 0,36	32,22 ± 1,77	389,90 ± 3,46	346,93 ± 17,07

Table 11.5: *Photoswitching was followed measuring the fluorescence emission on the one hand and absorption maxima at the other hand. In fluorescence mode, both the on- as the off-switching signal was fitted by a mono-exponential curve, giving parameters τ_{on} and τ_{off}. In absorption measurements, both peak increases and decreases were fitted with a mono-exponential, giving parameter for the on-switching of the protein (anionic peak going up (τ_A), neutral peak going down (τ_N)) and for the off-switching of the protein (anionic peak going down (τ_A), neutral peak going up (τ_N)). All τ values expressed in seconds.*

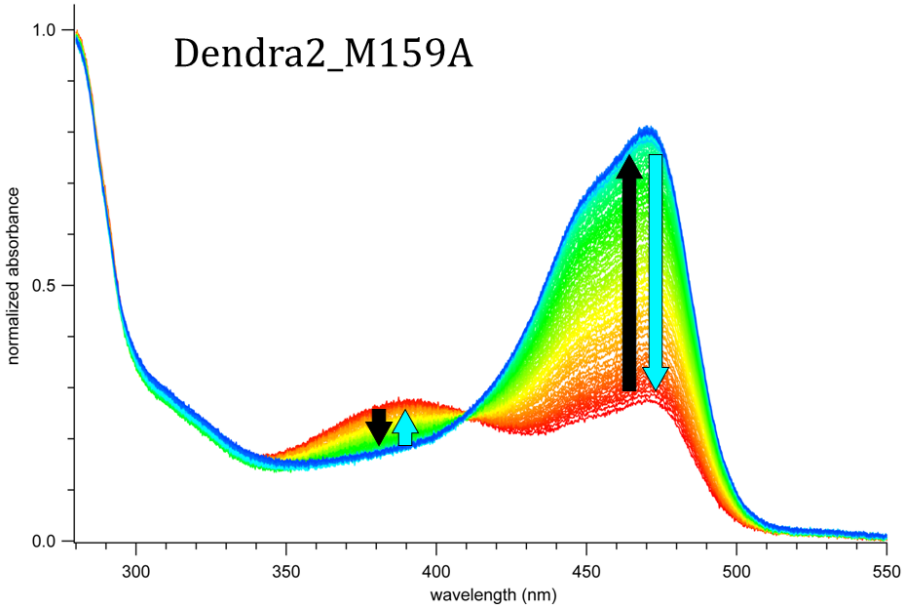

Figure 11.15: *Absorption spectrum series of Dendra2_M159A. After switching off the fluorescence by 488 nm light (cyan arrows), the protein was left in the dark, measuring absorption spectra at different timepoints. The red spectrum is at* $t = 0$ *s, the blue one is at* $t = 3600$ *s (black arrows).*

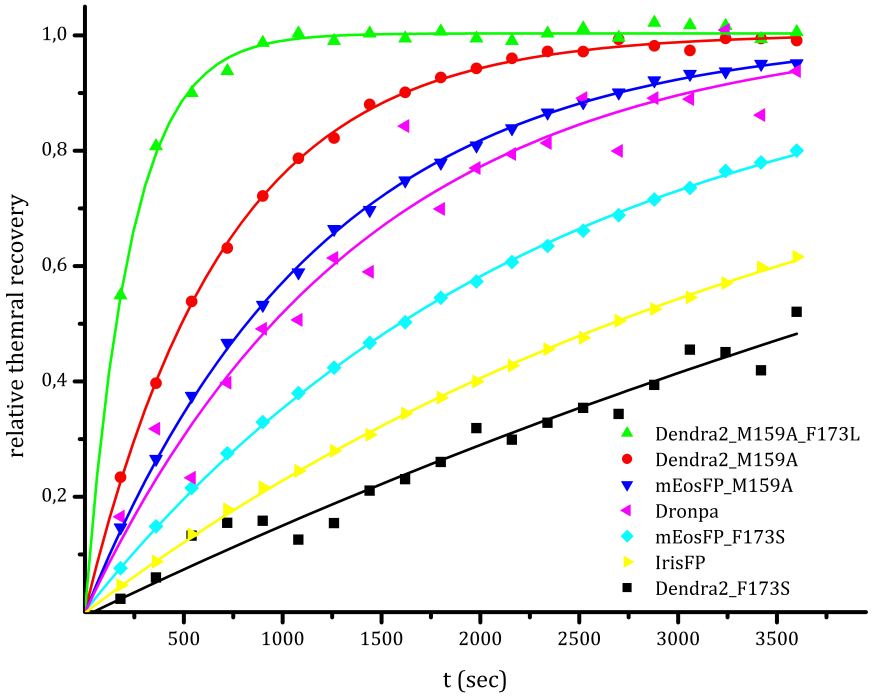

Figure 11.16: *Thermal recovery of RSFPs represented as the absorption maximum of the anionic species as a function of time. Circles, triangles or squares represent scaled data points, the line is the exponential fit according to Equation 11.4.*

Protein	τ (min)
Dendra2_M159A	11,7 ± 0,1
Dendra2_F173S	93,5 ± 23,8
Dendra2_M159A_F173L	3,79 ± 0,04
mEosFP_M159A	19,5 ± 0,1
mEosFP_F173S	38,1 ± 0,4
IrisFP	63,8 ± 1,5
Dronpa	23,9 ± 2,2

Table 11.6: *RSFP half-lifes for thermal recovery*

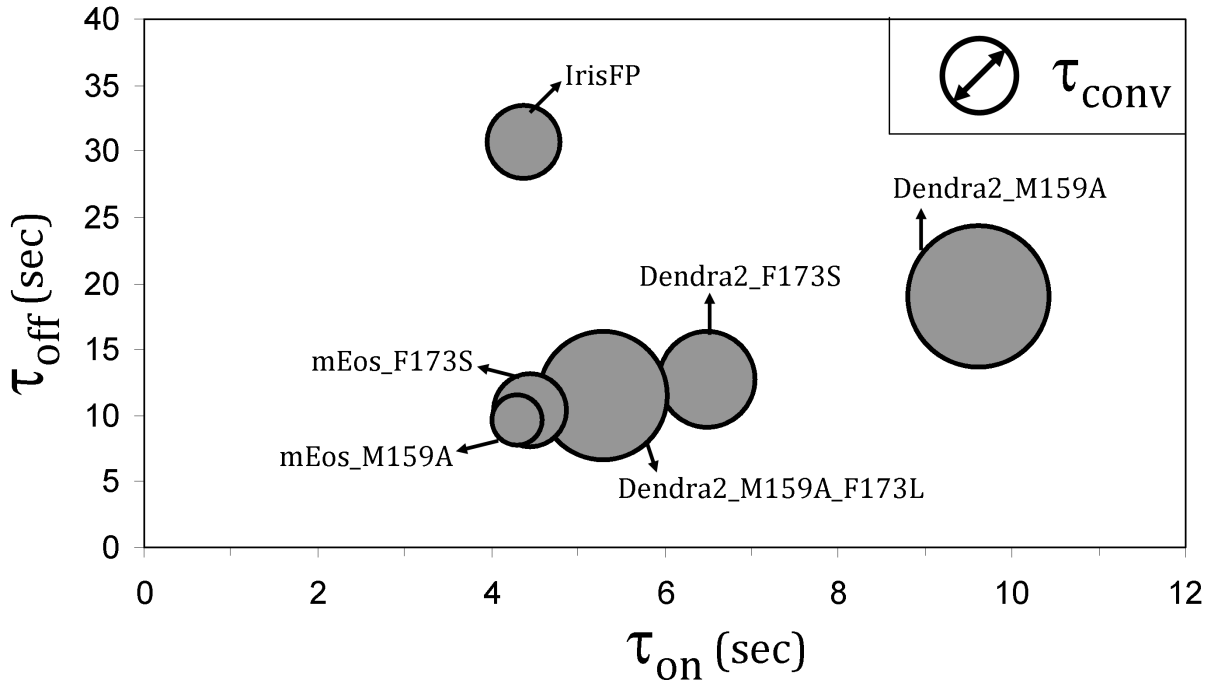

Figure 11.17: *Photoactivation properties for both photoconvertible and photoswitchable proteins. The value of τ_{conv} of IrisFP was arbitrarily set to the same value as mIrisFP.*

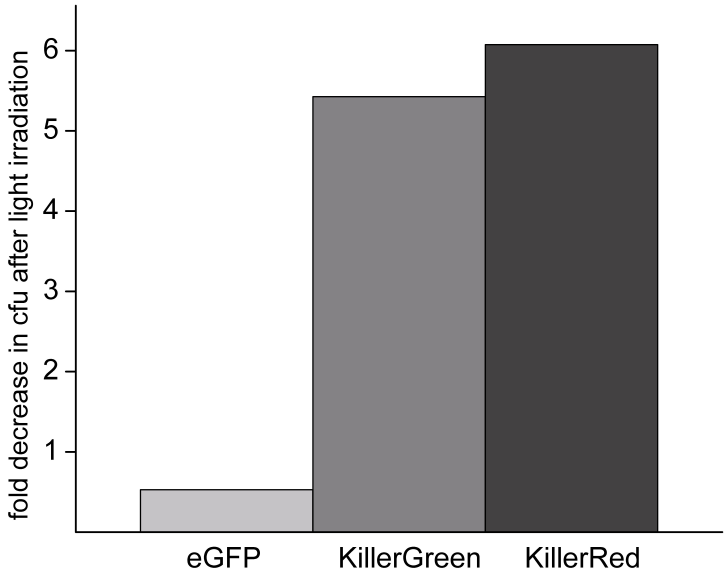

Figure 11.18: *Phototoxicity assessment of eGFP_V68E_Q69P with eGFP and KillerRed as negative and positive control, respectively.*

11.3 KillerGreen

The eGFP_V68E_Q69P mutant was successfully constructed and purified. However, the bacterial colonies as well as the purified protein proved to be non-fluorescent. Nevertheless, the phototoxic properties were checked as described in Section 10.5. For eGFP (negative control), eGFP_V68E_Q69P (sample) and KillerRed (positive control), the number of cfu with and without light irradiation were counted. The ratio of the two is represented in Figure 11.18.

Part E

Discussion

CHAPTER 12

Discussion

12.1 Selection of the best protein for two-color superresolution microscopy

The quality of a PALM experiment is determined by the color contrast of the images and for that reason depends on a number of factors. One of the most important ones is the number of detected photons from one protein during one on-time. The brightness thus plays a crucial role, but more important is the off-switching speed. The faster a protein is switched off, the less photons will be emitted before the actual off-switching event. Thus, it is interesting to use bright molecules with slow off-switching rate constants [23]. Moreover, using fluorescent proteins that are both photoswitchable and photoconvertible, it is important to use a protein that gets not too easily photoconverted. It has for instance been reported that Dendra2 can be photoconverted using 488 nm light [61]. This can cause photoconversion due to probe light irradiation. Not only are these proteins then no longer observed in the green channel, but more annoyingly, they show up in the red channel. This false positive protein detection in the red channel blurs out the image. On the other hand, the conversion should not be too slow, as irreversible bleaching could then take the upper hand and intended photoconversion would then not occur at all.

As can be seen from Figure 11.17, there is a positive linear correlation between the τ_{on} and

τ_{on} while IrisFP is an outlier. Its τ_{off} is three times bigger than mIrisFP (mEosFP_F173S), meaning that it switches off much slower. This deviation from all the other IrisFP-like proteins can be explained by the tetrameric nature of IrisFP. Similar results have been obtained by comparing Dronpa and its tetrameric parent molecule, 22G [50]. In Dronpa, light-induced increase in local flexibility of the β-barrel at the chromophore hydroxyphenyl moiety allows for efficient photoswitching. However, due to the tetrameric nature of 22G, this local flexibility is prevented and photoswitching is happening much slower [23]. We here propose the same mechanism for mIrisFP in respect to IrisFP.

Initially, we thought that M159A mutants of Dendra2 and mEosFP would show fast on-switching and slow off-switching. Figure 11.17 shows us that this is not the case. Instead of talking in terms of stability of the cis- or trans-conformation, it seems that the flexibility of the chromophore and its freedom to move plays an essential role. This means that we rather have to think in terms of energy barriers rather than energy levels. The more conformational freedom is given to the chromophore hydroxyphenyl moiety by mutating a given residue to less bulky one, the lower this energy barrier is and the faster both on- and off-switching take place. This insight explains the strong linear relationship of the datapoints in Figure 11.17.

From this work, we can conclude that both Dendra2_M159A and Dendra2_F173S are very promising monomeric fluorescent proteins for two-color PALM experiments. We tested Dendra2_F173S in early explorative super-resolution trials and already gave it a trivial name: NijiFP[1].

12.2 Met159 has a profound effect on the protonation state

Throughout this work, we have evidenced that the role of the Met159 residue has been underestimated what concerns its influence on the protonation state of the chromophore. In Figure 5.2, we see that the distance between the Met159 sulphur atom and the chromophore hydroxyphenyl hydroxyl oxygen is too big for strong and direct interaction in EosFP (3,5Å). However rather distant, 2,3Å could be close enough for a reasonable stabilization of the protonated species. Following this rationale, mutating Met159 to alanine or mutating Phe173 to serine and indirectly making the Met159 flip away from the chromophore should cause the pKa to be shifted

[1] While Iris is the ancient Greek goddess representing the rainbow, Niji is the Japanese word for rainbow.

downwards. This is apparent in Dendra2, where all the mutants have much lower pKa, resulting in an almost not present neutral absorption peak at pH 7,4. Also, from Table 11.4 we see that all mutants show lower photoconversion speeds, which is at least partly due to this decreased pKa. The effect is less pronounced in mEosFP, where the neutral species is less favored compared to Dendra2 due to the different interaction of Arg66 with the chromophore, as discussed in Section 5.3.

12.3 Two types of photoswitching

As has been described in Chapter 5, there is quite some doubt about the actual mechanism of photoswitching. Is cis-trans isomerization the key ingredient, is it protonation of the hydroxyphenyl moiety of the chromophore or is local flexibility the crucial factor? Apart from all possible mechanisms, it is clear that, during this project, we have observed at least two classes of fluorescent proteins with very different switching behaviors. The first class are the proteins that are considered to be non-switchers. Dendra2, mEosFP, eGFP and Dronpa_C62H are members of this class. Typical of their switching behavior is their very slow off-switching and their on-switching restores a reasonably bigger fraction of the initial fluorescence than the other class. This second class consists of the proteins that are known to be photoswitchable, like Dronpa, IrisFP, but also a lot of the mutants we made, like Dendra2_F173S and mEosFP_M159A. Their fluorescence can be switched off to a basic level, and restored, although to a substantially lower level than the initial fluorescence peak.

How can these two classes now be explained? In proteins that are believed to be non-switchable, we merely observe light-induced protonation (i.e. photoprotonation). Of course, this photoprotonation and subsequent deprotonation happens to a different extent in different proteins. Indeed, in eGFP we can merely see small fluctuations, while in mEosFP, the sharkfins look more like the shark's teeth. This susceptibility of the chromophore to be protonated or deprotonated under influence of light is dependent on the local environment and is therefore different from protein to protein.

It is only in the second class that the actual switching occurs. After the light-induced protonation, these proteins can indeed undergo cis-trans isomerization. Strangely enough, the fluorescence (and absorption) of these proteins does not return to the initial level after the first

off-switching. An explanation for the incomplete recovery might be that the conformation of the initial state is different from the back-switched state and that this back-switched state then has a lower extinction coefficient. To check this last hypothesis, we would need crystal structures or NMR models of the back-switched species for comparison to the native state. Also in this second class, there are differences between the members that have to be explained by the local environment of the chromophore. Some trans-conformations are more favored than the other, thus explaining thermal stability of the dark form en switching parameters. While IrisFP seems to be easily switched on and off, Dronpa and Dendra2_M159A show a behavior that can be called bistable: both on- and off-switching are relatively slow.

12.4 What renders Dronpa_C62H non-switchable

It is clear from this work that Dronpa_C62H is indeed a PCFP, but not a RSFP. This is quite remarkable, as Dronpa is one of the most well-know reversibly switchable fluorescent proteins. The immanent question is of course which structural theme has caused the loss of switching abilities. To answer this question precisely, obtaining an atomic model of the protein is crucial. However, some initial guesses can already be made. Mutating cysteine towards a histidine means mutating a rather small residue to a rather bulky one. Consequently, the chromophore might be pushed away from the side of the β-can where the cysteine normally is located and more towards the opposite side. This side is exactly where the chromophore hydroxyphenyl moiety resides in its trans conformation. In other words, this structural rearrangement might explain why bistable switching due to a cis-trans isomerization is prevented and photoprotonation and -deprotonation is not.

12.5 Blue-shifted spectra of Dendra2 mutants

As can be seen from Figure 11.1 and Figure 11.2 and is also obvious from Table 11.1, the mutants of Dendra2 and mEosFP have shorter wavelength absorption and excitation peaks compared to their parents. An explanation can be found in the crystal structure of these parents. In Figure 12.1, we clearly see that the chromophore hydroxyphenyl moiety forms a $\pi - \pi$ stacking interaction with the imidazole ring of the histidine residue at position 193 in Dendra2 (in

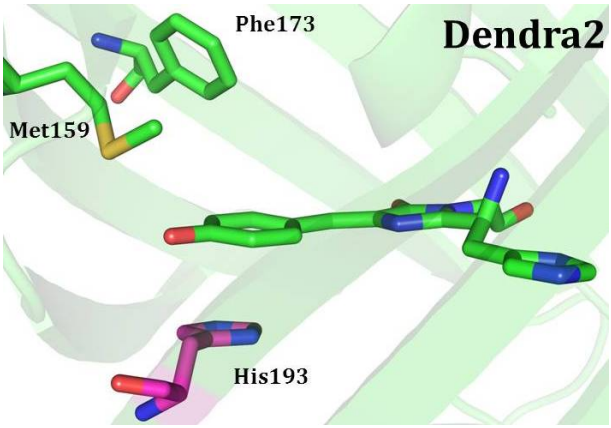

Figure 12.1: *Stacking interaction between the Dendra2 chromophore hydroxyphenyl moiety and His193. The chromophore and the two key mutated residues are shown in green while His194 is colored pink. Nitrogen atoms are depicted in blue, oxygen atoms are red and sulphur atoms are shown in yellow.*

mEosFP, this is position 194). This kind of stacking interaction usually shifts the excitation peak towards higher wavelengths.

In all of the mutants, one or both of the key residues (Met159 and Phe173) are mutated towards a less bulky amino acid. This gives more conformational freedom to the chromophore, so that it can perform a cis-trans isomerization during the reversible photoswitching event. However, this increased conformational freedom renders the interaction of the hydroxyphenyl moiety of the chromophore with the histidine imidazole ring less intense, ultimately leading to a smaller $\pi - \pi$ interaction effect and shorter absorption and excitation wavelengths. This is consistent with the broader absorption peaks and lower quantum yields, as has been discussed in Subsection 11.2.1.

12.6 An intermediate photoswitcher?

From all results, it is clear that Dendra2_M159A_F173S does not show switching behavior that is intermediate between Dendra2_M159A and Dendra2_F173S. Instead, a both photoconvertible and photoswitchable fluorescent protein has been made with rather low fluorescence brightness that is photoconverting slowly. The rather low fluorescence quantum yield can be explained by the increased flexibility of the chromophore due to replacing two residues to less bulky ones. This is also evidenced by the broad absorption peak and blue-shifted absorption and excitation peaks. In other words, is not very likely that this protein will make it to the next level, being two-color super-resolution microscopy.

12.7 KillerGreen revised

The results obtained from the cfu-counting experiment have to be interpreted with a lot of care. These measurements are very indirect and only carried out once. Maybe the most worrying observation is the absence of fluorescence of the KillerGreen mutant. The absorption spectrum contains a very small absorption peak at about 500 nm, but is extremely low compared to the 280 nm band (data not shown). A lot of optimization and further characterization and will thus be needed.

CHAPTER 13

A proof of concept

We would like to conclude in beauty. Figure 13.1 shows a proof of concept op two-color PALM using NijiFP. Image **A** is a high resolution image of NijiFP-fused actin filaments in HeLa cells, that was recorded only making use of 488 nm laser light. Image **B** is a high resolution image of a similar HeLa cell, having NijiFP-fused actin, where the proteins were first photoconverted to the red state en subsequently recorded only making use of 561 nm laser light. In the near future, similar experiments will be done using two lasers, two detectors, one cell and NijiFP.

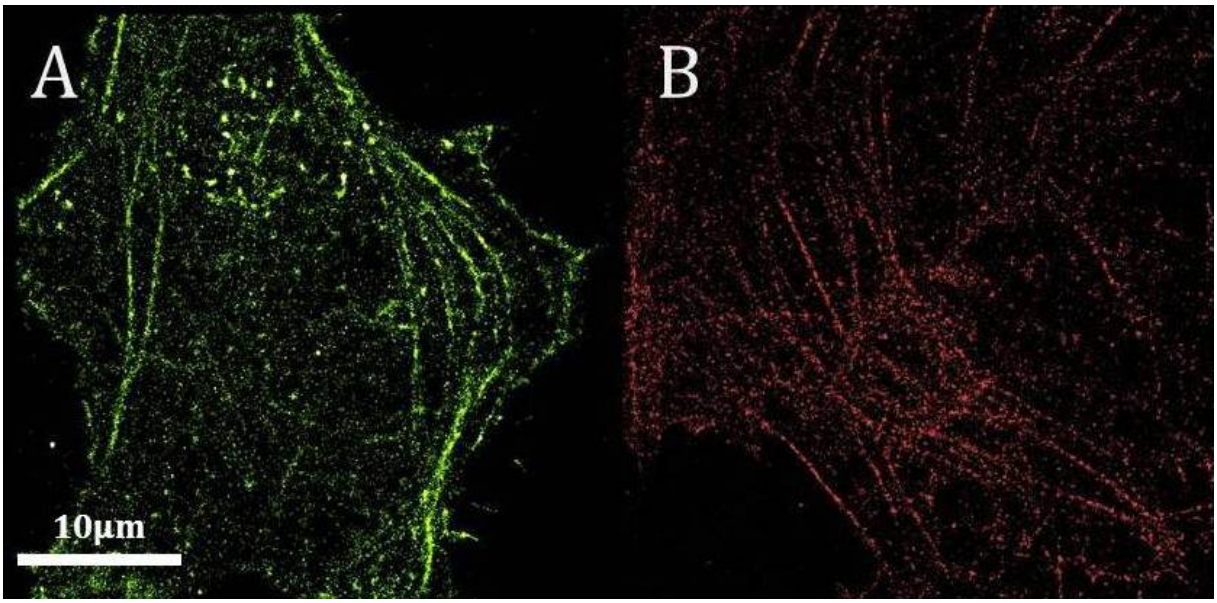

Figure 13.1: *Initial PALM images of NijiFP-fused actin filaments in HeLa cells using (**A**) only a 488 nm laser in the green from and (**B**) only a 561 nm laser in the photoconverted red form. This may serve as a proof of principle for dual-color PALM using only two lasers and one fluorescent protein.*

CHAPTER 14

Summary

In the 1960's, O. Shimomura was the first one to extract a fluorescent protein from *Aequorea victoria*, a jellyfish living at the North-American west coast. Soon after, the DNA coding for this remarkable protein was isolated and cloned in different organisms, from bacteria to plants and mice. The protein has the shape of a can formed by β-strands with a central α-helix that holds the heart of the protein: the chromophore. Mutating the chromophore or its surrounding residues changes the photophysical properties of the protein, for instance the excitation and emission wavelengths. This, combined with an ever growing array of organisms that naturally produce their own fluorescent proteins, led to a big diversity of fluorescent proteins, spanning almost the entire visible spectrum.

Since the start of the new millennium, a new type of fluorescent proteins has been discovered: photoactivatable fluorescent proteins. The first category are the photoconvertible proteins, that can be converted from a green-emitting to a red-emitting state by irradiation of a specific wavelength. A second category are the photoswitchable fluorescent proteins, that can be reversibly switched on and off (i.e. from a fluorescent to a non-fluorescent state) by means of irradiation of light with specific wavelengths. This kind of fluorescent proteins has enabled numerous advances in diffraction-unlimited far-field microscopy, especially what concerns the technique of photo-activated light microscopy. One of the latest discoveries in the field of photoactivatable fluorescent proteins is IrisFP, a fluorescent protein that is photoconvertible from

green to red and both the green and red species can reversibly switch from a bright to a dim state.

Another unexpected property of fluorescent proteins is that they can be engineered to produce reactive oxygen species upon excitation. Such kind of molecules are called photosensitizers. These highly active oxygen species react with almost any molecule, explaining its toxic nature. One such fluorescent protein is known to date, called KillerRed. Its effectiveness in chromophore assisted light inactivation in both prokaryotic and eukaryotic cells is proven.

The major question of this project was whether or not it is possible to get a grip on the properties of fluorescent proteins from a mechanistic point of view. This means, can we rationally engineer specific properties into fluorescent proteins, based on structural data?

Starting from two different photoconvertible fluorescent proteins (mEosFP and Dendra2) and based on structural studies on IrisFP, we have been able to rationally engineer IrisFP-like (i.e. a both photoconvertible as photoswitchable) fluorescent proteins. This has been done using a site-directed mutagenesis approach. The characteristics of these mutant proteins have been studied as to select the proteins that show the both photoswitchable and photoconvertible behavior we were looking for. In the course of this characterization, two such fluorescent proteins, appropriate for dual-color photo-activated light microscopy, have been selected and one of them was called NijiFP. Their behavior brings dual-color photo-activated light microscopy with only two laser beams in close reach. The same has been done starting from a photoswitchable fluorescent protein (Dronpa). The resulting protein proved to be photoconvertible, but has at the same time lost its photoswitching properties.

In the light of two-photon chromophore-assisted light inactivation, we reasoned that it would be very useful to make a green photosensitizer. Based on structural studies of KillerRed, we deduced the structural features that lay at the basis of the photosensitizing mechanism and have built them into eGFP, thus trying to make KillerGreen. This mutant seems to bear photosensitizing properties, although it is essentially non-fluorescent. Further, more in-depth characterization will be needed to confirm the first basic experiments with KillerGreen.

In this thesis, we have tried to provide enough convincing evidence of the fact that indeed the properties of fluorescent proteins can be altered by rational engineering. We hope to be able to extend this research to even more advanced systems leading to renewed insight in the structure, activity and applications of these remarkable proteins.

CHAPTER 15

Samenvatting

O. Shimomura extraheerde in de zestiger jaren voor het eerst een fluorescent proteïne dat voorkwam in een kwal (*Aequorea victoria*) die aan de Noord-Amerikaanse westkust leeft. Kort daarna werd het DNA dat voor dit merkwaardige proteïne codeert geïsoleerd en in verschillende organismen, gaande van bacteriën over planten tot muizen, gekloneerd en tot expressie gebracht. Het proteïne heeft de vorm van een cilinder waarvan de wand gevormd wordt door β-strengen. Axiaal loopt een α-helix die het hart van het proteïne, het chromofoor, vormt en op zijn plaats houdt. Door diverse mutaties in het chromofoor en zijn directe omgeving in te voeren, konden verschillende fotofysische parameters, bijvoorbeeld excitatie- en emissiegolflengten, veranderd worden. Samen met het feit dat steeds steeds meer organismen die fluorescent proteïnen maken gevonden worden, gaf dit aanleiding tot een grote diversiteit aan fluorescente proteïnen, met kleuren die ongeveer het hele zichtbare spectrum omvatten.

Aan het begin van het nieuwe millennium werd een nieuw soort fluorescente proteïnen ontdekt, die fotoactiveerbaar werden genoemd. Een eerste categorie waren de fotoconverteerbare fluorescente proteïnen, die van een groene naar een rode toestand kunnen worden gebracht door instralen van licht met een specifieke golflengte. Een tweede categorie zijn de fotoschakelbare fluorescente proteïnen. Deze kunnen aan- en uitgeschakeld worden (dit betekent, van een fluorescente naar niet-fluorescente toestand en omgekeerd gebracht worden) ook door instralen van licht met specifieke golflengten. Dit soort proteïnen kent reeds vele toepassingen,

als cellulaire merkers maar ook als label dat gebruikt kan worden in diffractie-ongelimiteerde microscopie (bijvoorbeeld in de techniek van foto-geactiveerde lichtmicroscopie (PALM)). Een van de laatste ontwikkelingen is de ontdekking van IrisFP, een fluorescent proteïne dat zowel fotoconverteerbaar als fotoschakelbaar is.

Een andere opmerkelijke eigenschap van fluorescente proteïnen is dat ze danig gemuteerd kunnen worden, dat ze reactieve zuurstofdeeltjes produceren. Deze zeer reactieve deeltjes interageren met zo goed als elk molecule en vernielen het veelal, vandaar de toxiciteit van dit soort proteïnen. Een dergelijk fluorescent proteïne werd ontwikkeld en KillerRed genoemd. Het kan gebruikt worden in chromofoor-geassisteerd licht inactivatie in zowel prokaryote als eukaryote celsystemen.

Deze grote vraag van dit masterproject is of het al dan niet mogelijk is om een danig begrip van fluorescente proteïnen op te bouwen, dat het mogelijk wordt om vanuit een structureel standpunt hun eigenschappen te begrijpen en naar de hand te zetten. Anders geformuleerd: is het mogelijk om rationeel bepaalde eigenschappen in fluorescente proteïnen in te bouwen, gebaseerd op structurele data?

Vertrekkende vanaf twee fotoconverteerbare fluorescente proteïnen (mEosFP en Dendra2) en ons baserend op structurele gegevens van IrisFP, zijn we erin geslaagd om IrisFP-achtige (i.e. zowel fotoconverteerbare als fotoschakelbare) proteïnen te maken. Dit gebeurde op rationele wijze met plaats-specifieke mutagenese. De karakteristieken van deze mutante proteïnen werden bepaald met het oog op het selecteren van een proteïne met de specifieke fotoconverteerbare en fotoschakelbare eigenschappen. Inderdaad, twee dergelijke mutanten werden geselecteerd en voorgesteld als een goede kandidaten voor twee-kleurs PALM door gebruik te maken van slechts twee (in vergelijking met de klassieke vier) lasers. Op dezelfde wijze werd vertrekkende van het fotoschakelbare Dronpa een mutant gemaakt die fotoconverteerbaar was, hoewel het zijn fotoschakelbare eigenschappen verloor.

Met het oog op twee-foton chromofoor-geassisteerde licht inactivatie, probeerden we een groen fluorescent proteïne te maken dat reactieve zuurstofdeeltjes maakt. We baseerden ons hiervoor op structurele studies op KillerRed en vertaalden de structurele elementen naar eGFP, om aldus KillerGreen te maken. De mutant die werd bekomen lijkt fototoxische eigenschappen te bezitten, maar is tevens niet fluorescent. Dit betekent dat verdere karakterisatie nodig is om deze eerste tests te confirmeren en meer inzicht te krijgen in de werking van dit KillerGreen.

Met deze thesis hebben we voldoende bewijs gegeven voor het feit dat het zonder twijfel mogelijk is de eigenschappen van fluorescente proteïnen dusdanig te vatten, dat we ze specifiek naar onze hand kunnen zetten. We hopen dat deze aanpak verder getrokken kan worden en tot vernieuwende inzichten in de structuur, functie en toepassingen van deze merkwaardige proteïnen zal leiden.

Paper published during the course of this thesis

During the course of this thesis, we have published a paper on 2D and 3D data storage based on the particular properties of photoswitchable, photoconvertible and both photoswitchable and photoconvertible proteins [52]. My contribution to this paper has been the expression and purification of the protein and preparation of the IrisFP-coated Ni-NTA beads. The paper is reproduced hereafter.

Journal of Biotechnology xxx (2010) xxx–xxx

Contents lists available at ScienceDirect

Journal of Biotechnology

journal homepage: www.elsevier.com/locate/jbiotec

Data storage based on photochromic and photoconvertible fluorescent proteins

Virgile Adam[a,b,*], Hideaki Mizuno[a,c], Alexei Grichine[d], Jun-ichi Hotta[a], Yutaka Yamagata[e], Benjamien Moeyaert[a], G. Ulrich Nienhaus[f,g,h], Atsushi Miyawaki[c], Dominique Bourgeois[i], Johan Hofkens[a]

[a] Laboratory of Photochemistry and Spectroscopy, Department of Chemistry, Katholieke Universiteit Leuven, Celestijnenlaan 200F, 3001 Heverlee, Belgium
[b] European Synchrotron Radiation Facility, 6, rue Jules Horowitz, BP 220, 38043 Grenoble, Cedex, France
[c] Laboratory for Cell Function and Dynamics, Advanced Technology Development Group, Brain Science Institute, RIKEN, 2-1 Hirosawa, Wako-City, Saitama 351-0198, Japan
[d] Platform 'Optical Microscopy – Cell Imaging' UJF-Grenoble 1, Inserm U823, Institut Albert Bonniot, 38042 La Tronche, France
[e] VCAD System Research Program, RIKEN (The Institute of Physical and Chemical Research), 2-1 Hirosawa, Wako-City, Saitama 351-0198, Japan
[f] Institute of Applied Physics and Center for Functional Nanostructures, Karlsruhe Institute of Technology (KIT), 76128 Karlsruhe, Germany
[g] Institute of Biophysics, University of Ulm, 89069 Ulm, Germany
[h] Department of Physics, University of Illinois at Urbana-Champaign, 1110 West Green Street, Urbana, IL 6180, USA
[i] IBS, Institut de Biologie Structurale Jean-Pierre Ebel, CEA, CNRS, Université Joseph Fourier, 41 rue Jules Horowitz, 38027 Grenoble, France

ARTICLE INFO

Article history:
Received 18 November 2009
Received in revised form 30 March 2010
Accepted 8 April 2010
Available online xxx

Keywords:
Optical data storage
Photoconversion
Photochromism
Fluorescent proteins
Protein crystals
3D data storage

ABSTRACT

The recent discovery of photoconvertible and photoswitchable fluorescent proteins (PCFPs and RSFPs, respectively) that can undergo photoinduced changes of their absorption/emission spectra opened new research possibilities in subdiffraction microscopy and optical data storage. Here we demonstrate the proof-of-principle for read only and rewritable data storage both in 2D and 3D, using PCFPs and RSFPs. The irreversible burning of information was achieved by photoconverting from green to red defined areas in a layer of the PCFP Kaede. Data were also written and erased several times in layers of the photochromic fluorescent protein Dronpa. Using IrisFP, which combines the properties of PCFPs and RSFPs, we performed the first encoding of data in four colours using only one type of fluorescent protein. Finally, three-dimensional optical data storage was demonstrated using three mutants of EosFP (d1EosFP, mEosFP and IrisFP) in their crystalline form. Two-photon excitation allowed the precise addressing of regions of interest (ROIs) within the three-dimensional crystalline matrix without excitation of out-of-focus optical planes. Hence, this contribution highlights several data storage schemes based on the remarkable properties of PCFPs/RSFPs.

1. Introduction

In the quest for optical data storage devices of ever-higher density, organic substrates have often been suggested as a potentially interesting storage medium. The possibility of using organic dyes displaying photochromic properties (i.e. that can be reversibly photoswitched between two states having distinct spectral properties) to design rewritable optical data storage devices was first suggested by Y. Hirschberg more than 50 years ago and further explored by numerous researchers (Berkovic et al., 2000; Irie, 2000; Kawata and Kawata, 2000; Yokoyama, 2000; Irie et al., 2002). The molecules which were first explored are known as spiropyrans. Spiropyrans can be reversibly photocyclised to their merocyanine forms that exhibit spectral properties distinct from those of their native forms (Hirschberg, 1956). While Hirschberg showed that most of the photochromic molecules in solution can be reversibly phototransformed after the absorption of a single photon at room temperature, other researchers demonstrated that some molecules retain photochromic properties in a rigid medium (Lewis and Lipkin, 1942). Furthermore it was demonstrated that photochromism can be produced by two-photon excitation (TPE) (Mandzhikov et al., 1973). The probability of simultaneous absorption of two photons is proportional to the square of the intensity and, therefore, two-photon excitation only allows the excitation of molecules at the very focus of the excitation beam in a bulk material. This latter point is crucial if one intends to address a particular volume of optically encoded information (voxel) within a three-dimensional matrix in order to encode more data than on a surface. For transparent materials, three-dimensional optical encoding was pioneered by the invention of holographic data storage (van Heerden, 1963), relying on the recording of interference patterns within a thick photosensitive material. It opened the way to the development of irreversible (Chen et al., 1968) and reversible (von der Linde and Glass, 1975) three-dimensional optical encoding techniques on various substrates such as mineral crystals (Andersen and Marrakchi, 1994; Heanue et al., 1996; Bai et al., 1997), glass (Cheben and Calvo, 2001), liquid crystals (Jang and Shin, 2001) or plastic polymers (Dubois et al., 2005; Sheridan et al., 2007). This technology obviously led to the creation of multilayer holographic discs, designed for optical mass storage application (McLeod et al., 2005; McLeod et al., 2008).

In thick non-transparent materials such as certain photochromic samples, the use of a non-linear process such as TPE ensures that the information stored outside the focal volume element does not interfere with the addressed data during the storage and/or readout process. The idea has thus been proposed to use TPE of photochromic dyes to create rewritable 3D data storage devices (Mitsunaga et al., 1988; Parthenopoulos and Rentzepis, 1989; Mitsunaga and Uesugi, 1990; Day et al., 1999; Gu and Day, 1999; Shen et al., 2001).

In contrast to the first attempts of using for this purpose small organic molecule, the idea of using biological macromolecules as a substrate for data storage was introduced only recently. While research on data storage based on DNA exists (Cox, 2001; Yachie et al., 2007), the use of the photochromic properties of proteins was pioneered with bacteriorhodopsin (bR) (Tallent et al., 1996). The spectral shifts between the different intermediate states of bR, assisted by the fact that the molecule easily forms 2D crystal-like arrangements, made this protein an interesting target to develop a rewritable storage medium (Bae et al., 1999; Fischer et al., 2003; Yao et al., 2005a,2005b; Ortiz-Lombardía and Verma, 2006) and led some researchers to propose the design of a biological DVD-like device by spin-coating a disk with bR (Renugopalakrishnan, 2006).

Since using fluorescence is an efficient and all-optical way of addressing the molecular state at specific locations in a structure, the use of fluorescent proteins for similar rewritable data storage devices was proposed shortly after the first reports based on using bR. In particular, the photoinduced cycling between the protonated and deprotonated forms of the green fluorescent protein (GFP) was suggested as an interesting research path for data storage at the single molecule level (Tsien, 1998).

Next to their invaluable role for cell imaging applications, fluorescent proteins (FPs) have been heavily used in a variety of biotechnological applications. For example, variants of FPs have been designed that serve as pH sensors (Hanson et al., 2002; McAnaney et al., 2002; Hess et al., 2004; Remington et al., 2004; McAnaney et al., 2005), calcium sensors (Miyawaki et al., 1997; Nagai et al., 2004), zinc sensors (Evers et al., 2008), ADP/ATP sensors (Berg et al., 2009), generators (Bulina et al., 2006) or sensors (Markvicheva et al., 2008) of reactive oxygen species, timers for gene expression (Terskikh et al., 2000) or for monitoring of time-dependent expression of proteins (Li et al., 2000; Shibasaki et al., 2003). More recently, the use of photoactivatable fluorescent proteins (PAFPs) contributed to the development of super-resolution microscopy schemes (Doose, 2008; Heilemann et al., 2009a) such as (F)PALM (Betzig et al., 2006; Hess et al., 2006)/(d)STORM (Rust et al., 2006; Heilemann et al., 2008; van de Linde et al., 2008; Heilemann et al., 2009b; van de Linde et al., 2009). The potential of PAFPs for nanobiotechnology applications, notably as being the active medium in novel biological data storage devices, has been suggested several times (Dickson et al., 1997; Andresen et al., 2005; Sauer, 2005; Schafer et al., 2008).

Current commercial optical data storage devices (e.g. CD, DVD, Blu-ray discs, etc.) are limited to a two-dimensional storage array in which molded pits encode binary information. Although efforts have been made to increase the storage density in these optical discs e.g. by using shorter wavelengths (Blu-ray technology) and by reducing the pit size (Kong et al., 2008), the two-dimensional approach evidently runs into a physical limitation in terms of achievable data density.

Expanding to the third dimension implies using an ordered pattern of perfectly aligned and highly condensed three-dimensional arrangement of photosensitive elements. Although several media were tested over the years, such as polymer matrices (Wang and Esener, 2000; Gindre et al., 2006), single 3D crystals (of proteins) represent the most condensed and perfectly self-assembled three-dimensional patterns one can possibly obtain.

This latter approach has actually been proposed in a patent (Hell et al., 2007) that introduces the concept of using single crystals of PCFPs/RSFPs to create a 3D data storage medium in which each protein molecule in the crystal would represent a data bit. Each molecule can indeed be considered as a binary encodable element, depending on whether the protein is in its bright or dark state. Note however that although the concept is valid, it is not yet possible to optically address a single molecule within a dense crystalline environment (typical concentrations of ~20 mM).

Some PAFPs (namely PCFPs) are capable of undergoing irreversible conversions by changing their fluorescence colour from green to red, due to a photoinduced cleavage of a peptide bond flanking their chromophore, ultimately leading to the extension of the chromophoric conjugated (Mizuno et al., 2003; Nienhaus et al., 2006; Lelimousin et al., 2009).

Other FPs (RSFPs) display a photochromic behaviour, undergoing reversible switching between a bright and a dim state. Initially, this photoswitching has been proposed to be due to a cis/trans isomerisation of the chromophore (Lukyanov et al., 2000), which was structurally verified later for certain FPs (Andresen et al., 2005). However, the mechanism can be more complicated for other FPs as has been demonstrated. Indeed, for the RSFP Dronpa it has been shown that switching results from a photoinduced protonation of the chromophore accompanied by a cis/trans isomerisation (Habuchi et al., 2005; Habuchi et al., 2006; Andresen et al., 2007; Flors et al., 2007; Fron et al., 2007; Adam et al., 2008; Mizuno et al., 2008).

These two types of photoactivation have been shown to be extremely useful for tracking motions of cells. Several examples of cell tracking after green-to-red photoconversion using PCFPs can be cited, such as the use of Kaede and KikGR to follow neurulation processes (Hatta et al., 2006; Sato et al., 2006) or the tracking of cell movements and cellular compartments trafficking using EosFP (Nieuwkoop and Faber, 1994; Nienhaus et al., 2006; Wiedenmann and Nienhaus, 2006). RSFPs, like Dronpa, have also been used to track such cell motions (Aramaki and Hatta, 2006).

PCFPs can also be used advantageously to track intracellular events such as protein movements in time, as it was the case in experiments using EosFP (Wiedenmann et al., 2004; Nienhaus et al., 2006; Wiedenmann and Nienhaus, 2006) or Dendra2 (Chudakov et al., 2004; Chudakov et al., 2007a,2007b) for example. Here again, the use of photochromic FPs allows similar observations (Ando et al., 2004; Fujioka et al., 2006).

These two different switching modes constitute alternative basis for data encoding and may potentially be combined in the same crystal. In addition, the biodegradability of these fluorescent proteins in principle provides a sustainable solution to the waste recycling of the current data storage media at their 'end of life'. However, significant problems imposed by their biolog-

Abbreviations: AOTF, Acousto-optic tunable filter; bR, Bacteriorhodopsin; CD, Compact disc; DVD, Digital versatile disc; (d)STORM, (direct) STochastic optical reconstruction microscopy; EDC, 1-Ethyl-3-[3-dimethylaminopropyl]carbodiimide hydrochloride; ESD, ElectroSpray deposition; (F)PALM, (Fluorescence) PhotoActivated localisation microscopy; FWHM, Full width at half maximum; ITO, Indium tin oxide; NHS, *N*-Hydroxysulphosuccinimide; OPE, One-photon excitation; PAFP, PhotoActivatable fluorescent protein; PCFP, PhotoConvertible fluorescent protein; PLL, Poly-L-lysine; RESOLFT, REversible saturable opticaL fluorescence transitions; RIKEN, Rikagaku KENkyusho; ROI, Region of interest; RSFP, Reversibly switchable fluorescent protein; STED, STimulated emission depletion microscopy; TPE, Two-photon excitation; WORM, Write-once–read-many; WMRM, Write-many–read-many.

* Corresponding author. Laboratory of Photochemistry and Spectroscopy, Department of Chemistry, Katholieke Universiteit Leuven, Celestijnenlaan 200F, bus 02404, 3001 Heverlee, Belgium. Tel.: +32 16 327399; fax: +32 16 327990.
E-mail address: virgile.adam@chem.kuleuven.be (V. Adam).

0168-1656/$ – see front matter © 2010 Elsevier B.V. All rights reserved.
doi:10.1016/j.jbiotec.2010.04.001

ical nature (photobleaching, need for a solvated state, sample aging, thermal instability) need to be tackled. The use of cryogenic temperatures could be eventually a (not very practical) solution, given that the phototransformations are preserved at such temperature. Alternatively, a systematic screening of FPs combined with random or rational mutagenesis could potentially generate more robust molecules, notably in terms of (photo)stability and fatigue resistance to ensure the robustness of encoded data. Although many practical issues stand in the way of a working device, the photoconvertible and photochromic properties of PCFPs/RSFPs form an interesting starting point for the development of write-once–read-many (WORM) (Wiedenmann et al., 2005) or write-many–read-many (WMRM) devices (Ando et al., 2004).

In this contribution, we show irreversible and reversible optical data storage using several PCFPs/RSFPs. We used the PCFP Kaede (Ando et al., 2002), the RSFP Dronpa (Ando et al., 2004), and three mutants of the PCFP EosFP (Wiedenmann et al., 2004; Nienhaus et al., 2006): the dimeric form d1EosFP, the monomeric form mEosFP (Wiedenmann et al., 2004), and IrisFP. IrisFP is a variant of EosFP that displays the unique property of being both irreversibly photoconvertible from green to red and reversibly switchable between a bright and a dark state in both the green and red forms (Adam et al., 2008). We show that IrisFP offers the possibility to encode data using a base-4 system. To demonstrate the potential of protein-based data storage methods, the FPs were used either by coating uniform layers of proteins on a variety of different surfaces, or by crystallising them to single 3D crystals.

2. Materials and methods

2.1. Surface coating techniques for Kaede, Dronpa and IrisFP

For the irreversible and reversible writing experiments performed on layers of FPs, a variety of coating techniques (cross-linking or immobilisation in a polymer matrix) were tested in order to deposit Kaede, Dronpa or IrisFP. Kaede was expressed and purified as described elsewhere (Ando et al., 2002) and was then deposited on an indium tin oxide (ITO) coated slide glass by electrospray deposition (ESD) using an Esprayer arrayer device (ES-3000, Fuence, Wako-City, Japan). Details of the ESD method are reported elsewhere (Lee et al., 2003). The resulting Kaede layer was covered with a cover glass and subjected to microscope-based light exposure for optical writing and reading steps.

For the preparation of Dronpa layers, the expression and the purification steps were performed as described elsewhere (Ando et al., 2004). A cover glass was first coated with 2.5 mg/ml of poly-L-lysine (PLL, MW 30,000–70,000) and kept overnight before a thorough washing step with 50 mM HEPES–NaOH buffer pH 7.5 was applied. Amino groups of PLL on the surface were coupled with carboxyl groups of Dronpa as follows: 1 mg/ml of protein in 50 mM HEPES–NaOH buffer pH 7.5, was mixed with same volume of a solution of (0.2 M EDC/0.05 M NHS) zero-length cross-linking agents and placed on the cover glass for ~15 min. The cover glass was then washed with the HEPES–NaOH buffer and mounted on a slide glass, facing the coated side to the slide glass.

For IrisFP, the expression and purification was carried out as previously described (Adam et al., 2008). The His-tag on the N-terminus of the protein was used to fix it on the surface of Ni-NTA agarose beads (Qiagen, bead diameter between 45 and 165 μm) as follows. A volume of 20 μl of IrisFP at 1.9 mg/ml in PBS (pH 7.4) was gently mixed with the same volume of 50% Ni-NTA agarose slurry for 5 min. The beads were washed with 1 ml of 20 mM HEPES–KOH buffer (pH 7.4) twice and suspended into 200 μl of the buffer. A small amount of the suspended beads were placed on a slide glass, a cover glass was finally sealed on the slide glass with clear manicure.

2.2. Protein crystallisation

Three mutants of the green-to-red photoconvertible fluorescent protein EosFP (Wiedenmann et al., 2004; Nienhaus et al., 2006) have been crystallised: a dimeric variant called d1EosFP and the monomeric form mEosFP (Wiedenmann et al., 2004) as well as the variant called IrisFP (Adam et al., 2008). The expression and purification of these mutants are described elsewhere (Wiedenmann et al., 2004; Adam et al., 2008).

Crystals of d1EosFP were grown using the hanging-drop vapour-diffusion method and by mixing 2 μl of a solution of d1EosFP at 10.3 mg/ml and 2 μl of a solution containing 2.2 M ammonium sulphate, 0.1 M bicine pH 8.6. To the final solution, 10% glycerol was added, which allowed obtaining much bigger and thicker crystals.

For mEosFP, crystals were obtained with the same method but mixing 0.2 μl of a solution of mEosFP at 9.2 mg/ml with 2 μl of a solution containing 2.2 M ammonium sulphate, 0.1 M Tris/HCl, pH 8.5.

Crystals of IrisFP were obtained as previously described (Adam et al., 2008). All crystals were grown at 20 °C and were obtained within a few days, reaching final dimensions of 470 μm × 130 μm × 90 μm, 430 μm × 45 μm × 15 μm and 430 μm × 100 μm × 100 μm for d1EosFP, mEosFP and IrisFP, respectively.

2.3. Writing with one-photon excitation on Kaede and Dronpa coated surfaces

For both Kaede and Dronpa, an inverted laser-scanning microscope was used (FluoView FV500, Olympus, Tokyo, Japan). The microscope was equipped with a 6-mW 405-nm laser diode (FV5-LD405, Olympus, Tokyo, Japan), a 20-mW 488-nm diode-pumped solid-state laser (Sapphire 488-20, Coherent, Santa Clara, CA, USA) and a 1-mW 543-nm He–Ne laser (05-LGP-193, Melles Griot, Bensheim, Germany). The objective lens was Apo40xWLSM/UV/0.90 (Olympus, Tokyo, Japan). The matrix size of the image was 512 × 512 pixels with a pixel size corresponding to 155 nm for the experiment with Kaede and 311 nm for the experiment with Dronpa.

To convert the protein Kaede to its red emitting state, the 405-nm laser beam (332 W/cm^2) was scanned (pixel dwell time of 10 μs) seven times. To readout the written pattern, the 488-nm (113 W/cm^2) and 543-nm (1.3 kW/cm^2) laser beams were used sequentially, and a Kalman filter with four times scan was applied to reduce the noise in the image.

To repeatedly write and erase patterns on the Dronpa layer, the scanning parameters to read, write, and erase these patterns were as follows: read, 488 nm (113 W/cm^2), scan once; write, 405 nm (332 W/cm^2), scan twice; erase, 488 nm (5.5 kW/cm^2), scan five times (pixel dwell time of 10 μs).

2.4. Encoding data using four colours on an IrisFP coated bead

Using the unique properties of IrisFP, data were encoded in four colours on the surface of a single microscopic bead coated with the protein. We performed our experiment by focusing on the center of a large bead having a diameter of 117 μm. The observed field of view was 22 μm × 22 μm, so that distortion of the image induced by the curvature of the bead surface was kept to a minimum.

An inverted confocal microscope was used (FluoView FV1000, Olympus, Tokyo, Japan). The microscope was equipped with a 50-mW 405-nm laser (Excelsior-405C-50, Spectra Physics), a 20-mW 488-nm laser (Cyan OEM, Spectra Physics) and a 50-mW 561-nm laser (Excelsior-561-50, Spectra Physics). An excitation beam splitter (BS 20/80) and an emission dichroic mirror (SDM 560) were used so that green and red channels collected signals at emission wavelengths between 500–535 nm and 575–620 nm, respectively. A UPlanSApo 60×/1.35 objective lens was used (Olympus, Tokyo, Japan). The matrix size of the image was 512 × 512 pixels, with a pixel size corresponding to 40 nm. Since we focused on a very small region, we performed all the different photoactivations using a short dwelling time (2 μs/pixel) in order to limit non-desired phototransformations.

The complete photoconversion of IrisFP to its red state was performed by scanning with the 405-nm laser light (263 W/cm^2) for 35 times (seven series of five scans). A partial photoconversion from green to red was achieved by scanning with the 405-nm laser light at the same power for three times (three series of one scan). To switch the green molecules to their dark state, we scanned with the 488-nm laser light (500 W/cm^2) for 40 times (two series of 20 scans). Finally, to switch the green molecules back to their bright state, we scanned with the 405-nm laser light (47 W/cm^2) for one time. To read the encoded letters, the imaging was performed using one scan of the 488-nm laser light (52 W/cm^2) for the green channel and of the 561-nm laser light (125 W/cm^2) for the red channel. A Kalman filter with four times scan was applied to reduce noise in the image.

2.5. Writing using one- and two-photon excitation inside crystals of d1EosFP, mEosFP and IrisFP

Single crystals were mounted by pipetting and depositing drops containing the crystals inside individual chambers of Lab-Tek trays. All the writing/recording experiments on protein crystals were performed using the two following systems.

For one-photon excitation (OPE) inside a crystal of d1EosFP, a mercury arc lamp was used, in combination with a DAPI filter (360–370 nm) during 5 s at 0.8 W/cm^2. The photoconverted area was limited by the field diaphragm and corresponds to an area of ~0.1 mm^2.

The matrix size of the image was 512 × 512 pixels with a pixel size corresponding to 394 nm (pixel dwell time of 2.5 μs).

Imaging was performed using 488-nm laser light (140 W/cm^2) for the green channel and 543-nm laser light (619 W/cm^2) for the red channel. An excitation dichroic beam splitter (HFT 488/543) and an emission long pass filter (NFT 545) were used. Filters were set so that green and red channels collected signals at emission wavelengths between 500–550 nm and 556–716 nm, respectively. A Kalman filter with two times scan was applied to reduce noise.

For experiments on mEosFP and IrisFP, an inverted multiphoton laser-scanning microscope was used (LSM 510 NLO Meta, Carl Zeiss, Jena, Germany). The microscope was equipped with a Tsunami Ti:Sa laser, 80 MHz, 120 fs, tunable between 690 nm and 1100 nm (Spectra Physics, Mountain View, CA, USA). The objective lens was a Plan-Apochromat 63×/1.4 (Carl Zeiss, Jena, Germany).

Phototransformations using two-photon excitation (TPE) were performed at 800 nm (2.6 MW/cm^2 average), 10 iterations. For this series of measurements, the matrix size of the images was 512 × 512 pixels with a pixel size corresponding to 70 nm (pixel dwell time of 1.6 μs).

The readout was performed here in OPE confocal mode using the lowest available laser power in order to minimise eventual heating, irreversible bleaching and dehydration effects. Still, the signal to noise ratio was good and the confocal alignment was maintained throughout the 30-μm thick crystal.

For mEosFP, imaging was performed in the sequential-scan 'multitrack' mode using the 488-nm and 543-nm lasers. An excitation dichroic beam splitter (HFT 488/543) and an emission long pass filter (NFT 545) were used. Filters were set so that green and red channels collected signals at emission wavelengths between 505–550 nm and 565–615 nm, respectively. A mean filter with eight times scan was applied to reduce noise.

For IrisFP, imaging was performed using 488-nm laser light (56 W/cm^2) and the 543-nm laser light (5 W/cm^2) for the red channel. An excitation dichroic beam splitter (HFT KP 700/488) and an emission long pass filter (NFT 545) were used, so that green and red channels collected signals at emission wavelengths between 500–550 nm and 556–716 nm, respectively. A mean filter with four times scan was applied to reduce noise.

For erasing letters written at the crystal surface of IrisFP, a mercury arc lamp was used, in combination with a DAPI filter (360–370 nm) during 1 s at 0.8 W/cm^2.

3. Results and discussion

3.1. Two-dimensional encoding on Kaede and Dronpa coated surfaces

Using FPs as optical memory media requires that the proteins are rigidly fixed on a support in order to avoid the loss of written information by protein diffusion. One possibility to achieve this goal is to coat the protein on a surface.

We first used an ITO coated glass as a support and deposited the green-to-red photoconvertible fluorescent protein Kaede by electrospray, to produce a homogeneous protein layer that originally emitted green fluorescence (Fig. 1a). A numeric mask representing the logo of the RIKEN Brain Science Institute (Japan) was prepared and loaded into the controlling software of the Olympus FV500 laser-scanning microscope. Green-to-red photoconversion of the proteins at specific pixels inside this mask was achieved by gating of a 405-nm laser beam with an acousto-optic tunable filter (AOTF) during the laser scanning. The results (Fig. 1b and Supplementary movie S1) show an excellent contrast between green and red molecules, with a clear identification of each written letter having a line width of less than 3 μm. Fluorescent colours of each pixels could be read out multiple times. The photoconversion of Kaede being irreversible, the layer of Kaede worked as a write-once–read-many (WORM) data storage device.

In contrast to this irreversible writing and in order to use a fluorescent protein as a rewritable medium, a photochromic FP must be used. A thin layer of the reversibly switchable FP Dronpa was produced by covalently binding the protein carboxyl groups to the amino groups coated on a treated glass surface. Several masks depicting logos and names (in English and Japanese) of the RIKEN, Brain Science Institute and Laboratory for Cell Function and Dynamics (Japan) were prepared and loaded into the controlling software of the Olympus FV500 laser-scanning microscope. The initial green fluorescence of the layer was erased by conversion to the dark state upon strong illumination of a 488-nm laser, and pattern conversion to the bright state was achieved by AOTF gating of 405 nm laser light during the scanning. The results (Fig. 2 and Supplementary movie S2) show that the contrast between bright and dark molecules is excellent although after several cycles, a certain photofatigue (40%) of the protein can be noticed (Fig. 2d and p, and Fig. S3). This photofatigue is much larger than the one reported previously (Ando et al., 2004) where only 25% loss of contrast was observed after 100 cycles. In this experiment, we used higher laser powers for generating the switching and for increasing the contrast between bright patterns and dark zones, inducing a faster irreversible photobleaching..

Since the photoswitching of Dronpa is a reversible process, the erase/write process could be repeated multiple times on exactly the same area of the Dronpa layer, and thus, this layer can be considered as a write-many–read-many (WMRM) data storage device. In spite of their advantages, there are two major difficulties using RSFPs as data storage media: the first one is that fluorescent proteins are rather 'weak' molecules, sensitive to photobleaching and, as mentioned above, with a photofatigue-limited number of achievable

G Model
BIOTEC 5463 1–11
ARTICLE IN PRESS

Please cite this article in press as: Adam, V., et al., Data storage based on photochromic and photoconvertible fluorescent proteins. J. Biotechnol. (2010), doi:10.1016/j.jbiotec.2010.04.001

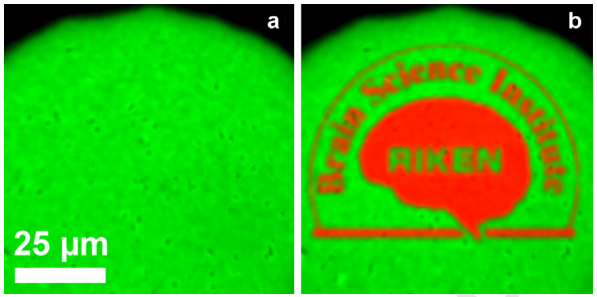

Fig. 1. 2D irreversible data storage using Kaede. A surface on which the green-to-red PAFP Kaede was coated by electrospray deposition was imaged by sequential excitations at 488 nm (green channel) and 543 nm (red channel) at 113 W/cm² and 1.3 kW/cm², respectively. (a) The logo of the RIKEN Brain Science Institute (Japan) was then drawn on the surface, photoconverting with a 405-nm laser (332 W/cm²) the green emitting proteins to their red form (pixel dwell time of 10 μs, seven scans). (b) The obtained contrast is excellent and reveals no blurring even for details as small as 3 μm.

write/erase cycles as compared with existing optical data storage media, capable of undergoing several thousands of cycles. Another major drawback concerns the long-term data storage of encoded elements using such photochromic fluorescent proteins due to their limited thermal stability. Once photoswitched, RSFPs have indeed a clear tendency to thermally switch back to their initial state (Andresen et al., 2005; Habuchi et al., 2005; Adam et al., 2008). This slow autorecovery could be avoided for example by keeping the samples at cryogenic temperatures once the data encoded or by screening for variants of RSFPs with bistable conformations, but it obviously represents currently a difficulty to the development of efficient optical data storage devices using photochromic FPs.

Fig. 2. 2D reversible data storage using Dronpa. The photochromic fluorescent protein Dronpa was cross-linked on a surface coated with poly-L-lysine. The whole field of view of this surface was then illuminated 488-nm laser light (5.5 kW/cm², pixel dwell time 10 μs, five scans) to switch the protein to its non-fluorescent state (a, c, e, g, i, k, m, o) and by a weak 405-nm laser light (332 W/cm², pixel dwell time 10 μs, two scans) to switch the protein back to its fluorescent state, drawing defined patterns (b, d, f, h, j, l, n, p). Using this method, the logos of the RIKEN, Brain Science Institute and laboratory for cell function and dynamics, both in English and Japanese were sequentially drawn and erased on the very same surface. The images were obtained by scanning the surface with 488-nm light (113 W/cm²). The contrast between bright and dark molecules is excellent although after several cycles, a certain photofatigue of the protein can be noticed as one can see by comparing images d and p.

Please cite this article in press as: Adam, V., et al., Data storage based on photochromic and photoconvertible fluorescent proteins. J. Biotechnol. (2010), doi:10.1016/j.jbiotec.2010.04.001

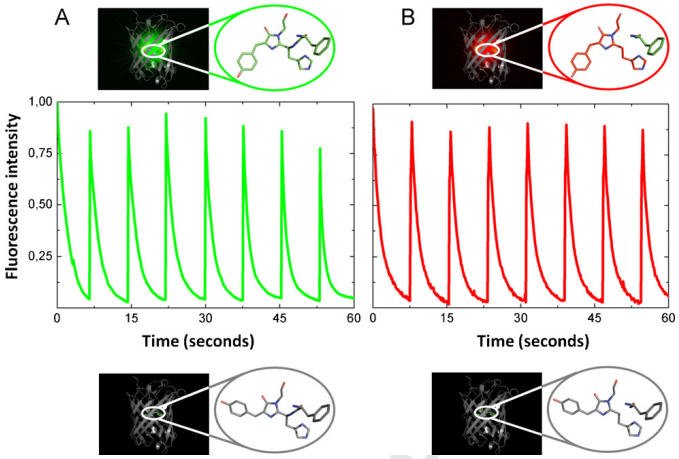

Fig. 3. Reversible photoswitching of green and red forms of IrisFP in crystals. (A) A crystal of IrisFP in its green form was mounted into a capillary and exposed to continuous illumination with 488-nm light (2.5 W/cm²), while 405-nm light (1 W/cm²) was switched on every 7.5 s for 25 ms. (B) After green-to-red photoconversion was visually checked (by strong illumination at 405 nm, using the direct light output from an optic fiber for ~1 mn), a crystal of IrisFP was mounted into a capillary and exposed to continuous illumination with 532-nm light (7.5 W/cm²) while 440-nm light (1 W/cm²) was switched on every 7.5 s for 200 ms. Insets show representations of the β-barrel structure of IrisFP and structural models of its chromophore in its two bright and two dark states.

3.2. Four-states data storage on an IrisFP coated surface

IrisFP is a newly characterised PAFP that is both capable of undergoing irreversible green-to-red photoconversion like Kaede and also reversibly photoswitching between a bright and a dark state, both in its green and red forms. These phototransformations are not only achievable in solution but also in crystals, with an excellent contrast between dark and bright states that can be cycled many times (Fig. 3). To combine the photochromic and photoconversion capabilities offered by IrisFP in order to create storage media for data encoded in four colours, green and red molecules of IrisFP can be photoswitched to their light-emitting state or kept to their dark state, forming a mosaic of dark, green, red or green + red = yellow areas.

On a surface coated with molecules of IrisFP, ensuring that half of the many molecules probed by the laser beam were previously irreversibly photoconverted to their red form, it becomes possible to perform the selective on/off reversible switching of both the green and red subpopulations and to encode data in 2 bits (four colours). This system allows the clear identification in a base-4 numeral system of the protein states numbered 0, 1, 2 and 3, corresponding to the proteins in their dark + dark = dark, green + dark = green, dark + red = red or green + red = yellow states (respectively 00, 01, 10 and 11 in binary format).

Multicolour rewritable encoding of data has already been successfully demonstrated but combining the photochromic properties of three different molecules (Uchida et al., 2005). Furthermore, for several organic compounds a multimode photochromism has been observed (Iyoda et al., 1989; Achatz et al., 1991; Spreitzer and Daub, 1996; Pina et al., 1997; Mrozek et al., 2001). However, all of these systems need combined light excitation and a second external stimulus (rise of temperature or oxidation/reduction of the system) to perform a complete change between the different states. The two-bit encoding presented here is, to our knowledge, the only all-optically biphotochromic system reported to date and is achievable thanks to the complex photoreactions allowed, at the molecular level, by the interactions between the chromophore of IrisFP and its protein matrix environment.

Practically, on the surface of a bead coated with IrisFP (Fig. 4a), we performed by strong illumination at 405 nm the green-to-red photoconversion of a ROI defining the letter "K" (Fig. 4b–d) and the partial photoconversion (by reducing the 405-nm time exposure) of a ROI defining the letter "U" (Fig. 4e–f). After the complete switching of all the green molecules in the sample, including the non-converted ones in the ROI forming the letter U, to their dark state (Fig. 4g), green molecules previously switched off within ROIs defining the letters "U" and "L" were back-switched to their bright state, resulting in an image composed of four colours (Fig. 4h): on a black background, the word KUL, standing for the Katholieke Universiteit Leuven (Leuven, Belgium) was thus written with its three letters coloured in red, yellow (red + green) and green, respectively.

With this method, we were able to obtain a surprisingly good contrast between each colour, even for ~5-μm letters having a line width of less than 650 nm (FWHM). This result suggests that this method can easily compete with photomicrolithography experiments and that we can in principle push forward our efforts by reducing the size of the encoded elements down to the diffraction limit of resolution (~200 nm) and maybe even further, by applying a 4Pi configuration and STED-like subdiffractional methods compatible with the super-resolution imaging of photoswitchable FPs (Hell et al., 2003; Hell, 2004; Hofmann et al., 2005; Dedecker et al., 2007). Such an enhancement would allow creating patterns comparable with those created by nanolithographic processes and with the size of pits in DVDs and Blu-ray discs.

The use of such a base-4 system obviously allows the doubling of the storage capacity as compared with a simple on/off switcher. While the 6-letter word "IrisFP" for example, is coded with 48 dig-

Please cite this article in press as: Adam, V., et al., Data storage based on photochromic and photoconvertible fluorescent proteins. J. Biotechnol. (2010), doi:10.1016/j.jbiotec.2010.04.001

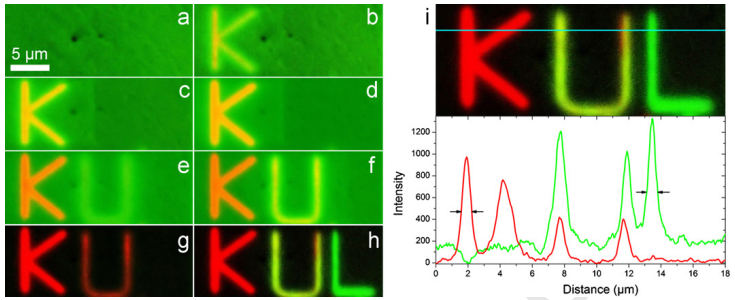

Fig. 4. Encoding in four colours using IrisFP. The surface of a large agarose-Ni-NTA bead (117 μm diameter) coated with IrisFP was imaged at 488 nm (52 W/cm^2) and 561 nm (125 W/cm^2) for green and red channels, respectively. (a) The pixel dwell time was set to 2 μs all along the experiment. Using a 405-nm laser light (263 W/cm^2, 35 scans), the letter "K" was written, photoconverting the initially green molecules to their red emitting state (b–e). A partial photoconversion of the molecules contained in a ROI defining the letter "U" was then performed by using the same power of 405-nm light during a least time exposure: three scans (e–f). The whole field of view was then illuminated at 488 nm (500 W/cm^2, 40 scans) to switch the green emitting molecules to their dark state, also turning the few unphotoconverted molecules in red regions to their dim state (g). Finally, the letter "L" was shaped in a dark region by using 405-nm light (47 W/cm^2, one scan) and the letter "U" in the region previously partially photoconverted to red, switching green molecules (non-converted in the second step of the writing process) back to their bright state. This ultimately wrote a yellow "U" (red + green) and a green "L" (h). Overall, an image in four colours (black, red, yellow and green) is obtained, forming the multicolour word KUL standing for Katholieke Universiteit Leuven (Belgium). An intensity profile (i) across the three letters (cyan line) shows the fraction of each states (detected by the green and red channels) and an average line thickness at FWHM for both red and green letters of 650 nm.

its in binary code, it will only require 24 digits in the quaternary system.

3.3. From 2D to 3D data storage using crystals of PAFPs

Encouraged by the results discussed above and by recent work successfully demonstrating the two-photon induced photoconversion from green to red in EosFP (Ivanchenko et al., 2007), we decided to expand our experiments to 3D protein crystals of EosFP variants using TPE. Assuming a single crystal of IrisFP measuring 100 μm × 100 μm × 100 μm, using 4-colour encoding, and assuming that TPE addresses voxels of about 1 fL (containing about 10^{12} individual molecules), we could in principle store as much as 250 KB in a volume as small as 1 nl.

We first used crystals of two variants of EosFP: a dimeric form called d1EosFP and the monomeric form called mEosFP. While d1EosFP forms rather lenticular-shaped and thick crystals, mEosFP forms long and thin rod-shaped crystals. In order to assess the added value of TPE versus OPE, we compared both excitation conditions. We first irradiated a crystal of d1EosFP with the near-UV part of the emission spectrum of a mercury arc lamp, thereby photoconverting a fraction of the crystal from green to red. The three-dimensional reconstruction of the crystal obtained by confocal microscopy shows that the irradiated part of the crystal underwent green-to-red photoconversion in a typical hourglass-shaped volume (Fig. 5a and Supplementary movie S5). In spite of a higher photon concentration at the focal plane and a reduced absorption along the optical axis due to the large optical density of the crystal, the whole thickness of the irradiated crystal volume photoconverted to the red form. Overall, the pronounced photoconversion throughout the whole excitation volume made it impossible to address a precise voxel within the crystal without altering neighbouring voxels at different depths. The data therefore demonstrate that one-photon excitation is obviously not the preferred method to perform 3D data storage within crystals. Such experiments have to resort to non-linear photochemistry.

Next, a 14-μm thick crystal of mEosFP was exposed to two-photon excitation at 800 nm. The photoconversion was shown to be more difficult in hydrated crystals than in dried crystals, for reasons that are not fully understood. No obvious differences in the phototransformation efficiency were observed for excitation wavelengths in the range from 760 nm to 840 nm. The excitation of a square ROI successfully led to the irreversible printing deep within the crystal. The thickness of the photoconverted square layer that could be imprinted this way was less than 3 μm (Fig. 5b).

3.4. Multicolour 3D data storage using crystals of IrisFP

Based on the results of 3D photoconversions obtained in crystals of EosFP and the multicolour writing experiments on surfaces coated with IrisFP, we set out to test if multicolour phototransformations in IrisFP were achievable using TPE writing inside

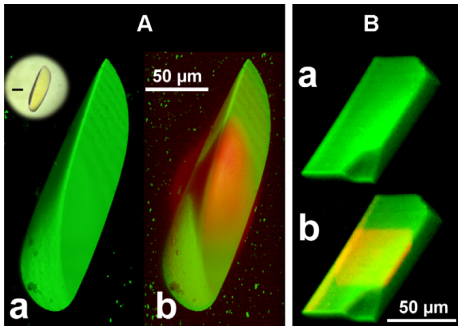

Fig. 5. One- and two-photon conversion within crystals of PCFPs. Crystals of d1EosFP (A) and mEosFP (B) were imaged at 488 nm (140 W/cm^2) for the green channel (a, b) and 543 nm (619 W/cm^2) for the red channel (b), prior (a) and after (b) green-to-red photoconversion. d1EosFP was photoconverted by a one-photon irradiation at 370 nm (0.8 W/cm^2, 5 s). mEosFP was photoconverted by two-photon irradiation at 800 nm (2.6 MW/cm^2 average, pixel dwell time 1.6 μs, four scans). When a crystal was converted by one-photon excitation, the typical hourglass shape of the 405-nm light entering and exiting the three-dimensional structure could be observed (A, b) – inset: bright field image of a d1EosFP crystal. When a crystal was converted by two-photon excitation, a thin shell (<4 μm) could be easily shaped within the crystal without altering neighbouring planes out of focus (B, b).

Please cite this article in press as: Adam, V., et al., Data storage based on photochromic and photoconvertible fluorescent proteins. J. Biotechnol. (2010), doi:10.1016/j.jbiotec.2010.04.001

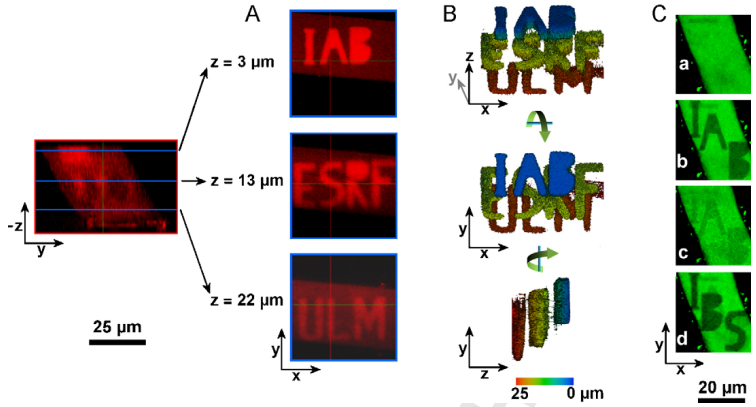

Fig. 6. 3D irreversible and reversible data storage using IrisFP. Using two-photon excitation at 800 nm (2.6 MW/cm^2 average, pixel dwell time: 1.6 μs), it was possible to photoconvert IrisFP from green-to-red at several depths within a single crystal (A), writing on three different crystal planes (<5 μm thick) the words "IAB", "ESRF" and "ULM", standing for the Institut Albert Bonniot (France), the European Synchrotron Radiation Facility (France) and the University of Ulm (Germany), respectively. Imaging occurred at 3 μm, 13 μm and 22 μm depths. A three-dimensional view of these three words is rendered colour-coded as a function of depth within the crystal (B). Surprisingly, while green-to-red photoconversion was particularly efficient when the crystal was dried, the main photoreaction at the same excitation wavelength (800 nm, 2.6 MW/cm^2 average, pixel dwell time: 1.6 μs) using fresh wet crystals revealed reversible on/off switching rather than just photoconversion (C). On the surface of a crystal of IrisFP (a), the word "IAB" was written (b) and erased by an illumination of the whole field of view at 370 nm (c), prior to the writing of the word "IBS" (d), standing for the Institut de Biologie Structurale (France). Although the photochromic properties of IrisFP seem to be retained in solvated crystals, we can notice a weak after-imagery of the word "IAB" due to an insufficient UV illumination or, on the contrary, from over-exposure to 800-nm light leading to partial irreversible photoconversion to the red state.

three-dimensional crystals. While the multicolour encoding mode that can be achieved with IrisFP can be mimicked by mixing several photochromic dyes on a surface, the fact that we can form crystals of a single multimode molecule would give IrisFP a clear advantage when considering dense 3D data encoding.

After having checked that the spectral properties of IrisFP were unchanged in the single crystal and observable by fluorescence microscopy (Fig. S4), we attempted to photoconvert (from green to red) defined regions of interest in a crystal of IrisFP at different depths. As already experienced for the other EosFP mutants (*vide supra*), we observed a significant effect of the humidity on the phototransformation yield. Irreversible green-to-red photoconversion under TPE occurred much more efficiently in dried crystals (contrary to reversible photoswitching using OPE, which did not appear to depend on humidity). This puzzling behaviour was reproducibly observed and corroborates recent experiments suggesting that the degree of moisture induces significant spectral changes in PAFPs (Aline Faro, personal communication). The mechanistic aspects of this phenomenon remain unclear but this could imply halochromic processes, meaning that dried samples could be more protonated than hydrated samples, hence favouring photoconversion in preference to photoswitching. Using TPE excitation, we noticed that while green-to-red photoconversion occurs preferentially in dry samples, reversible photoswitching becomes the main photoresponse pathway when crystals are kept hydrated. Since two-photon excitation spectra are generally broader and blue-shifted as compared to one-photon excitation spectra, different photochemical events eventually could be involved. Whatever the process involved, having crystals that easily photoconvert from green to red in dried conditions could potentially be a great advantage in terms of robustness of the biological matter used as optical data storage media. Since there would be no need to maintain and control the humidity in the sample, we could even envisage preserving and embedding single crystals inside a plastic polymer matrix as it has been already shown to be possible (Ravelli et al., 2007).

Next, we used a combination of OPE and TPE to store patterns in the crystals, similar to those burnt in protein layers. A single crystal of IrisFP was kept in the dark until evaporation of the microdroplet which confined it, and was then submitted to TPE excitation at 800 nm. Three different crystal depths (z_1 = 3 μm, z_2 = 13 μm, z_3 = 22 μm) were scanned in ROIs defining the three words "IAB", "ESRF" and "ULM", standing for the Institut Albert Bonniot (Grenoble, France), the European Synchrotron Radiation Facility (Grenoble, France) and the University of Ulm (Ulm, Germany). The confocal readout of the crystal clearly revealed the three words each written in a layer with a thickness of less than 5 μm (Fig. 6A and Supplementary movies S6 and S7). These results, which present the first successful demonstration of the potential use of activatable and switchable FPs for three-dimensional optical data storage, become even more interesting when realising that IrisFP crystals offer the possibility of combining irreversible and reversible data storage in multicolour and in three dimensions.

In order to demonstrate reversible data encoding in 3D, a fresh and hydrated crystal was selected. The microscope was focused on the bottom surface of the crystal. By irradiating the crystal at 800 nm (Fig. 6B, a), a two-photon-induced on-to-off switching was performed inside a ROI forming the word "IAB", standing for the Institut Albert Bonniot (Grenoble, France), which allowed to visualize this word with negative contrast (Fig. 6B, b). Next, the fluorescence was recovered by 5 s of wide field illumination with a mercury arc lamp in order to erase the word and reset the crystal (Fig. 6B, c).

After this step, we could however observe that some weak traces of the word "IAB" were still present. This could result from insufficient UV illumination or, on the contrary, from over-exposure to 800-nm light leading to partial irreversible photoconversion to the red state. Clearly the optimal use of IrisFP requires fine-tuned calibration of the UV light intensity.

Finally, a new ROI was prepared and, using the same TPE excitation at 800 nm, the word "IBS", standing for the Institut de Biologie Structurale (Grenoble, France) was written on the very same crystal

Please cite this article in press as: Adam, V., et al., Data storage based on photochromic and photoconvertible fluorescent proteins. J. Biotechnol. (2010), doi:10.1016/j.jbiotec.2010.04.001

surface (Fig. 6C, d). Between each step, the images were obtained by exciting the sample with weak illumination at 488 nm. This final experiment confirms that reversible data storage in FP crystals is indeed possible.

4. Conclusion

In this paper, we have demonstrated the potential applicability of photoactivatable fluorescent proteins as recording media for optical data storage. We showed that information can be irreversibly or reversibly written on surfaces coated with PCFPs and RSFPs. As IrisFP combines the properties of these two classes of proteins, it was possible, by activating at different wavelengths, to store information in four colours, thus enabling the development of a 4-base system. The very fast reversible photoswitching capabilities of IrisFP compared to other photochromic FPs (Regis Faro et al., 2010) provide a clear advantage to this protein for optical reversible data storage applications. Moreover, different to other reported publications in which protein-based patterns were written via a lithographic method and the use of homemade masks to create a contrast between irradiated and non-irradiated regions (Sorribas et al., 2002; Christman and Maynard, 2005; Howland et al., 2005; Nakayama et al., 2008), the direct photoactivation/photoswitching of FPs with precise laser scanning (and especially TPE) allows reducing the size of encoded elements. By using crystals of IrisFP and other EosFP mutants in combination with TPE, 3D data storage with FPs was demonstrated. Future experiments will aim at writing and addressing smaller voxels. In this way it can be established whether or not the approach proposed here can compete with other recently reported optical encoding schemes (De Cremer et al., 2010).

Uncited references

Belousov et al. (2006), Cook et al. (2004), Cowell et al. (2009), Hoffman (2005), Kogure et al. (2006), Kurokawa et al. (2001), Miyawaki et al. (1999), Mizuno et al. (2001), Mochizuki et al. (2001), Nakai et al. (2001) and Takemoto et al. (2003).

Acknowledgments

Financial support of the “Fonds voor Wetenschappelijk Onderzoek FWO” (Grant G.0366.06), the K.U. Leuven Research Fund (GOA 2006/2, Center of Excellence CECAT, Center of Excellence INPAC, CREA2007), the Flemish government (long-term structural funding – Methusalem funding) and the Federal Science Policy of Belgium (IAP-VI/27, Tournesol 2009 project T2009.05) is gratefully acknowledged. VA acknowledges the European Synchrotron Radiation Facility (France), the State of Baden-Württemberg (Germany) for financial support and the FWO for a postdoctoral grant, HM and JH acknowledge support from the Katholieke Universiteit Leuven (Belgium). GUN acknowledges funding of this work by the Deutsche Forschungsgemeinschaft (DFG) and the State of Baden-Württemberg through the Center for Functional Nanostructures and by DFG grant NI 291/9. DB acknowledges support by the “Agence Nationale de la Recherche” (ANR-07-BLAN-0107-01).

Appendix A. Supplementary data

Supplementary data associated with this article can be found, in the online version, at doi:10.1016/j.jbiotec.2010.04.001.

References

Achatz, J., Fischer, C., Salbeck, J., Daub, J., 1991. Functionalized photochromics for molecular switching – the multistabilities of a dihydroazulene anthraquinone system. J. Chem. Soc. Chem. Commun., 504–507.

Adam, V., Lelimousin, M., Boehme, S., Desfonds, G., Nienhaus, K., Field, M.J., Wiedenmann, J., McSweeney, S., Nienhaus, G.U., Bourgeois, D., 2008. Structural characterization of IrisFP, an optical highlighter undergoing multiple photo-induced transformations. Proc. Natl. Acad. Sci. U.S.A. 105, 18343–18348.

Andersen, P.E., Marrakchi, A., 1994. Noise-free holographic storage in iron-doped lithium niobate crystals. Opt. Lett. 19, 1583–1585.

Ando, R., Hama, H., Yamamoto-Hino, M., Mizuno, H., Miyawaki, A., 2002. An optical marker based on the UV-induced green-to-red photoconversion of a fluorescent protein. Proc. Natl. Acad. Sci. U.S.A. 99, 12651–12656.

Ando, R., Mizuno, H., Miyawaki, A., 2004. Regulated fast nucleocytoplasmic shuttling observed by reversible protein highlighting. Science 306, 1370–1373.

Andresen, M., Stiel, A.C., Trowitzsch, S., Weber, G., Eggeling, C., Wahl, M.C., Hell, S.W., Jakobs, S., 2007. Structural basis for reversible photoswitching in Dronpa. Proc. Natl. Acad. Sci. U.S.A. 104, 13005–13009.

Andresen, M., Wahl, M.C., Stiel, A.C., Grater, F., Schafer, L.V., Trowitzsch, S., Weber, G., Eggeling, C., Grubmuller, H., Hell, S.W., Jakobs, S., 2005. Structure and mechanism of the reversible photoswitch of a fluorescent protein. Proc. Natl. Acad. Sci. U.S.A. 102, 13070–13074.

Aramaki, S., Hatta, K., 2006. Visualizing neurons one-by-one in vivo: optical dissection and reconstruction of neural networks with reversible fluorescent proteins. Dev. Dynam. 235, 2192–2199.

Bae, Y.S., Yang, J., Jin, S., Lee, S.Y., Park, C.H., 1999. Optical CDMA system using bacteriorhodopsin for optical data storage. Biotechnol. Prog. 15, 971–973.

Bai, Y.S., Neurgaonkar, R.R., Kachru, R., 1997. High-efficiency nonvolatile holographic storage with two-step recording in praseodymium-doped lithium niobate by use of continuous-wave lasers. Opt. Lett. 22, 334–336.

Belousov, V.V., Fradkov, A.F., Lukyanov, K.A., Staroverov, D.B., Shakhbazov, K.S., Terskikh, A.V., Lukyanov, S., 2006. Genetically encoded fluorescent indicator for intracellular hydrogen peroxide. Nat. Methods 3, 281–286.

Berg, J., Hung, Y.P., Yellen, G., 2009. A genetically encoded fluorescent reporter of ATP:ADP ratio. Nat. Methods 6, 161–166.

Berkovic, G., Krongauz, V., Weiss, V., 2000. Spiropyrans and spirooxazines for memories and switches. Chem. Rev. 100, 1741–1753.

Betzig, E., Patterson, G.H., Sougrat, R., Lindwasser, O.W., Olenych, S., Bonifacino, J.S., Davidson, M.W., Lippincott-Schwartz, J., Hess, H.F., 2006. Imaging intracellular fluorescent proteins at nanometer resolution. Science 313, 1642–1645.

Bulina, M.E., Chudakov, D.M., Britanova, O.V., Yanushevich, Y.G., Staroverov, D.B., Chepurnykh, T.V., Merzlyak, E.M., Shkrob, M.A., Lukyanov, S., Lukyanov, K.A., 2006. A genetically encoded photosensitizer. Nat. Biotechnol. 24, 95–99.

Cheben, P., Calvo, M.L., 2001. A photopolymerizable glass with diffraction efficiency near 100% for holographic storage. Appl. Phys. Lett. 78, 1490.

Chen, F.S., Lamacchia, J.T., Fraser, D.B., 1968. Holographic storage in lithium niobate. Appl. Phys. Lett. 13, 223–225.

Christman, K.L., Maynard, H.D., 2005. Protein micropatterns using a pH-responsive polymer and light. Langmuir 21, 8389–8393.

Chudakov, D.M., Lukyanov, S., Lukyanov, K.A., 2007a. Tracking intracellular protein movements using photoswitchable fluorescent proteins PS-CFP2 and Dendra2. Nat. Protoc. 2, 2024–2032.

Chudakov, D.M., Lukyanov, S., Lukyanov, K.A., 2007b. Using photoactivatable fluorescent protein Dendra2 to track protein movement. Biotechniques 42, 553, 555, 557 passim.

Chudakov, D.M., Verkhusha, V.V., Staroverov, D.B., Souslova, E.A., Lukyanov, S., Lukyanov, K.A., 2004. Photoswitchable cyan fluorescent protein for protein tracking. Nat. Biotechnol. 22, 1435–1439.

Cook, J.L., Re, R., Alam, J., Hart, M., Zhang, Z., 2004. Intracellular angiotensin II fusion protein alters AT1 receptor fusion protein distribution and activates CREB. J. Mol. Cell Cardiol. 36, 75–90.

Cowell, C.F., Doppler, H., Yan, I.K., Hausser, A., Umezawa, Y., Storz, P., 2009. Mitochondrial diacylglycerol initiates protein-kinase D1-mediated ROS signaling. J. Cell Sci. 122, 919–928.

Cox, J.P., 2001. Long-term data storage in DNA. Trends Biotechnol. 19, 247–250.

Day, D., Gu, M., Smallridge, A., 1999. Use of two-photon excitation for erasable-rewritable three-dimensional bit optical data storage in a photorefractive polymer. Opt. Lett. 24, 948–950.

De Cremer, G., Sels, B.F., Hotta, J., Roeffaers, M.B.J., Bartholomeeusen, E., Coutiño-Gonzalez, E., Valtchev, V., De Vos, D.E., Vosch, T., Hofkens, J., 2010. Optical encoding of silver zeolite microcarriers. Adv. Mater. 22, 957–960.

Dedecker, P., Hotta, J., Flors, C., Sliwa, M., Uji-i, H., Roeffaers, M.B., Ando, R., Mizuno, H., Miyawaki, A., Hofkens, J., 2007. Subdiffraction imaging through the selective donut-mode depletion of thermally stable photoswitchable fluorophores: numerical analysis and application to the fluorescent protein Dronpa. J. Am. Chem. Soc. 129, 16132–16141.

Dickson, R.M., Cubitt, A.B., Tsien, R.Y., Moerner, W.E., 1997. On/off blinking and switching behaviour of single molecules of green fluorescent protein. Nature 388, 355–358.

Doose, S., 2008. Trends in biological optical microscopy. Chemphyschem 9, 523–528.

Dubois, M., Shi, X., Erben, C., Longley, K.L., Boden, E.P., Lawrence, B.L., 2005. Characterization of microholograms recorded in a thermoplastic medium for three-dimensional optical data storage. Opt. Lett. 30, 1947–1949.

Evers, T.H., Appelhof, M.A., Meijer, E.W., Merkx, M., 2008. His-tags as Zn(II) binding motifs in a protein-based fluorescent sensor. Protein Eng. Des. Sel. 21, 529–536.

Fischer, T., Neebe, M., Juchem, T., Hampp, N.A., 2003. Biomolecular optical data storage and data encryption. IEEE Trans. Nanobiosci. 2, 1–5.

Flors, C., Hotta, J., Uji-i, H., Dedecker, P., Ando, R., Mizuno, H., Miyawaki, A., Hofkens, J., 2007. A stroboscopic approach for fast photoactivation-localization microscopy with Dronpa mutants. J. Am. Chem. Soc. 129, 13970–13977.

Fron, E., Flors, C., Schweitzer, G., Habuchi, S., Mizuno, H., Ando, R., De Schryver, F.C., Miyawaki, A., Hofkens, J., 2007. Ultrafast excited-state dynamics of the photoswitchable protein Dronpa. J. Am. Chem. Soc. 129, 4870-+.

Fujioka, A., Terai, K., Itoh, R.E., Aoki, K., Nakamura, T., Kuroda, S., Nishida, E., Matsuda, M., 2006. Dynamics of the Ras/ERK MAPK cascade as monitored by fluorescent probes. J. Biol. Chem. 281, 8917–8926.

Gindre, D., Boeglin, A., Fort, A., Mager, L., Dorkenoo, K.D., 2006. Rewritable optical data storage in azobenzene copolymers. Opt. Expr. 14, 9896–9901.

Gu, M., Day, D., 1999. Use of continuous-wave illumination for two-photon three-dimensional optical bit data storage in a photobleaching polymer. Opt. Lett. 24, 288–290.

Habuchi, S., Ando, R., Dedecker, P., Verheijen, W., Mizuno, H., Miyawaki, A., Hofkens, J., 2005. Reversible single-molecule photoswitching in the GFP-like fluorescent protein Dronpa. Proc. Natl. Acad. Sci. U.S.A. 102, 9511–9516.

Habuchi, S., Dedecker, P., Hotta, J.I., Flors, C., Ando, R., Mizuno, H., Miyawaki, A., Hofkens, J., 2006. Photo-induced protonation/deprotonation in the GFP-like fluorescent protein Dronpa: mechanism responsible for the reversible photoswitching. Photochem. Photobiol. Sci. 5, 567–576.

Hanson, G.T., McAnaney, T.B., Park, E.S., Rendell, M.E.P., Yarbrough, D.K., Chu, S.Y., Xi, L.X., Boxer, S.G., Montrose, M.H., Remington, S.J., 2002. Green fluorescent protein variants as ratiometric dual emission pH sensors. 1. Structural characterization and preliminary application. Biochemistry 41, 15477–15488.

Hatta, K., Tsujii, H., Omura, T., 2006. Cell tracking using a photoconvertible fluorescent protein. Nat. Protoc. 1, 960–967.

Heanue, J.F., Bashaw, M.C., Daiber, A.J., Snyder, R., Hesselink, L., 1996. Digital holographic storage system incorporating thermal fixing in lithium niobate. Opt. Lett. 21, 1615–1617.

Heilemann, M., Dedecker, P., Hofkens, J., Sauer, M., 2009a. Photoswitches: Key molecules for subdiffraction-resolution fluorescence imaging and molecular quantification. Laser Photonics Rev. 3, 180–202.

Heilemann, M., van de Linde, S., Mukherjee, A., Sauer, M., 2009b. Super-resolution imaging with small organic fluorophores. Angew. Chem. Int. Ed. Engl. 48, 6903–6908.

Heilemann, M., van de Linde, S., Schuttpelz, M., Kasper, R., Seefeldt, B., Mukherjee, A., Tinnefeld, P., Sauer, M., 2008. Subdiffraction-resolution fluorescence imaging with conventional fluorescent probes. Angew. Chem. Int. Ed. Engl. 47, 6172–6176.

Hell, S.W., 2004. Strategy for far-field optical imaging and writing without diffraction limit. Phys. Lett. A 326, 140–145.

Hell, S.W., Jakobs, S., Andresen, M., Stiel, A.C.,Eggeling, C., 2007. Method and apparatus for storing a three-dimensional arrangement of data bits in a solid-state body. Patents #US20070047287, DE102005040671, EP1763024.

Hell, S.W., Jakobs, S., Kastrup, L., 2003. Imaging and writing at the nanoscale with focused visible light through saturable optical transitions. Appl. Phys. A: Mater. Sci. 77, 859–860.

Hess, S.T., Girirajan, T.P., Mason, M.D., 2006. Ultra-high resolution imaging by fluorescence photoactivation localization microscopy. Biophys. J. 91, 4258–4272.

Hess, S.T., Heikal, A.A., Webb, W.W., 2004. Fluorescence photoconversion kinetics in novel green fluorescent protein pH sensors (pHluorins). J. Phys. Chem. B 108, 10138–10148.

Hirschberg, Y., 1956. Reversible formation and eradication of colors by irradiation at low temperatures a photochemical memory model. J. Am. Chem. Soc. 78, 2304–2312.

Hoffman, R.M., 2005. Advantages of multi-color fluorescent proteins for whole-body and in vivo cellular imaging. J. Biomed. Opt. 10, 41202.

Hofmann, M., Eggeling, C., Jakobs, S., Hell, S.W., 2005. Breaking the diffraction barrier in fluorescence microscopy at low light intensities by using reversibly photoswitchable proteins. Proc. Natl. Acad. Sci. U.S.A. 102, 17565–17569.

Howland, M.C., Sapuri-Butti, A.R., Dixit, S.S., Dattelbaum, A.M., Shreve, A.P., Parikh, A.N., 2005. Phospholipid morphologies on photochemically patterned silane monolayers. J. Am. Chem. Soc. 127, 6752–6765.

Irie, M., 2000. Diarylethenes for memories and switches. Chem. Rev. 100, 1685–1716.

Irie, M., Fukaminato, T., Sasaki, T., Tamai, N., Kawai, T., 2002. Organic chemistry: a digital fluorescent molecular photoswitch. Nature 420, 759–760.

Ivanchenko, S., Glaschick, S., Rocker, C., Oswald, F., Wiedenmann, J., Nienhaus, G.U., 2007. Two-photon excitation and photoconversion of EosFP in dual-color 4Pi confocal microscopy. Biophys. J. 92, 4451–4457.

Iyoda, T., Saika, T., Honda, K., Shimidzu, T., 1989. A multi-mode chemical transducer-1 new conjugated function of photochromism and electrochromism of azo-quinone compound. Tetrahedron Lett. 30, 5429–5432.

Jang, J.S., Shin, D.H., 2001. Optical representation of binary data based on both intensity and phase modulation with a twisted-nematic liquid-crystal display for holographic digital data storage. Opt. Lett. 26, 1797–1799.

Kawata, S., Kawata, Y., 2000. Three-dimensional optical data storage using photochromic materials. Chem. Rev. 100, 1777–1788.

Kogure, T., Karasawa, S., Araki, T., Saito, K., Kinjo, M., Miyawaki, A., 2006. A fluorescent variant of a protein from the stony coral Montipora facilitates dual-color single-laser fluorescence cross-correlation spectroscopy. Nat. Biotechnol. 24, 577–581.

Kong, S.C., Sahakian, A., Taflove, A., Backman, V., 2008. Photonic nanojet-enabled optical data storage. Opt. Express 16, 13713–13719.

Kurokawa, K., Mochizuki, N., Ohba, Y., Mizuno, H., Miyawaki, A., Matsuda, M., 2001. A pair of fluorescent resonance energy transfer-based probes for tyrosine phosphorylation of the CrkII adaptor protein in vivo. J. Biol. Chem. 276, 31305–31310.

Lee, B., Kim, J., Ishimoto, K., Yamagata, Y., Tanioka, A., Nagamune, T., 2003. Fabrication of protein microarrays for immunoassay using the electrospray deposition (ESD) method. J. Chem. Eng. Jpn. 36, 1370–1375.

Lelimousin, M., Adam, V., Nienhaus, G.U., Bourgeois, D., Field, M.J., 2009. Photoconversion of the fluorescent protein EosFP: a hybrid potential simulation study reveals intersystem crossings. J. Am. Chem. Soc. 131, 16814–16823.

Lewis, G.N., Lipkin, D., 1942. Reversible photochemical processes in rigid media: The dissociation of organic molecules into radicals and ions. J. Am. Chem. Soc. 64, 2801–2808.

Li, J., Wang, S., VanDusen, W.J., Schultz, L.D., George, H.A., Herber, W.K., Chae, H.J., Bentley, W.E., Rao, G., 2000. Green fluorescent protein in *Saccharomyces cerevisiae*: real-time studies of the GAL1 promoter. Biotechnol. Bioeng. 70, 187–196.

Lukyanov, K.A., Fradkov, A.F., Gurskaya, N.G., Matz, M.V., Labas, Y.A., Savitsky, A.P., Markelov, M.L., Zaraisky, A.G., Zhao, X., Fang, Y., Tan, W., Lukyanov, S.A., 2000. Natural animal coloration can be determined by a nonfluorescent green fluorescent protein homolog. J. Biol. Chem. 275, 25879–25882.

Mandzhikov, V.F., Murin, V.A., Barachevskii, V.A., 1973. Nonlinear coloration of photochromic spiropyran solutions. Sov. J. Quant. Electron. 3, 128–129.

Markvicheva, K.N., Bogdanova, E.A., Staroverov, D.B., Lukyanov, S., Belousov, V.V., 2008. Imaging of intracellular hydrogen peroxide production with HyPer upon stimulation of HeLa cells with epidermal growth factor. Methods Mol. Biol. 476, 79–86.

McAnaney, T.B., Park, E.S., Hanson, G.T., Remington, S.J., Boxer, S.G., 2002. Green fluorescent protein variants as ratiometric dual emission pH sensors 2. Excited-state dynamics. Biochemistry 41, 15489–15494.

McAnaney, T.B., Shi, X.H., Abbyad, P., Jung, H., Remington, S.J., Boxer, S.G., 2005. Green fluorescent protein variants as ratiometric dual emission pH sensors. 3. Temperature dependence of proton transfer. Biochemistry 44, 8701–8711.

McLeod, R.R., Daiber, A.J., Honda, T., McDonald, M.E., Robertson, T.L., Slagle, T., Sochava, S.L., Hesselink, L., 2008. Three-dimensional optical disk data storage via the localized alteration of a format hologram. Appl. Opt. 47, 2696–2707.

McLeod, R.R., Daiber, A.J., McDonald, M.E., Robertson, T.L., Slagle, T., Sochava, S.L., Hesselink, L., 2005. Microholographic multilayer optical disk data storage. Appl. Opt. 44, 3197–3207.

Mitsunaga, M., Kim, M.K., Kachru, R., 1988. Degenerate photon echoes: simultaneous storage of multiple optical data. Opt. Lett. 13, 536–538.

Mitsunaga, M., Uesugi, N., 1990. 248-Bit optical data storage in Eu(3+):YAlO(3) by accumulated photon echoes. Opt. Lett. 15, 195–197.

Miyawaki, A., Griesbeck, O., Heim, R., Tsien, R.Y., 1999. Dynamic and quantitative Ca^{2+} measurements using improved cameleons. Proc. Natl. Acad. Sci. U.S.A. 96, 2135–2140.

Miyawaki, A., Llopis, J., Heim, R., McCaffery, J.M., Adams, J.A., Ikura, M., Tsien, R.Y., 1997. Fluorescent indicators for Ca^{2+} based on green fluorescent proteins and calmodulin. Nature 388, 882–887.

Mizuno, H., Mal, T.K., Tong, K.I., Ando, R., Furuta, T., Ikura, M., Miyawaki, A., 2003. Photo-induced peptide cleavage in the green-to-red conversion of a fluorescent protein. Mol. Cell. 12, 1051–1058.

Mizuno, H., Mal, T.K., Walchli, M., Kikuchi, A., Fukano, T., Ando, R., Jeyakanthan, J., Taka, J., Shiro, Y., Ikura, M., Miyawaki, A., 2008. Light-dependent regulation of structural flexibility in a photochromic fluorescent protein. Proc. Natl. Acad. Sci. U.S.A. 105, 9227–9232.

Mizuno, H., Sawano, A., Eli, P., Hama, H., Miyawaki, A., 2001. Red fluorescent protein from Discosoma as a fusion tag and a partner for fluorescence resonance energy transfer. Biochemistry 40, 2502–2510.

Mochizuki, N., Yamashita, S., Kurokawa, K., Ohba, Y., Nagai, T., Miyawaki, A., Matsuda, M., 2001. Spatio-temporal images of growth-factor-induced activation of Ras and Rap1. Nature 411, 1065–1068.

Mrozek, T., Gorner, H., Daub, J., 2001. Multimode-photochromism based on strongly coupled dihydroazulene and diarylethene. Chem. A: Eur. J. 7, 1028–1040.

Nagai, T., Yamada, S., Tominaga, T., Ichikawa, M., Miyawaki, A., 2004. Expanded dynamic range of fluorescent indicators for Ca(2+) by circularly permuted yellow fluorescent proteins. Proc. Natl. Acad. Sci. U.S.A. 101, 10554–10559.

Nakai, J., Ohkura, M., Imoto, K., 2001. A high signal-to-noise Ca(2+) probe composed of a single green fluorescent protein. Nat. Biotechnol. 19, 137–141.

Nakayama, K., Tachikawa, T., Majima, T., 2008. Protein recording material: photorecord/erasable protein array using a UV-eliminative linker. Langmuir 24, 1625–1628.

Nienhaus, G.U., Nienhaus, K., Holzle, A., Ivanchenko, S., Renzi, F., Oswald, F., Wolff, M., Schmitt, F., Rocker, C., Vallone, B., Weidemann, W., Heilker, R., Nar, H., Wiedenmann, J., 2006. Photoconvertible fluorescent protein EosFP: biophysical properties and cell biology applications. Photochem. Photobiol. 82, 351–358.

Nieuwkoop, P.D., Faber, J., 1994. Normal Table of *Xenopus laevis* (Daudin). Garland Publishing Inc., NY, USA.

Ortiz-Lombardía, M., Verma, C.S., 2006. Proteins as data storage devices: insights from computer models. J. Phys. Conf. Ser. 34, 7–14.

Parthenopoulos, D.A., Rentzepis, P.M., 1989. Three-dimensional optical storage memory. Science 245, 843–845.

Pina, F., Melo, M.J., Maestri, M., Ballardini, R., Balzani, V., 1997. Photochromism of 4′-methoxyflavylium perchlorate. A “write-lock-read-unlock-erase” molecular switching system. J. Am. Chem. Soc. 119, 5556–5561.

Ravelli, R.B., Haselmann-Weiss, U., McGeehan, J.E., McCarthy, A.A., Marquez, J.A., Antony, C., Frangakis, A.S., Stranzl, G., 2007. Plastic-embedded protein crystals. J. Synchrotron Radiat. 14, 128–132.

Regis Faro, A., Adam, V., Carpentier, P., Darnault, C., Bourgeois, D., de Rosny, E., 2010. Low-temperature photoinduced protonation in photochromic fluorescent proteins. Photochem. Photobiol. Sci. 9, 254–262.

Remington, et al., 2004 Remington, S.J., Hanson, G.T., Canon, M., Aggeler, R., Oglesbe, D., Capaldi, R.A., Tsien, R.Y., 2004. Third generation GFP biosensors for real time readout of pH and redox potential in living cells. In: Savitsky, A.P., Brovko, L.Y.,

Bornhop, D.J., Raghavachari, R., Achilefu, S.I. (Eds.), Genetically Engineered and Optical Probes for Biomedical Applications II, vol. 5329, pp. 1–12.
Rust, M.J., Bates, M., Zhuang, X., 2006. Sub-diffraction-limit imaging by stochastic optical reconstruction microscopy (STORM). Nat. Methods 3, 793–795.
Sato, T., Takahoko, M., Okamoto, H., 2006. HuC:Kaede, a useful tool to label neural morphologies in networks in vivo. Genesis 44, 136–142.
Sauer, M., 2005. Reversible molecular photoswitches: a key technology for nanoscience and fluorescence imaging. Proc. Natl. Acad. Sci. U.S.A. 102, 9433–9434.
Schafer, L.V., Groenhof, G., Boggio-Pasqua, M., Robb, M.A., Grubmuller, H., 2008. Chromophore protonation state controls photoswitching of the fluoroprotein asFP595. PLoS Comput. Biol. 4, e1000034.
Shen, Y., Swiatkiewicz, J., Jakubczyk, D., Xu, F., Prasad, P.N., Vaia, R.A., Reinhardt, B.A., 2001. High-density optical data storage with one-photon and two-photon near-field fluorescence microscopy. Appl. Opt. 40, 938–940.
Sheridan, J.T., Gleeson, M.R., Close, C.E., Kelly, J.V., 2007. Optical response of photopolymer materials for holographic data storage applications. J. Nanosci. Nanotechnol. 7, 232–242.
Shibasaki, S., Tanaka, A., Ueda, M., 2003. Development of combinatorial bioengineering using yeast cell surface display—order-made design of cell and protein for bio-monitoring. Biosens. Bioelectron 19, 123–130.
Sorribas, H., Padeste, C., Tiefenauer, L., 2002. Photolithographic generation of protein micropatterns for neuron culture applications. Biomaterials 23, 893–900.
Spreitzer, H., Daub, J., 1996. Multi-mode switching based on dihydroazulene/vinylheptafulvene photochromism: synergism of photochromism and redox switching in heteroaryl-functionalized systems. Chem. A: Eur. J. 2, 1150–1158.
Takemoto, K., Nagai, T., Miyawaki, A., Miura, M., 2003. Spatio-temporal activation of caspase revealed by indicator that is insensitive to environmental effects. J. Cell Biol. 160, 235–243.
Tallent, J., Song, Q.W., Li, Z., Stuart, J., Birge, R.R., 1996. Effective photochromic nonlinearity of dried blue-membrane bacteriorhodopsin films. Opt. Lett. 21, 1339–1341.
Terskikh, A., Fradkov, A., Ermakova, G., Zaraisky, A., Tan, P., Kajava, A.V., Zhao, X., Lukyanov, S., Matz, M., Kim, S., Weissman, I., Siebert, P., 2000. "Fluorescent timer": protein that changes color with time. Science 290, 1585–1588.
Tsien, R.Y., 1998. The green fluorescent protein. Annu. Rev. Biochem. 67, 509–544.
Uchida, K., Saito, M., Murakami, A., Kobayashi, T., Nakamura, S., Irie, M., 2005. Three bits eight states photochromic recording and nondestructive readout by using IR light. Chem. A: Eur. J. 11, 534–542.
van de Linde, S., Endesfelder, U., Mukherjee, A., Schuttpelz, M., Wiebusch, G., Wolter, S., Heilemann, M., Sauer, M., 2009. Multicolor photoswitching microscopy for subdiffraction-resolution fluorescence imaging. Photochem. Photobiol. Sci. 8, 465–469.
van de Linde, S., Sauer, M., Heilemann, M., 2008. Subdiffraction-resolution fluorescence imaging of proteins in the mitochondrial inner membrane with photoswitchable fluorophores. J. Struct. Biol. 164, 250–254.
van Heerden, P.J., 1963. A new optical method of storing and retrieving information. Appl. Opt. 2, 387–392.
von der Linde, D., Glass, A.M., 1975. Photorefractive effects for reversible holographic storage of information. Appl. Phys. 8, 85–100.
Wang, M.M., Esener, S.C., 2000. Three-dimensional optical data storage in a fluorescent dye-doped photopolymer. Appl. Opt. 39, 1826–1834.
Wiedenmann, J., Ivanchenko, S., Oswald, F., Schmitt, F., Rocker, C., Salih, A., Spindler, K.D., Nienhaus, G.U., 2004. EosFP, a fluorescent marker protein with UV-inducible green-to-red fluorescence conversion. Proc. Natl. Acad. Sci. U.S.A. 101, 15905–15910.
Wiedenmann, J., Nienhaus, G.U., 2006. Live-cell imaging with EosFP and other photoactivatable marker proteins of the GFP family. Expert Rev. Proteomics 3, 361–374.
Wiedenmann, J., Oswald, F., Nienhaus, G.U., 2005. EosFP: Neues fluoreszentes Protein vorgestellt. Uni Ulm Intern. 273, 30–31.
Yachie, N., Sekiyama, K., Sugahara, J., Ohashi, Y., Tomita, M., 2007. Alignment-based approach for durable data storage into living organisms. Biotechnol. Prog. 23, 501–505.
Yao, B., Lei, M., Ren, L., Menke, N., Wang, Y., Fischer, T., Hampp, N., 2005a. Polarization multiplexed write-once–read-many optical data storage in bacteriorhodopsin films. Opt. Lett. 30, 3060–3062.
Yao, B., Ren, Z., Menke, N., Wang, Y., Zheng, Y., Lei, M., Chen, G., Hampp, N., 2005b. Polarization holographic high-density optical data storage in bacteriorhodopsin film. Appl. Opt. 44, 7344–7348.
Yokoyama, Y., 2000. Fulgides for memories and switches. Chem. Rev. 100, 1717–1739.

Please cite this article in press as: Adam, V., et al., Data storage based on photochromic and photoconvertible fluorescent proteins. J. Biotechnol. (2010), doi:10.1016/j.jbiotec.2010.04.001

Bibliography

[1] Osamu Shimomura, Frank H. Johnson, and Yo Saiga. Extraction, purification and properties of aequorin, a bioluminescent protein from the luminous hydromedusan, aequorea. *Journal of Cellular and Comparative Physiology*, 59:223–239, 1962.

[2] Douglas C. Prasher, Virginia K. Eckenrode, William W. Ward, Frank G. Prendergast, and Milton J. Cormier. Primary structure of the aequorea victoria green-fluorescent protein. *Gene*, 111(2):229–233, 1992.

[3] Martin Chalfie, Yuan Tu, Ghia Euskirchen, William W. Ward, and Douglas C. Prasher. Green fluorescent protein as a marker for gene expression. *Science*, 263(5148):802–805, 1994.

[4] Mats Ormö, Andrew B. Cubitt, Karen Kallio, Larry A. Gross, Roger Y. Tsien, and S. James Remington. Crystal structure of the aequorea victoria green fluorescent protein. *Science*, 273(5280):1392–1395, 1996.

[5] Fan Yang, Larry G. Moss, and George N. Phillips. The molecular structure of green fluorescent protein. *Nature Biotechnology*, 14(10):1246–1251, 1996.

[6] Andrew B. Cubitt, Roger Heim, Stephen R. Adams, Aileen E. Boyd, Larry A. Gross, and Roger Y. Tsien. Understanding, improving and using green fluorescent proteins. *Trends in Biochemical Sciences*, 20(11):448–455, 1995.

[7] Jason A. Kahana, Bruce J. Schnapp, and Pamela A. Silver. Kinetics of spindle pole body separation in budding yeast. *Proceedings of the National Academy of Sciences of the United States of America*, 92(21):9707–9711, 1995.

[8] Jim Haseloff and Brad Amos. GFP in plants. *Trends in Genetics*, 11(8):328–329, 1995.

[9] Shengxian Wang and Tulle Hazelrigg. Implications for bcd mRNA localization from spatial distribution of exu protein in drosophila oogenesis. *Nature*, 369(6479):400–403, 1994.

[10] Adam Amsterdam, Shuo Lin, Larry G. Moss, and Nancy Hopkins. Requirements for green fluorescent protein detection in transgenic zebrafish embryos. *Gene*, 173(1 Spec No):99–103, 1996.

[11] Hiromi Masuda, Yasuhiro Takenaka, Atsushi Yamaguchi, Satoshi Nishikawa, and Hiroshi Mizuno. A novel yellowish-green fluorescent protein from the marine copepod, chiridius poppei, and its use as a reporter protein in HeLa cells. *Gene*, 372:18–25, 2006.

[12] Dimitri D. Deheyn, Kaoru Kubokawa, James K. McCarthy, Akio Murakami, Magali Porrachia, Greg W. Rouse, and Nicholas D. Holland. Endogenous green fluorescent protein (GFP) in amphioxus. *Biological Bulletin*, 213(2):95–100, 2007.

[13] Xiaokun Shu, Antoine Royant, Michael Z. Lin, Todd A. Aguilera, Varda Lev-Ram, Paul A. Steinbach, and Roger Y. Tsien. Mammalian expression of infrared fluorescent proteins engineered from a bacterial phytochrome. *Science*, 324(5928):804–807, 2009.

[14] Roger Heim, Andrew B. Cubitt, and Roger Y. Tsien. Improved green fluorescence. *Nature*, 373(6516):663–664, 1995.

[15] Nathan C. Shaner, Robert E. Campbell, Paul A. Steinbach, Ben N. G. Giepmans, Amy E. Palmer, and Roger Y. Tsien. Improved monomeric red, orange and yellow fluorescent proteins derived from discosoma sp. red fluorescent protein. *Nature Biotechnology*, 22(12):1567–1572, 2004.

[16] Lei Wang, W. Coyt Jackson, Paul A. Steinbach, and Roger Y. Tsien. Evolution of new nonantibody proteins via iterative somatic hypermutation. *Proceedings of the National Academy of Sciences of the United States of America*, 101(48):16745–16749, 2004.

[17] Xiaokun Shu, Nathan C. Shaner, Corinne A. Yarbrough, Roger Y. Tsien, and S. James Remington. Novel chromophores and buried charges control color in mFruits. *Biochemistry*, 45(32):9639–9647, 2006.

[18] Roger Y. Tsien. Nobel lecture: constructing and exploiting the fluorescent protein paintbox. *Integrative Biology*, 2(2-3):77, 2010.

[19] Virgile Adam, Mickaël Lelimousin, Susan Boehme, Guillaume Desfonds, Karin Nienhaus, Martin J. Field, Joerg Wiedenmann, Sean McSweeney, G. Ulrich Nienhaus, and Dominique Bourgeois. Structural characterization of IrisFP, an optical highlighter undergoing multiple photo-induced transformations. *Proceedings of the National Academy of Sciences of the United States of America*, 105(47):1834318348, 2008.

[20] Ryoko Ando, Hideaki Mizuno, and Atsushi Miyawaki. Regulated fast nucleocytoplasmic shuttling observed by reversible protein highlighting. *Science*, 306(5700):1370–1373, 2004.

[21] Satoshi Habuchi, Ryoko Ando, Peter Dedecker, Wendy Verheijen, Hideaki Mizuno, Atsushi Miyawaki, and Johan Hofkens. Reversible single-molecule photoswitching in the GFP-like fluorescent protein dronpa. *Proceedings of the National Academy of Sciences of the United States of America*, 102(27):9511–9516, 2005.

[22] AndreC. Stiel, Simon Trowitzsch, Gert Weber, Martin Andresen, Christian Eggeling, StefanW. Hell, Stefan Jakobs, and MarkusC. Wahl. 1.8 å bright-state structure of the reversibly switchable fluorescent protein dronpa guides the generation of fast switching variants. *Biochemical Journal*, 402(Pt 1):35–42, 2007.

[23] Hideaki Mizuno, Peter Dedecker, Ryoko Ando, Takashi Fukano, Johan Hofkens, and Atsushi Miyawaki. Higher resolution in localization microscopy by slower switching of a photochromic protein. *Photochemical & Photobiological Sciences*, 9(2):239–248, 2010.

[24] Martin Andresen, Andre C. Stiel, Jonas Folling, Dirk Wenzel, Andreas Schonle, Alexander Egner, Christian Eggeling, Stefan W. Hell, and Stefan Jakobs. Photoswitchable fluorescent proteins enable monochromatic multilabel imaging and dual color fluorescence nanoscopy. *Nature Biotechnology*, 26(9):1035–1040, 2008.

[25] George H. Patterson and Jennifer Lippincott-Schwartz. A photoactivatable GFP for selective photolabeling of proteins and cells. *Science*, 297(5588):1873–1877, 2002.

[26] Dmitriy M. Chudakov, Vladislav V. Verkhusha, Dmitry B. Staroverov, Ekaterina A. Souslova, Sergey Lukyanov, and Konstantin A. Lukyanov. Photoswitchable cyan fluorescent protein for protein tracking. *Nature Biotechnology*, 22(11):1435–1439, 2004.

[27] Ryoko Ando, Hiroshi Hama, Miki Yamamoto-Hino, Hideaki Mizuno, and Atsushi Miyawaki. An optical marker based on the UV-induced green-to-red photoconversion of a fluorescent protein. *Proceedings of the National Academy of Sciences of the United States of America*, 99(20):12651–12656, 2002.

[28] Hidekazu Tsutsui, Satoshi Karasawa, Hideaki Shimizu, Nobuyuki Nukina, and Atsushi Miyawaki. Semi-rational engineering of a coral fluorescent protein into an efficient highlighter. *EMBO Reports*, 6(3):233–238, 2005.

[29] Jörg Wiedenmann, Sergey Ivanchenko, Franz Oswald, Florian Schmitt, Carlheinz Röcker, Anya Salih, Klaus-Dieter Spindler, and G. Ulrich Nienhaus. EosFP, a fluorescent marker protein with UV-inducible green-to-red fluorescence conversion. *Proceedings of the National Academy of Sciences of the United States of America*, 101(45):15905–15910, 2004.

[30] Nadya G. Gurskaya, Vladislav V. Verkhusha, Alexander S. Shcheglov, Dmitry B. Staroverov, Tatyana V. Chepurnykh, Arkady F. Fradkov, Sergey Lukyanov, and Konstantin A. Lukyanov. Engineering of a monomeric green-to-red photoactivatable fluorescent protein induced by blue light. *Nature Biotechnology*, 24(4):461–465, 2006.

[31] Virgile Adam, Karin Nienhaus, Dominique Bourgeois, and G. Ulrich Nienhaus. Structural basis of enhanced photoconversion yield in green fluorescent protein-like protein dendra2. *Biochemistry*, 48(22):4905–4915, 2009.

[32] Hideaki Mizuno, Tapas Kumar Mal, Kit I. Tong, Ryoko Ando, Toshiaki Furuta, Mitsuhiko Ikura, and Atsushi Miyawaki. Photo-induced peptide cleavage in the green-to-red conversion of a fluorescent protein. *Molecular Cell*, 12(4):1051–1058, 2003.

[33] Konstantin A. Lukyanov, Dmitry M. Chudakov, Sergey Lukyanov, and Vladislav V. Verkhusha. Photoactivatable fluorescent proteins. *Nature Reviews Molecular Cell Biology*, 6(11):885–890, 2005.

[34] George T. Hanson, Tim B. McAnaney, Eun Sun Park, Marla E. P. Rendell, Daniel K. Yarbrough, Shaoyou Chu, Lixuan Xi, Steven G. Boxer, Marshall H. Montrose, and S. James Remington. Green fluorescent protein variants as ratiometric dual emission pH sensors. 1. structural characterization and preliminary application. *Biochemistry*, 41(52):15477–15488, 2002.

[35] Atsushi Miyawaki, Juan Llopis, Roger Heim, J. Michael McCaffery, Joseph A. Adams, Mitsuhiko Ikura, and Roger Y. Tsien. Fluorescent indicators for Ca^{2+} based on green fluorescent proteins and calmodulin. *Nature*, 388(6645):882–887, 1997.

[36] Wolf B. Frommer, Michael W. Davidson, and Robert E. Campbell. Genetically encoded biosensors based on engineered fluorescent proteins. *Chemical Society Reviews*, 38(10):2833, 2009.

[37] Daniel G. Jay. Selective destruction of protein function by chromophore-assisted laser inactivation. *Proceedings of the National Academy of Sciences of the United States of America*, 85(15):5454–5458, 1988.

[38] Ken Jacobson, Zenon Rajfur, Eric Vitriol, and Klaus Hahn. Chromophore-assisted laser inactivation in cell biology. *Trends in Cell Biology*, 18(9):443–450, 2008.

[39] C.A. Robertson, D. Hawkins Evans, and Heidi Abrahamse. Photodynamic therapy (PDT): a short review on cellular mechanisms and cancer research applications for PDT. *Journal of Photochemistry and Photobiology B: Biology*, 96(1):1–8, 2009.

[40] Dmitry A. Shagin, Ekaterina V. Barsova, Yurii G. Yanushevich, Arkady F. Fradkov, Konstantin A. Lukyanov, Yulii A. Labas, Tatiana N. Semenova, Juan A. Ugalde, Ann Meyers, Jose M. Nunez, Edith A. Widder, Sergey A. Lukyanov, and Mikhail V. Matz. GFP-like proteins as ubiquitous metazoan superfamily: evolution of functional features and structural complexity. *Molecular Biololgy and Evolution*, 21(5):841–850, 2004.

[41] Maria E. Bulina, Dmitriy M. Chudakov, Olga V. Britanova, Yurii G. Yanushevich, Dmitry B. Staroverov, Tatyana V. Chepurnykh, Ekaterina M. Merzlyak, Maria A. Shkrob, Sergey Lukyanov, and Konstantin A. Lukyanov. A genetically encoded photosensitizer. *Nature Biotechnology*, 24(1):95–99, 2006.

[42] Sergei Pletnev, Nadya G. Gurskaya, Nadya V. Pletneva, Konstantin A. Lukyanov, Dmitriy M. Chudakov, Vladimir I. Martynov, Vladimir O. Popov, Mikhail V. Kovalchuk, Alexander Wlodawer, Zbigniew Dauter, and Vladimir Pletnev. Structural basis for phototoxicity of the genetically encoded photosensitizer KillerRed. *The Journal of Biological Chemistry*, 2009.

[43] Philippe Carpentier, Sebastien Violot, Laurent Blanchoin, and Dominique Bourgeois. Structural basis for the phototoxicity of the fluorescent protein KillerRed. *FEBS Letters*, 583(17):2839–2842, 2009.

[44] Stefan W. Hell. Far-field optical nanoscopy. *Science*, 316(5828):1153–1158, 2007.

[45] Stefan W. Hell and Jan Wichmann. Breaking the diffraction resolution limit by stimulated emission: stimulated-emission-depletion fluorescence microscopy. *Optics Letters*, 19(11):780–782, 1994.

[46] Eric Betzig, George H. Patterson, Rachid Sougrat, O. Wolf Lindwasser, Scott Olenych, Juan S. Bonifacino, Michael W. Davidson, Jennifer Lippincott-Schwartz, and Harald F. Hess. Imaging intracellular fluorescent proteins at nanometer resolution. *Science*, 313(5793):1642–1645, 2006.

[47] Michael J. Rust, Mark Bates, and Xiaowei Zhuang. Sub-diffraction-limit imaging by stochastic optical reconstruction microscopy (STORM). *Nature Methods*, 3(10):793–796, 2006.

[48] Jennifer Lippincott-Schwartz and George H. Patterson. Development and use of fluorescent protein markers in living cells. *Science*, 300(5616):87–91, 2003.

[49] Samuel T. Hess, Thanu P. K. Girirajan, and Michael D. Mason. Ultra-high resolution imaging by fluorescence photoactivation localization microscopy. *Biophysical Journal*, 91(11):4258–4272, 2006.

[50] Hideaki Mizuno, Tapas Kumar Mal, Markus Wälchli, Akihiro Kikuchi, Takashi Fukano, Ryoko Ando, Jeyaraman Jeyakanthan, Junichiro Taka, Yoshitsugu Shiro, Mitsuhiko Ikura, and Atsushi Miyawaki. Light-dependent regulation of structural flexibility in a photochromic fluorescent protein. *Proceedings of the National Academy of Sciences of the United States of America*, 105(27):9227–9232, 2008.

[51] Aline Regis Faro, Virgile Adam, Philippe Carpentier, Claudine Darnault, Dominique Bourgeois, and Eve de Rosny. Low-temperature switching by photoinduced protonation in photochromic fluorescent proteins. *Photochemical & Photobiological Sciences*, 9(2):254–262, 2010.

[52] Virgile Adam, Hideaki Mizuno, Alexei Grichine, Jun-Ichi Hotta, Yutaka Yamagata, Benjamien Moeyaert, G. Ulrich Nienhaus, Atsushi Miyawaki, Dominique Bourgeois, and Johan Hofkens. Data storage based on photochromic and photoconvertible fluorescent proteins. *Journal of Biotechnology*, April 2010.

[53] G. Ulrich Nienhaus, Karin Nienhaus, Angela Hölzle, Sergey Ivanchenko, Fabiana Renzi, Franz Oswald, Michael Wolff, Florian Schmitt, Carlheinz Röcker, Beatrice Vallone, Wolfgang Weidemann, Ralf Heilker, Herbert Nar, and Jörg Wiedenmann. Photoconvertible fluorescent protein EosFP: biophysical properties and cell biology applications. *Photochemistry and Photobiology*, 82(2):351358, 2006.

[54] Martin Andresen, Markus C. Wahl, André C. Stiel, Frauke Gräter, Lars V. Schäfer, Simon Trowitzsch, Gert Weber, Christian Eggeling, Helmut Grubmüller, Stefan W. Hell, and Stefan Jakobs. Structure and mechanism of the reversible photoswitch of a fluorescent protein. *Proceedings of the National Academy of Sciences of the United States of America*, 102(37):13070–13074, 2005.

[55] Eduard Fron, Cristina Flors, Gerd Schweitzer, Satoshi Habuchi, Hideaki Mizuno, Ryoko Ando, Frans C. De Schryver, Atsushi Miyawaki, and Johan Hofkens. Ultrafast excited-state dynamics of the photoswitchable protein dronpa. *Journal of the American Chemical Society*, 129(16):4870–4871, 2007.

[56] Karin Nienhaus, G. Ulrich Nienhaus, Jörg Wiedenmann, and Herbert Nar. Structural basis for photo-induced protein cleavage and green-to-red conversion of fluorescent protein

EosFP. *Proceedings of the National Academy of Sciences of the United States of America*, 102(26):9156–9159, 2005.

[57] Ikuko Hayashi, Hideaki Mizuno, Kit I. Tong, Toshiaki Furuta, Fujie Tanaka, Masato Yoshimura, Atsushi Miyawaki, and Mitsuhiko Ikura. Crystallographic evidence for water-assisted photo-induced peptide cleavage in the stony coral fluorescent protein kaede. *Journal of Molecular Biology*, 372(4):918–926, 2007.

[58] Mickaël Lelimousin, Virgile Adam, G. Ulrich Nienhaus, Dominique Bourgeois, and Martin J. Field. Photoconversion of the fluorescent protein EosFP: a hybrid potential simulation study reveals intersystem crossings. *Journal of the American Chemical Society*, 2009.

[59] Joseph Sambrook and David Russell. *Molecular Cloning: A Laboratory Manual*. Cold Spring Harbor Laboratory Press, 2001.

[60] Gerd Schweitzer, Li Xu, Bruce Craig, and Frans C. De Schryver. A double OPA femtosecond laser system for transient absorption spectroscopy. *Optics Communications*, 142(4-6):283–288, 1997.

[61] Dmitriy M. Chudakov, Sergey Lukyanov, and Konstantin A. Lukyanov. Using photoactivatable fluorescent protein dendra2 to track protein movement. *BioTechniques*, 42(5):553, 555, 557 passim, 2007.